UNIVERSITY OF MILANO-BICOCCA
Department of Environmental Sciences

- Nanoparticles -

Biological effects on *in vivo*

and *in vitro* systems

Elisa Moschini

Thesis for the degree of philosophiae doctor (ph.d)

Tutor: Prof. Marina Camatini
Co-tutor: Dr. Paride Mantecca

2012

Table of contents

PREFACE

Aim and structure of the research

The present research is focused on the comprehension of the (eco)toxicology of a specific category of inorganic engineered nanoparticles: metal nanoxides (indicated in text as MONs).

In *Chapter 1* the main criticisms related to the production, diffusion and potential release of these compounds in the environment are discussed. *Chapter 2* describes the aim of the project, which intends to evaluate the potential biological effects of three representative transition metal nanoxides ($nTiO_2$, nCuO, nZnO) on two different experimental models: an *in vivo* model and an *in vitro* one . The *in vivo* model has been used to assess MONs aquatic toxicity, which has been evaluated by the use of the FETAX assay (Frog embryo teratogenesis assay - Xenopus). *Chapter 3* (and related Supporting information – PART I) reports and discusses the results obtained by this approach.

The human alveolar epithelial cell line A459 has been used as *in vitro* model to assess the potential toxicity on the respiratory system of humans exposed to MONs. In *Chapter 4* the nanotoxicological study has been approached with the aim to estabilish a correlation between the biochemical analyses and the morphological evidences, to better characterize the phenomena at the nano-level. Thus a comparative study on the cytotoxicity and cell-particle interactions of $nTiO_2$ and nCuO was performed on A549 cells. Since nCuO resulted to be a strong cytotoxic agent, *Chapter 5* and *6* are focused on the mechanisms of action of this MON. The sensitive cellular targets to nCuO and the potential mechanisms of toxicity involved were investigated. Ion dissolution, oxidative stress and cell cycle alterations were analysed as possible responsible of the cytotoxic effects. Supporting information

regarding this section, PART II, are reported at the end of the work. Finally, in *Chapter 7*, a general conclusion on the MON toxicity in aquatic developing embryos and in human respiratory cells has been delineated. The implications of the MONs toxic potential on the environment and human health, as well as the future developments are discussed.

CHAPTER 1

Nanoparticles, what risks? An overview of the criticisms of the nanoworld focused on metal oxide nanoparticles

1.1 Abstract

The advent of nanotechnology and the commercialization of several nanoparticle-containing-products call to a serious assessment of the environmental and human risks derived from the exposure to these new materials. Among nanomaterials, metal oxide nanoparticles (MONs) can be considered an interesting and critical group. The most important criticisms of new nano-structured materials are represented by the emerging properties, the absence of a dedicate regulation, the increasing world-market, the implementation of the application fields and finally by the several potential scenarios , which expose humans and ecosystems to nanoparticles (NPs). These aspects pose the necessity to improve our knowledge about the environmental fate and the effects of these new materials on biological systems, in order to define adequate guidelines for toxicity studies and to harmonise the production of new and safe materials.

1.2 Introduction

1.2.1 Engineered Nanoparticles: definitions and application fields

It is now recognized that exposure to particulate matter in ambient air can be associated with the increase of human health outcomes such as respiratory and cardiovascular diseases, exacerbation of asthma, pulmonary inflammation. Moreover several epidemiological studies found a correlation between atmospheric mass concentration of coarse and fine particles and mortality or cancer incidence (WHO 2003; Dockery et al., 1993; Pope et al., 2002), but little is known about finest fractions. So, in the last years, the investigators moved their attention on the smallest particles, called ultrafine particles (UFP), because they are predicted to have a higher toxic potential as a result of their high surface/mass ratios (Konkzol et al., 2011). The contribute in mass of this fraction is negligible to the respect of the total particulate matter but they dominate in number. In literature are reported different values regarding the environmental concentration of UFPs: for example in Luther (2004) and SCENIHR/002/05 are reported similar contents ranging from 10^6 to 10^8 particles per litre of air in urban and rural areas with man-made dust more abundant in urban areas.

Although it has been estimated that anthropogenic aerosol represent only 10% of the total atmospheric dust (SCENIHR/002/05; Buzea et al., 2007) the main concerns arise from the broad diffusion of *nanotechnological materials* having their size in the ultrafine range because they represent new substances with unpredictable properties. To distinguish the manufactured origin of these products from naturally occurring particles with similar size, they have been defined as "*engineered nanoparticles*" (ENPs). They are in fact synthesized with specific properties and characteristics. This clarification is useful because in the scientific community there was some

confusion about the definition of nano-scaled particles and quite frequently the terms “nano” and “ultrafine” were interchangeably used.

An official definition of these new compounds derives from the International Standard Organization which proposed a pre-normative terminology to define the products coming from nanotechnology: “N**anoparticles** indicate **nano-objects with the three external dimensions ranging from 1 to 100nm** (ISO TS27687 2008).

ENPs include a huge variety of different materials classified on the basis of their composition. Ostiguy and co-workers (2009) distinguished ENPs in three distinct large categories:

1) Carbon based nanoparticles:

- Fullerene (C_{60})
- Carbon nanofibers
- Carbon nanofoams
- Graphene
- Graphene nanofoils
- Carbon Nanotubes (CNT)
    - Single-walled carbon nanotubes (SWCNT)
    - Multi-walled carbon nanotubes (MWCNT)
- Carbon Black (CB)

2) Organic nanoparticles:

- Organic polymers
- Biologically-Inspired Nanoparticles

3) Inorganic nanoparticles:

- Metal nanoparticles
- Metal oxide nanoparticles (MONs)
- Quantum dots (QDs)

Each of these categories presents specific features. Thanks to their crystalline structure and electrical properties *carbon-based nanoparticles* are mainly used in the electronic field. Thanks to the great surface area, some of these NPs are also used for molecular absorption (i.e. gas storage). CBs are diffusely applied as pigments or strengthening agents in tires.

Organic nanoparticles are investigated for their application in medical, biomedical and cosmetic field. Finally *inorganic nanoparticles* show a broad spectrum of properties so they are used in many applications such as catalysis, cosmetics, optic, diagnostic, and drug delivery.

Among these inorganic NPs, metal oxides are of great interest in nanotechnology (Rice et al., 2009) and represent at the same time an attractive and critical group. The reasons of this consideration (emerging properties, growing market, hazard, (eco)toxicity) are reported in the sections below.

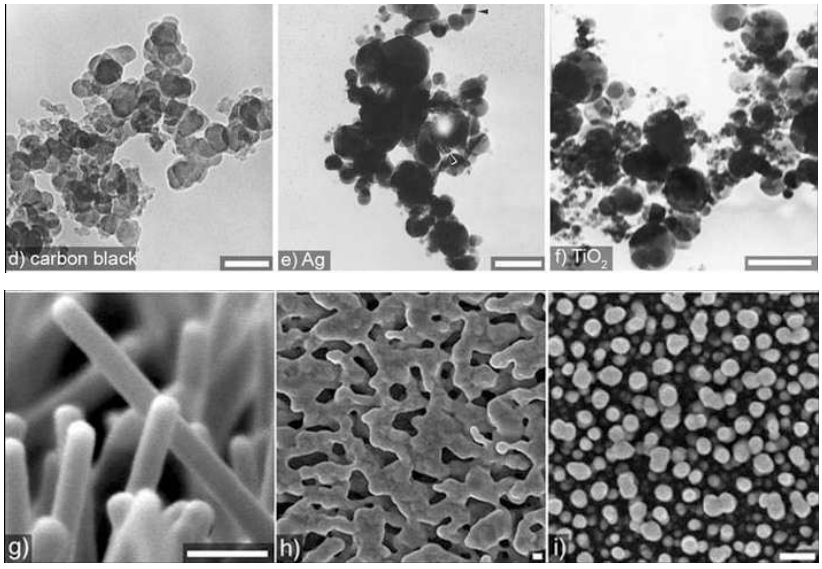

Fig. 1 Examples of nanoparticles and nanostructured materials in thin film form, d) Carbon black NPs; e) silver; f) titanium oxide; g) ZnO nanowires; h) porous Ag; (i) porous Si. The scale bars represent 100 nm. (Buzea et al., 2007).

1.3 Metal oxide nanoparticles: characteristics and critical aspects

1.3.1 Emerging properties

As well as other natural NPs, metal oxides exist in all ecosystems and play an important role in biogeochemical processes (Wigginton et al., 2007) so, during the evolution, living organisms have adapted to the presence of these compounds in the environment (Blinova et al., 2010).

Criticisms arise for manufactured metal nanoxides since their dimensions at the nanoscale confer emerging properties which differ from single atoms, individual molecules or bulk materials. For this reason MONs should be considered as new chemical compounds which don't obey to classical physic laws (SCENIHR/002/05; Vippola et al., 2009).

Firstly they have a surface area to volume ratio greater than microparticles with the same chemical composition; this means that the atoms on the surface are more than in the core and the binding energy is lower if compared to the bulk material. With the reduction in size also the electrons can be confined in a very little space and the result can be both a quantized spectrum of energy and a quantized ability to accept and donate electrical charge (Kamat 2002). Some nanoxide (e.g. TiO_2, ZnO) shows the ability to generate electron-hole pairs when photo-activated: when particles with a specific size (5÷20 nm) are excited by energy greater than their band gap, a positive holes in the valence band occur because electrons are promoted to the conduction band (Hurst et al., 2011). This electronic unbalance can lead to redox processes on particle surface and further recombination reactions can occur with the subsequent loss of the absorbed energy. Another consequence of the quantum effect is the appearance of magnetic moment in materials which do not present this property at the bulk state (Buzea et al., 2007).

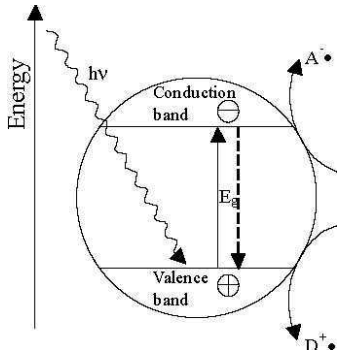

Fig. 2 Representative scheme of photoactivation inTiO_2 a with formation of radicals (Stamate and Lazar, 2007).

MONs differ in elemental composition (metal or transition metal), oxidation state, solubility, speciation (depending on the medium), mineralogy (e.g. TiO_2), crystallinity and electronic charge.

This basic spectrum of properties can be further amplified and modified firstly by different manufacture's preparation. Below a representative list of the main MON-specific production processes (Ostiguy et al., 2009) is reported.

Chemical processes:

- Vapour phase reactions
- Reactions and precipitations in liquid media
- Reactions in solid media
- Sol-gel techniques (i.e. nanocristallyne CuO, ZnO, NiO for catalysis)
- Supercritical fluids with chemical reaction
- Chemical co-precipitation or hydrolysis reactions

Physical processes:

- Evaporation / condensation under inert or reactive partial pressure
- Laser pyrolysis
- Plasma synthesis or electric arc methods

- Combustion flames
- Supercritical fluid without chemical reaction (Materials for vectorization of active principles)
- Thermal plasma

Mechanical processes:
- Mechanosynthesis processes and mechanical activation of powder metallurgy processes
- Consolidation and densification
- Strong deformation by torsion, lamination or friction

Also the post synthesis treatments plays a fundamental role in determining surface characteristics. By functionalization or derivatization, it is possible to modify the surface characteristics in order to obtain materials with peculiar properties or reactivity. For example the functionalization of the NP surface with a surfactant is used to reduce the aggregation (Li et al., 2003).

Emerging properties are of actual interest in the nanotechnological world. They have opened new frontiers in several fields such as biology, medicine, electronic, cosmetics and allowed to develop new devices or innovative analytical systems. Several MONs in powder form are commercially available and currently used as fillers, opacifiers, semiconductors, cosmetics, microelectronics coating agents, additives (i.e in food) or embedded in different matrix to improve mechanical or optical characteristics (Nel et al., 2006; Reijnders 2006).

These new characteristics are usefully employed to develop new technological applications and benefits, but, at the same time, such changes in chemical-physical behaviour may determine different environmental fate and/or toxic properties, making necessary a risk assessment on case by case

basis. For these reasons these chemicals should be treated as new substances and therefore regulated by a specific discipline.

1.3.2 Global market of MON

Nanotechnology is a relatively young research field increased rapidly since 1980s and in dynamical development despite the global economic crisis (Kessler 2011).

Recent updated reports focused on world market of metal oxide nanopowders estimated a current worldwide production of about 9000 tons, with the perspective to further increase until 18000 tons by 2016. These projections involve also applications, demand by material type and revenues of 15 of the most used metal nanoxides.

The enormous diffusion of MONs finds explanation in the wide spectrum of properties previously described which promote broad application fields. Among ENPs, MONs are the most commercially important nanomaterials after carbon black (Landsiedel et al., 2010) and it has been estimated that they account for over 80% of world nanopowder production (http://www.abercade.ru/en/materials/analytics/130.html).

On the market the number of consumer products containing NPs exceeds 800 and MONs (specifically TiO_2) are in the fourth position among the most mentioned materials in the product description (Bryce et al., 2009; Kahru et al., 2010). The market of metal oxide nanoparticles is dominated by silicon dioxide, followed by aluminum dioxide, stannic oxide, titanium dioxide, zinc oxide, iron oxide, cerium oxide and indium tin oxide (ITO) (nano.DE-Report 2009). Already in 2004 The Royal Society affirmed that TiO_2 and ZnO NPs were produced in industrial amounts (Heinlaan et al., 2008).

Another indicator of the rapid growth and development of metal oxide nanoparticles is the EPA Basic Program. EPA invited manufacturers, processors, importers, and users of chemical nanoscaled materials to

voluntarily submit existing information on these compounds in order to improve the knowledge about physical and chemical properties, hazard, exposure, use, and risk management practices (NMSPI-Report 2009). About 106 submissions of new products have been received by September 2008: 25% of these requests were metal nanoxides and the major part of them consists in commercial products as shown in the figure below.

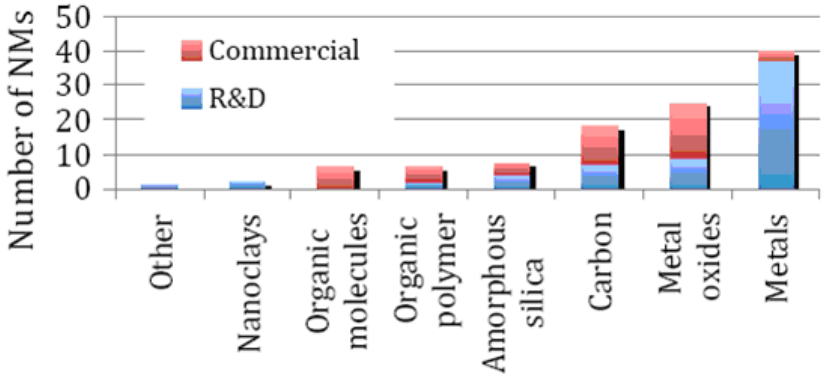

Fig. 3 Submissions of the nanoscale materials (NMs) in the NMSP grouped by chemical category (NMSPI-Report 2009).

1.3.3 Environmental concentrations of MONs and exposure scenarios

Data relative to the environmental concentrations of metal oxide nanoparticles are actually lacking. The reasons of the little knowledge in this field depend on the gaps in the monitoring systems which, at present, do not allow a realistic identification and quantification of ENPs in the environmental compartments. Accordingly, a description or even a realistic prediction of the exposure levels for the biological systems is not yet possible.

Instrumentation normally used to characterize particulate matter is often inadequate to quantify trace concentrations of nanoparticles because of their small size and the negligible mass. Moreover it is experimentally difficult to

distinguish particles of interest from the natural background even an when using expensive multidisciplinary approaches with TEM, SEM, ICP OES, ICP-MS, EDX techniques (Peralta-Videa et al., 2011).

So, when real exposure data are not available, predictive models are used. In this case the extent of the starting production volume, the phases of the NP-life cycle considered (synthesis/handling of pristine NP_i and/or fate of NP_i-containing products) and the possible transformations occurring in the environment are some of the main variables which can affect these predictions. Moreover the calculated concentrations are often referred to a limited area (local, regional scale), making difficult to compare the different predicted scenarios. Considering $nTiO_2$ as a representative MON produced in industrial quantity, in literature different estimates of predicted environmental concentrations (PECs) can be found, depending on the modelling approach used. For example Gottschalk et al. (2009) calculated environmental concentrations of this substance basing on a probabilistic material flow analysis which considered only the life-cycle perspective of TiO_2 containing products. By their model they calculated a concentration of 21 ng/L for surface waters, of 4 μg/L for sewage treatment effluents and of 3–16 μg/l in treated wastewater (Gottschalk et al., 2009).

In another study Mueller and Nowack (2008) estimated an expected concentration for the water compartment ranging from 0.7–16 to μg/L, and ranging from 0,0015 to 0,042 $\mu g/m^3$ for air. These predictions were made considering both a realistic and high exposure scenario on the regional scale of Switzerland.

Anyway, because existing data are very limited to few scenarios and often they derived from extrapolations, it has been hypothesized that environmental concentrations of MONs (and generally NPs) have been underestimated if we consider the exponential increase in their production.

Furthermore in each scenario it has been considered an homogeneous distribution of nanoparticles which cannot reflect a realistic situation.

1.3.3.4 Environmental hazard

Since metal oxides are widely use for antimicrobial purposes and environmental remediation it is likely that also natural ecosystems are potential targets of these substances. Often the antimicrobial concentrations investigated are very high (100÷5000 mg/L) (Adams et al., 2006; Ren et al., 2009) thus they pose serious risks for a potential contamination.

Water is considered as the main sink where the most part of contaminants tend to accumulate. In this compartment the fate of MONs and the potential interactions with aquatic organisms depend on a series of variables. Aggregation, degradation, solubilization, photoactivation of these compounds are some of the main processes which can modify the behaviour of pristine metal oxides in water as well as in soil. Soil and sediments are more complex matrices so it is still difficult to determine the concentration of NPs in these ecosystems. Moreover there is a large background of nanoparticles, such as iron oxide, so it is difficult to differentiate the natural and manufactured NPs in soil. Finally it has been demonstrated that also the presence (concentration) of organic matter modifies the bioavailability of these compounds (Peralta-Videa et al., 2011).

At present, only few studies have been performed on the environmental hazard posed by metal nanoxides, but their number is rapidly growing. They considered organisms ranging from bacteria to aquatic vertebrates and terrestrial invertebrates (nematodes). Bacteria and algae, followed by organisms as *Daphnia* and Cyclops, represented the first step in the evaluation of the potential biomagnification of MONs through the food chain (Peralta Videa et al., 2011). On the basis of the current knowledge the LC50 estimated for aquatic invertebrates spanned over three orders of magnitude (Blaise et al., 2008). Considering aquatic vertebrates, fishes as

Danio rerio or *Oncorhynchus mykiss* were used for the assessment of metal oxide nanoparticle toxicity.

Preliminary researches on hazard for terrestrial organisms (*Caenorhabditis elegans*) demonstrated that nZnO, nAl_2O_3, and $nTiO_2$ affected the growth and reproduction capability of this nematode.

In some of these cases toxicity of the particles where tested in parallel to the bulk form or correspondent cation in order to address the observed effects to solubilization of particles (Blinova et al., 2010). Anyway the key role of the particles themselves was often highlighted.

1.3.3.5 Human safety

Indoor

Occupational exposure may represent a serious scenario for a direct contact with MONs and involve both the industrial scale and the research scale such as university laboratories.

In this case the main exposure routes are represented by inhalation and dermal contact which can occur in all phases of the manufacturing process. Firstly investigations about monitoring of occupational worker revealed that human exposure to engineered nanomaterials by inhalation is very limited during production (Luther 2004) but there are several concerns about safety of the other phases of the commercialization process such as powder handling, packaging and manufacturing of MON –based products.

The extent of particle release during these stages depends on many variables including work practices, type and quantity of the material handled, environmental conditions and the adequacy of the system exhaust (Kaluza et al., 2010).

Outdoor

Although metal nanoxides represent a negligible fraction in mass of the total atmospheric aerosol there are several possibilities to come in contact with these materials during their whole life cycle as shown in Fig.4. Their wide diffusion in fact determines a variety of exposure scenarios for both nanopowder themselves and derived consumer products. For this reason the potential involvement of human populations and other living systems to the uncontrolled release of MONs from application of these materials is cause of several concerns (Rice et al., 2009). Environmental release of metal oxide nanoparticles can derive from intentional emissions (i.e antimicrobial applications, remediation processes) or unintentional sources such as spillage, degradation of MON-based devices, disposal waste of consumer products. Moreover for some metal nanoxides the removal procedures used during incineration or wastewater treatment are not sufficient to destroy them, so they will persist (Gottschalk et al., 2011). An example of persistent compound is titanium dioxide that it was predicted to accumulate in the highest concentrations at orders of magnitude larger than any other NPs (Gottschalk et al., 2009).

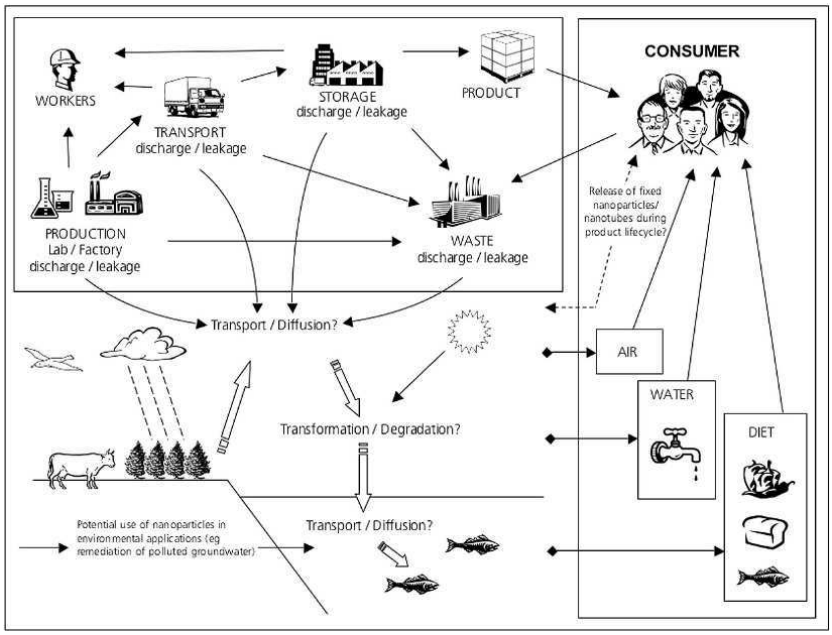

Fig. 4. Some possible exposure routes for nanoparticles and nanotubes based on current and potential future applications. Human exposure can theoretically occur indoor (production phases) or outdoor during transport, use and discharge of nanoparticles and nanostructured materials. MON used for environmental remediation can distributed in soil, water and to contaminate air, water and food (R.S. & R.A. Eng. 2004 - Final report).

Deliberated exposure

Finally we must consider the personal exposure to MON due to the use of personal care products and cosmetics in which MON are the main component. This aspect represent today a big concern for both human and environmental safety because the large use of metal nanoxides in sunscreens and medical or cosmetic purposes. A clear example of the extent of this aspect comes from Australia where it has been estimated that there are more than 300 registered sunscreen products containing nanoscaled titanium dioxide (Mueller and Nowak 2008).

Anyway the few data available about indoor or outdoor concentrations of MONs are hardly comparable because they are often obtained with different measuring systems and expressed with a different metrology. So it is difficult to get a good overall picture of the potential exposure resulting from activities related to metal oxide nanoparticles and an estimate of the potential for worker exposure has been defined actually as not possible (Brouwer et al., 2011).

1.4 Regulation: state of the art

At the moment no specific discipline completely dedicate to production, use and commercialization of metal nanoxides (as for any other nanoparticles) does exist. It means that the reference discipline is based on the general existing laws for chemicals and their applications to which nanoxides (NPs) can be ascribed. The following considerations are made taking into account the European scenario.

With regard to occupational exposure, the references are represented by the EU Directive 89/391/EEC and the Council Directive 98/24/EC (which regulate specifically the production of chemical substances). In order to prevent human risk deriving for use of commercial products-containing nanoxides it must be adopted the existing discipline for the specific commercial category to which belong the compound. Where not possible it must be applied the General Product Safety Directive (Directive 2001/95/EC). If the metal oxide containing-product is used for antimicrobial applications we must refer to the Directive 98/8/EC for biocidal compounds. For environmental pollution (atmospheric, aquatic contaminations, waste management) the Seveso II Directive (96/82/EC), the The Water Framework Directive (2000/60/EC) and the 2006/12/EC pose the basis for the respective evaluations. When necessary there is the possibility to include water or

waste in the “List of the priority substances” or “List of hazardous waste” if the hazardous properties of the contained nanomaterial are testified.

Anyway the European commission, in the “Regulatory Aspects of Nanomaterials”, recently assessed that both nanoparticles themselves and NPs containing products must satisfy REACH (Registration, Evaluation, Authorization and restriction of Chemicals) criteria, since they can be generally defined as new substances or existing compounds for new applications (Kaluza et al., 2011). After that, with another communication, EC opened to the possibility to create a specific section of the REACH, specifically dedicated to the NP regulation. This in order to ensure the efficient assessment of manufactured nanomaterials so prevent adverse effects from the use of these materials in the short, medium and long term. The consultations is now opened and the results of the works will be available in the 2012.

Finally, on 2009, also another regulatory body (the Organisation for Economic Co-operation and Development-OECD) elaborated general guidelines for testing nanomaterials, in order to harmonize and uniform the different protocols used (ENV/JM/MONO(2009)21). In another document it listed representative nanoparticles “for inclusion in a set of reference materials to support measurement, toxicology and risk” and these list included also metal oxide nanoparticles such as nTiO_2, nZnO and nSiO_2 (ENV/JM/MONO(2009)20/REV).

References

Adams L.K., Lyon D.Y., Alvarez P.J.J. 2006. Comparative eco-toxicity of nanoscale TiO_2, SiO_2, and ZnO water suspensions. Water research 40, 3527 – 3532.

Blinova I, Ivask A, Heinlaan M, Mortimer M, Kahru A. 2010. Ecotoxicity of nanoparticles of CuO and ZnO in natural water. Environ Pollut 158, 41–47.

Brouwer B. 2010. Exposure to manufactured nanoparticles in different workplaces. Toxicology 269, 120–127.

Buzea C., Pacheco Blandino I.I., Robbie K. 2007. Nanomaterials and nanoparticles: Sources and toxicity. Biointerphases 2, MR17 - MR172.

Council Directive 89/391/EEC of 12 June 1989 on the introduction of measures to encourage improvements in the safety and health of workers at work, Official Journal of the European Communities L, 29.06.1989, pp. 1-8, accessed on 13 November 2008. http:// eurlex. europa. eu/ LexUriServ/ LexUriServ.do?uri=CELEX:31989L0391:EN:HTML

Council Directive 96/82/EC of 9 December 1996 on the control of major-accident hazards involving dangerous substances, Official Journal of the European Communities L 10, 14.1.1997, pp. 13-33, accessed on 13 November 2008. http://eurlex.europa.eu/LexUriServ/LexUriServ.do? uri= CELEX:31996 L0082 :EN:HTML

Council Directive 98/24/EC of 7 April 1998 on the protection of the health and safety of workers from the risks related to chemical agents at work (fourteenth individual Directive within the meaning of Article 16(1) of Directive 89/391/ EEC), Official Journal of the European Communities L 131, 5.5.1998, pp. 11-23, accessed on 13 November 2008. http://eurlex.europa.eu/LexUriServ/ Lex UriServ.do?uri=OJ:L:1998:131:0011:0023:EN:PDF

Council Directive 2000/60/EC of the European Parliament and of the Council of 23 October 2000 establishing a framework for Community action in the field of water policy, Official Journal of the European Communities L 327, 22.12.2000, pp. 1-72, accessed on 13 November 2008. http://eur-lex.europa.eu/LexUriServ / LexUriServ.do?uri=OJ:L:2000:327:0001:0072:EN:PDF

Directive 98/8/EC of the European Parliament and of the Council of 16 February 1998 concerning the placing of biocidal products on the market, Official Journal of the European Communities L 123, 24.4.1998, pp. 1-63, accessed on 13 November 2008. http://eurlex.europa.eu/LexUriServ/ LexUriServ.do?uri =OJ: L:1998:123:0001:0063:EN:PDF

Directive 2001/95/EC of the European Parliament and of the Council of 3 December 2001 on general product safety, Official Journal of the European Communities

L 11, 15.1.2002, pp. 4-17, accessed on 13 November 2008. http://eurlex.europa .eu/LexUriServ/LexUriServ.do? uri=OJ:L:2002:011:0004:0017:EN:PDF

Directive 2006/12/EC of the European Parliament and of the Council of 5 April 2006 on waste, Official Journal of the European Communities L 114, 27.4.2006, pp. 9-21, accessed on 13 November 2008. http://eurlex.europa.eu/ LexUriServ/LexUriServ.do?uri=OJ:L:2006:114:0009:0021:EN:PDF

Dockery D.W., Pope 3rd. C.A., Xu X., Spengler J.D., Ware J.H., Fay M.E., Ferris Jr. B.G., Speizer F.E., 1993. An association between air pollution and mortality in six U.S. cities. N. Engl. J. Med. 329, 1753–1759.

ENV/JM/MONO(2009)21 - ENVIRONMENT DIRECTORATE, JOINT MEETING OF THE CHEMICALS COMMITTEE AND THE WORKING PARTY ON CHEMICALS, PESTICIDES AND BIOTECHNOLOGY - Preliminary Review of OECD Test Guidelines for their Applicability to Manufactured Nanomaterials

ENV/JM/MONO(2009)20/REV - ENVIRONMENT DIRECTORATE JOINT MEETING OF THE CHEMICALS COMMITTEE AND THE WORKING PARTY ON CHEMICALS, PESTICIDES AND BIOTECHNOLOGY - Guidance manual for the testing of manufactured nanomaterials: OECD's sponsorship programme; first revision.

Gottschalk F., Sonderer T., Scholz R.W., Nowack B. 2009. Environ Sci Technol 43, 9216–9222.

Gottschalk F., Nowack B. 2011. The release of engineered nanomaterials to the environment. J. Environ. Monit., 13, 1145.

Heinlaan M., Ivask A., Blinova I., Dubourguier H-C., Kahru A. 2008. Toxicity of nanosized and bulk ZnO, CuO and TiO2 to bacteria Vibrio fischeri and crustaceans Daphnia magna and Thamnocephalus platyurus. Chemosphere 71, 1308–1316.

Huang Y-W., Wu C-H., Aronstam R.S. 2010. Toxicity of transition metals oxide nanoparticles: recent insights from *in vitro* studies. Materials 3, 4842-4859.

Hurst S.J., Fry H.C., Gosztola D.J., Rajh T. 2011. Utilizing Chemical Raman Enhancement: A Route for Metal Oxide Support-Based Biodetection. J. Phys. Chem. C 115, 620-630.

ISO / TS 276872 2008 "Nanotechnology - terminology and definitions for the “nano-objects", i.e. Nanoparticle, nanofiber and nanoplate".

Kahru A, Dubourguier H-C. 2010. From ecotoxicology to nanoecotoxicology. Toxicology 269, 105–119.

Kaluza S., Balderhaar J.K., Orthen B., Honnert B., Jankowska E., Pietrowski P., Rosell M.G., Tabarro C., Tejedor J, Zugasti A. 2010. Workplace exposure to nanoparticles. European Agency for Safety and Health at Work (EU-OSHA), Spain.

Kamat P.V. 2002. Photophysical, photochemical and photocatalytic aspects of metal nanoparticles. J Phys Chem B, 106, 7729-7744.

Kessler R. 2011. Engineered Nanoparticles in Consumer Products - Understanding a new ingredient. Environmental Health Perspectives 119, A121-A125.

Konczol M., Ebeling S., Goldenberg E., Treude F., Gminski R., Giere R., Grobety B., Rothen-Rutishauser B., Merfort I., Mersch-Sundermann V. 2011. Cytotoxicity and Genotoxicity of Size-Fractionated Iron Oxide (Magnetite) in A549 Human Lung Epithelial Cells: Role of ROS, JNK, and NF-jB. Chem. Res. Toxicol. dx.doi.org/10.1021/tx200051s

Landsiedel R., Ma-Hock L., Kroll A., Hahn D., Schnekenburger J., Wiench K., Wohlleben W. 2010. Testing Metal-Oxide Nanomaterials for Human Safety. Adv. Mater. 22, 2601–2627.

Li N., Hao M., Phalen R.F., Hinds W.C., Nel A.E. 2003. Particulate air pollutants and asthma. A paradigm for the role of oxidative stress in PM-induced adverse health effects. Clin. Immunol. 109, 250–265.

Luther W. 2004 Technological analysis - Industrial applications of nanomaterials – chances and risks.

Marquis B.J., Love S.A., Braun K.L., Haynes C.L. 2009. Analytical methods to assess nanoparticle toxicity. Analyst, 2009, 134, 425–439.

Mueller N., Nowack B. 2008. Exposure Modeling of Engineered Nanoparticles in the Environment. Environ. Sci. Technol. 42, 4447–4453

nano.DE-Report 2009: Status Quo of Nanotechnology in Germany. Federal Ministry of Education and Research.

Nanoscale Materials Stewardship Program Interim Report - U.S. Environmental Protection Agency Office of Pollution Prevention and Toxics. January 2009.

Nel A.E., Xia T., Madler L., Li N. 2006. Toxic potential of materials at the nanolevel. Science 311, 622–627.

Nel A.E., Xia T., Madler L., Li N. 2006. Toxic potential of materials at the nanolevel. Science 311, 622–627.

Oberdörster G., Oberdörster E., Oberdörster J., 2005, Nanotoxicology: An Emerging Discipline Evolving from Studies of Ultrafine Particles, Environ. Health Persp. 113, 823-839.

Ostiguy C., Roberge B., Woods C., Soucy B. 2009. Engineered Nanoparticles: Current Knowledge about OHS Risks and Prevention Measures. REPORT R-656.

Peralta-Videa J.R., Zhao L., Lopez-Moreno M.L., de la Rosa G., Hong J., Gardea-Torresdey J.L. 2011. Nanomaterials and the environment: A review for the biennium 2008–2010. Journal of Hazardous Materials 186, 1–15.

Pope C.A., Burnett R.T., Thun M.J., Calle E.E., Krewski D., Ito K., Thurston G.D., 2002. Lung cancer, cardiopulmonary mortality, and long-term exposure to fine particulate air pollution. JAMA 287, 1132–1141.

Reijnders, L., 2006. Cleaner nanotechnology and hazard reduction of manufactured nanoparticles. J. Cleaner Prod. 14, 124–133.

Ren G., D. Hu, Cheng E.W.C., Vargas-Reus M. A., Reip P., Allaker R. P. 2009. Characterisation of copper oxide nanoparticles for antimicrobial applications. International Journal of Antimicrobial Agents 33, 587–590.

Rice R.H., Vidrio E.A., Kumfer B.M., Qin Q., Willits N.H. Kennedy I.M., Anastasio C. 2009. Generation of oxidant response to copper and iron nanoparticles and salts: Stimulation by ascorbate. Chemico-Biological Interactions 181, 359–365.

SCENIHR/002/05. The appropriateness of existing methodologies to assess the potential risks associated with engineered and adventitious products of nanotechnologies.

Stamate M., Lazar G. 2007. Application of titanium dioxide photocatalysis to create self-cleaning materials. Romanian technical sciences academy.

The Royal Society & The Royal Academy of Engineering. Nanoscience and nanotechnologies: opportunities and uncertainties. Final report. Nanoscience and nanotechnologies. 2004.

Vippola M., Falck G.C.M., Lindberg H.K. Suhonen S., Vanhala S., Norppa H., Savolainen K., Tossavainen A., Tuomi T. 2009. Preparation of nanoparticle dispersions for in-vitro toxicity testing. Human & Experimental Toxicology 28, 377–385.

WHO (2003) Health Aspects of Air Pollution with Particulate Matter, Ozone and Nitrogen Dioxide, Report on a WHO Working Group, Bonn, Germany.

Wigginton N.S., Haus K.L., Hochella M.F. 2007. J. Environ. Monit. 9, 1306.

CHAPTER 2

Approaching the toxicity of three relevant metal oxide nanoparticles: TiO_2, ZnO and CuO

2.1 Abstract

At the present, the few studies focused on toxicity metal oxide nanoparticles consider different *in vivo* and *in vitro* models to test the potentiality of these materials. With regard to the environmental toxicity in this work we have addressed the attention to the aquatic ecosystem by the use of FETAX assay (Frog Embryo Teratogenesis Assay – *Xenopus)*, a sensitive test which allows to investigate the embryotoxic effects induced by commercial metal nanoxides (nCuO, $nTiO_2$ and nZnO). At the end of the test the main end points of growth retardation, mortality, absolute and relative frequency of malformations have been analysed.

In parallel another critical aspect related to MONs diffusion has been analysed by the evaluation of the potential toxicity to the human respiratory apparatus. Biological effects induced by $nTiO_2$ and nCuO were investigated on the epithelial alveolar cell line (A549), an *in vitro* model for NPs inhalation. Different techniques able to characterize the main end points of cytotoxicity, internalization mechanisms, oxidative stress potential, mitochondrial and lysosomal perturbation, cell cycle alteration have been used. In particular low concentrations of particles for mechanicistic studies and the early events produced by particle exposure

have been evaluated

Keywords: *Xenopus laevis*, aquatic ecotoxicity, respiratory toxicity, A549.

2.2 Introduction

Among the transition metal oxides, titanium dioxide, zinc oxide and cupric oxide have received particular attention due to their unique physical and chemical properties (Huang et al., 2010) and their environmental and economical relevance.

Titanium dioxide exist in three different crystal structures (i.e. anatase, rutile and brookite) and is used as main ingredient in cosmetics products and sunscreens. Since $nTiO_2$ is widely used as whitening pigment in exterior paints (e.g. for house façades) or as biocide, thanks to its photoactivating properties (Kaegi et al., 2008), it may pose serious risks after environmental release. $nTiO_2$ is expected to be found in the highest concentrations in the environment, thus it is retained the most promising nano-pollutants. First (eco)toxicological data about adverse effects on aquatic organism and cell lines suggest different potential hazards coming from $nTiO_2$, depending on the crystalline form investigated (Aruoja et al., 2009; Hund-Rinke and Simon 2006).

Cosmetics (and suncreens) excluded, zinc oxide is widely studied also as antimicrobial agent in coated textiles. This kind of application rise concerns for aquatic environment, that can be endangered by the leaking NPs and/or metal ions, as well as for human safety that may be potentially harmed by the contact with functionalized textiles.

Copper oxide (CuO) is currently developed in the nanoscaled form to be used as catalyst for NO abatement, methanol synthesis and gas sensors or element for the implementation of high-critical-temperature superconductors. It is also diffuse as pigment in ceramics, additive for inks and antimicrobial agent (Huang et al., 2010).

All these particles are currently available in different size and the same oxide can be obtained from different synthesis processes as previously reported in

Chapter1. For the purposes of this study we consider commercial forms of TiO_2, ZnO and CuO nanopowders obtained from the same distributor (Sigma-Aldrich).

In particular, after a preliminary chemical-physical characterization, these materials were investigated on two different models representative of *in vivo* and *in vitro* systems respectively. We used *Xenopus laevis* for the *in vivo* aquatic toxicity screening while human lung epithelial cell line A549 was investigated for the *in vitro* respiratory toxicity studies.

2.3 Aquatic toxicity

Although the aquatic ecosystems likely represent a sink for most metal oxides, data demonstrating the effects of $nTiO_2$, nZnO and nCuO on aquatic vertebrates remain scarce. The African amphibian *Xenopus laevis* was frequently used for testing chemicals with the standardized procedure FETAX (Frog Embryo Teratogenesis Assay-*Xenopus*) (Bantle and Dawson 1988), but its application as model for nanotoxicological purposes is still rather scarce (Bacchetta et al., 2011). This kind of test allow to investigate the potential embryotoxicity of chemical compounds in the first stage of the amphibian (0-96h) by monitoring, day by day, the correct development of the embryos. At the end of the test the main endpoints (mortality, malformations and growth retardation) induced by the tested substance can be evaluated. The FETAX assay provides a large number of embryos useful to perform a solid statistical analysis and allows the calculation of the lethal and teratogenic concentrations (e.g. LC50 and TC50). A teratogenic index (TI) can also be derived to establish if the tested compound is (or not) an effective teratogen agent.

Specific terata are evaluated by the screening of the gross malformations throughout the whole embryo. Below, a short description of the main

categories of detectable malformations is reported according to (Bantle et al., 1998).

Axial malformations/shortening: they are represented by an altered curvature of the axis which determine a dorsal, ventral or lateral flexure of the tail. Sometime this malformation can affect also the head development and the correct gut coiling.

Edema: it is a pathologic condition which involve regional or somatic areas. It is characterized by formation of swollen and transparent areas fluid-filled or by comparison of epidermal blisters.

Eyes abnormalities: this category includes a series of conditions such as microophtalmia (mono/bi-lateral), altered choroid fissure closure, altered development of the optic cup and uncorrected localization of the lens. Sometimes eyes can show inappropriate pigmentation.

Extreme head abnormalities: in this case the malformation lead to an altered development of the brain. It means that it can be partially or totally lacking. This is usually accompanied by other severe malformations.

Head and facial malformations: embryo affected by this kind of malformation can show shape and size alterations of head and facial structures. Further also the distances among the facial structures (e.g. eyes and nares,) and their position are not kept.

Heart malformations: sometimes, as result of toxicant exposure, the heart can develop as an amorphous mass or showing an altered coiling of the tubes.

Gut abnormalities: they are referred to a partially o completely lacking of gut coiling. Gut can appear as a simple straight tube without any coiling. Sometimes they are accompanied with abdominal edema.

In addition to the screening of the external malformations, more detailed histopathological analyses can allow researchers to identify specific lesions to embryo organs and tissues. In particular, in this work, we associated chemical and biochemical evaluations to advanced microscopic analyses in order to better understand the effects observed and to define the potential targets of the MONs investigated at tissutal and cellular levels. To detect the presence of the particles inside the tissues confocal laser scanning microscopy was used in reflection mode on histological sections. Transmission electron microscopy was applied in bright field to investigate the ultrastructure of the organs mainly affected by the exposure to $nTiO_2$, nZnO and nCuO. Then Electron Spectroscopic Imaging (ESI) analysis was used to track NPs in fixed tissues, by mapping the distribution of the NP-constituting elements (Ti, Zn, Cu). When possible, Electron Energy Loss spectra were obtained in specific subcellular area. Biochemical procedures were applied to investigate metabolic alterations (in particular oxidative damages, i.e lipid peroxidation) induced by metal oxides (data included in the Supporting Information- PART I).

2.4 Respiratory toxicity

Becker et al. (2011) defined inhalation as the most critical route for human exposure to airborne nanoparticulate. Preliminary studies on the toxicity of metal oxide nanoparticles also confirmed the respiratory system as the most sensitive target, while human skin appeared to be an efficient barrier (Landsiedel et al., 2010; Kaluza et al., 2010). The main factors affecting the

inhalation toxicology of metal nanoxides are related to their size. The distribution of inhaled particles in the respiratory tree varies greatly as a function of particle or aggregate granulometry. Basing on classical particle deposition model, objects measuring one nm cannot reach the pulmonary alveoli so they are probably deposited in the upper regions of the lungs as well large agglomerates. Particles smaller than 5nm are deposited relatively evenly in the nose and pharynx, while more than 50% of nanoparticles measuring 20 nm can reach and be deposited in the alveoli (Ostiguy et al., 2009) as shown in (Fig.1).

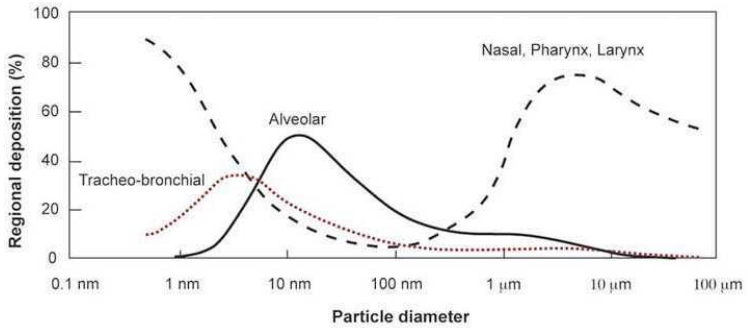

Fig. 1. Distribution of inhaled particles in the respiratory tree (Buzea et al., 2007). Most of the particles measuring 20nm can reach the alveolar region.

Once reached the alveolar space, NPs can by-pass the macrophagic clearance, overwhelm the air-blood barrier and translocate to other districts of the organism, where they might exert additional toxicity (Oberdoster 2005). To investigate *in vitro* human respiratory toxicity different cell lines were used (A549, BEAS-2B, HEp-2 etc.) and the main end points investigated in order to explain the adverse effects induced by MONs generally are:

- cellular uptake
- oxidative stress
- DNA damage
- cell cycle (alteration)

Below a short description of these processes is presented.

2.4.1 Cellular uptake

Depending on agglomeration state, shape and surface charge, nanoparticles can enter into the cell by different mechanisms. When considering the size of particles and their aggregates, macropynocytosis and phagocytosis are described as the most probable mechanisms of TiO_2 uptake in exposed cells (Barillet et al., 2010), while pynocytosis is involved in the internalization of very small objects.

In literature different explanations for the sequence of events characterising the fate of endocytic vesicles can be found, but their maturation from early to late endosomes after clathrin mediated endocytosis (CME) seems to be one the preferential route for NPs to reach lysosomes (Fig.2).

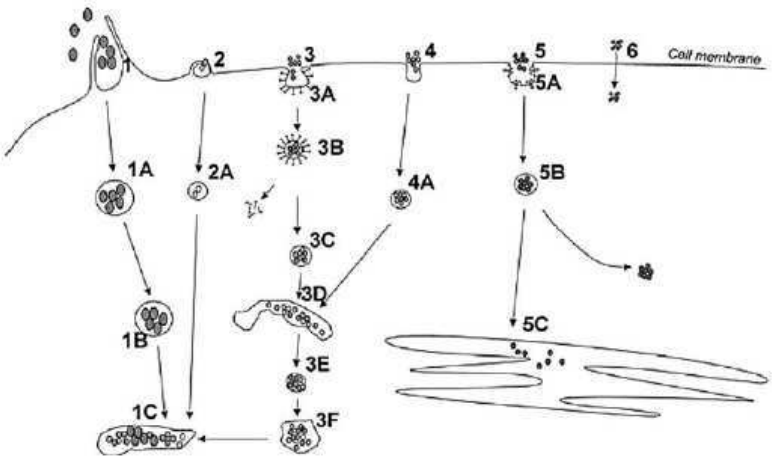

Fig. 2. **M**echanisms for the uptake of nanoparticles by the cells: (1) phagocytosis, (2) macropinocytosis, (3) clathrin-mediated endocytosis, (4) non-clathrin, non-caveolae mediated endocytosis, (5) caveolae-mediated endocytosis, (6) diffusion (Unfried et al., 2007).

Also the z-potential can affect the internalization route (Patil et al., 2007; Gratton et al., 2008). It is well known that plasma membranes (PM) are negatively charged. This determines that cationic nanoparticles interact with PM and are internalized by cells much more easily than negatively-charged ones. Nevertheless it has been found some evidence of massive internalization of negatively-charged NPs. This event could be due to 1) formation of nanoparticle clusters near the few PM cationic domains; 2) non specific processes of adsorption on the cell membrane which reduce the charge density of the NP and may favour the internalization of single nanoparticles (Wilhelm et al., 2003); 3) nano-scale surface roughness which minimizes repulsive interactions promoting adhesion and internalization (Nel et al., 2009).

Since the presence of free nanoparticles in the cytoplasm has been documented, the occurring of adhesive interactions, transport through membrane pores, diffusion or formation of transient holes should be considered as potential mechanisms of particle uptake (Geiser et al., 2005; Unfried et al., 2007; Gratton et al., 2008; Verma et al., 2008).

2.4.2 Oxidative stress

Nanoparticles, especially metal nanoxides, can interact with cell bio-interfaces leading to production of reactive oxygen species (ROS) by different mechanism, thanks to their surface properties and in some case their nature of semiconductors (Fig.3).

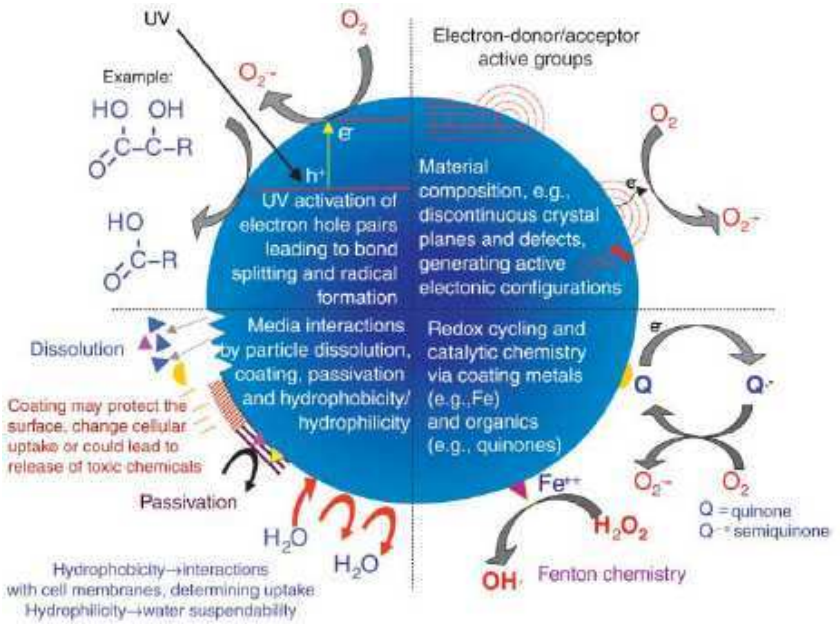

Fig. 3. Possible mechanisms by which nanomaterials, specially metal-containing NPs, induce free radical formation and interact with biological tissue. Importance of material composition, electronic structure, surface coatings, solubility, and interactions with environmental factors (e.g., UV) are reported (Nel et al., 2006).

Increasing concentrations of free radicals in the cellular environment can promote oxidative stress. This condition is characterised by an unbalance between the presence of oxidant agents and antioxidant intracellular defences. The biological response and the consequences of the oxidative stress change depending on the extent of the oxidative pressure and the cellular components involved as summarised in Fig.4.

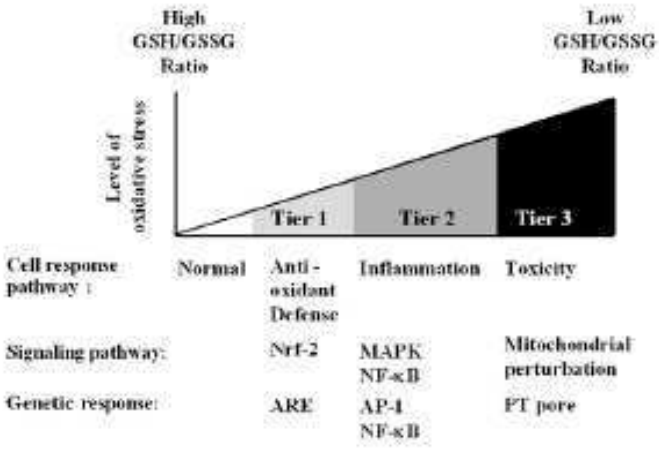

Fig. 4. Hierarchical oxidative stress responses; GSH/GSSG ratio is considered as index of the oxidative pressure. For low level (Tier 1), antioxidant enzymes restore cellular redox homeostasis. At an intermediate level of oxidative stress (Tier 2) proinflammatory responses (e.g., cytokines and chemokines.) are induced. At the higher level of oxidative stress (Tier 3) correspond the perturbation of the mitochondrial permeability transition pore the consequential disruption of electron transfer resulting in cell death (Li et al., 2008).

At cellular level it has been observed that endoplasmic reticulum, plasma membranes an mitochondria are sensitive targets of free radicals.

The consequence of this interactions can determine a cytoplasmic deregulation of Ca^{++} release which may promote cytoskeletal disfunctions, affect the correct microtubules polimerization or activate specific proteases inducing apoptosis (Zong and Thompson 2006).

Lipid peroxidation (LPO) and protein degradation are the two most probable events mediated by oxidative stress. The process of lipid peroxidation, catalysed by iron and copper ions, lead to formation of peroxyl radicals (ROO•) from unsatured fatty acids, after reaction with an hydroxyl radical. Once formed, peroxyl radicals tend to rearrange by a cyclisation reaction and this process results in formation of malondialdehyde (MDA) and its

precursors. Then MDA can react with DNA bases to form DNA adducts (Marnett 1999). Moreover has been found that copper-induced LPO can promote an increase in the levels of a signalling molecule HNE which acts as a second messenger in phosphorylation and activation of the c-Jun N-terminal kinase/stress-activated protein kinase and p38 pathways (Jomova et al., 2011). As consequence of the oxidative stress also respiration, oxidative phosphorylation and the correct folding of the proteins could may be impaired.

2.4.3 DNA damage

The overproduction of free radicals can be responsible also for DNA (nuclear and mitochondrial) damages by initiation of mutations, DNA strand breaks or nucleotide oxidation. The cell can adopt different mechanisms to react to the insult, for example by activating a DNA repair action mediate by cycle check points, or by activating of excision repair mechanisms. Another possible response to ROS induce DNA damage involves the activation of p53 pathway which promote apoptosis or cell cycle arrest (Ahamed et al., 2010).

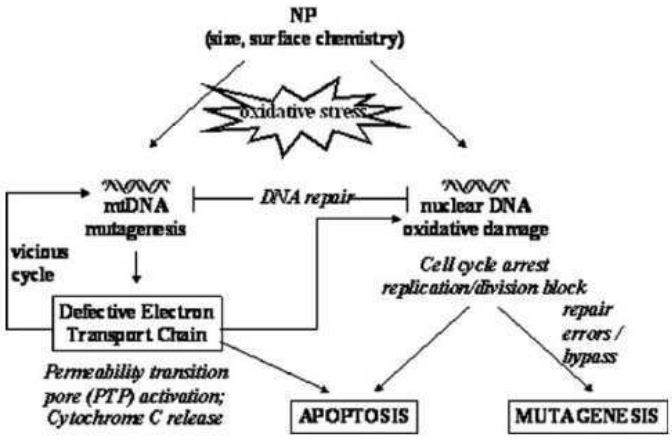

Fig. 5. Effect of nanoparticle-induced oxidative stress on the mitochondrial and nuclear DNA and potential consequences (Unfried et al., 2007).

2.4.4 Cell cycle

Cell cycle summarizes the sequence of events which lead to growth, DNA replication and cell division (Fig.4). It is generally represented by four different phases: Mitosis and G1, S, G2 phases which constitute the interphase. During mitosis the nuclear and cellular division physically occur. During interphase the cell growths (G1,G2) and duplicates its genome (S).

The cell cycle progression is controlled by a complex system of regulatory proteins with own specific function during a specific phase. They promote or inhibit the normal progression depending on the surrounding conditions. So the beginning of one phase is subject to the correct course of the previous stage. This strategy has been developed by cell to reduce the probability to transfer DNA modifications to the daughter cells and so to guarantee their growth in favorable conditions. Presence of toxicants, stressful conditions or other disturbing agents like nanoparticles can alter the normal progression of cell cycle by DNA damages or intracellular homeostasis alteration leading to cell cycle arrest. When the recovery is not possible cells may exit the cell cycle (G0 phase) or undergo to apoptosis (Martinenaite et al., 2011).

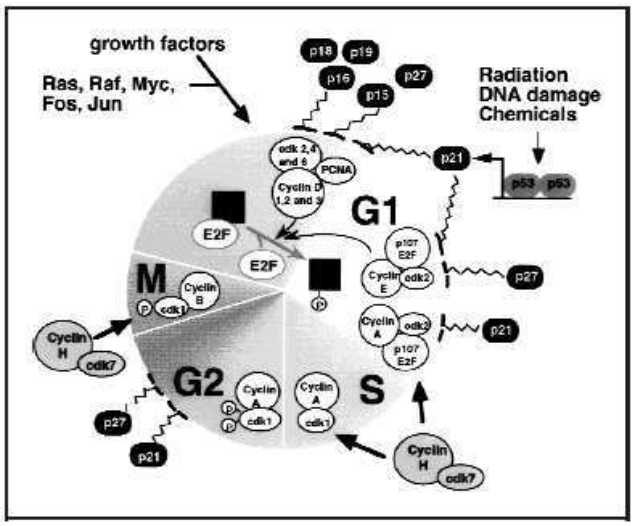

Fig. 6. Representative sequence of cell cycle phases and their regulation (Senderowitch et al., 2000).

Previous studies on the respiratory toxicity of nCuO and nZnO demonstrated the very high toxic potential of these MONs in human cell lines, often coupled with genotoxic effects (Sharma et al., 2009; Ahmed et al., 2010; Petersen et al., 2010) but the mechanisms occurring at the biointerfaces are not well clarified.

The three main studies focused on the toxicity of nCuO (Karlsson et al., 2008; 2009; Fahmy et al., 2009) agree to indicate the oxidative stress as mainly cause of cytotoxicity. Effects such as mitochondrial depolarization and oxidative DNA damage were observed after prolonged exposure times (16h) or after administration of very high exposure concentrations of particles (80μg/ml) respectively. Although these findings were attributed to the nanoparticle rather the ionic component dissolved is not completely clear wheter the internalization is a prerogative for the cyto/genoxicity and what is exactly the extent of its contribute to these effects.

To study the mechanisms of action of nCuO, we used lower concentrations of nanoparticles (10μg/ml = 2,6μg/cm^2) than those reported in literature, focusing our observations on the early stages of exposure. Further we investigated the main events proposed to explain the oxidative stress generation (extracellular vs lysosomal release of copper ions and mitochondrial damage) in order to understand the extent of these phenomena and the hierarchical sequence in promoting of cell death. Finally different microscopic techniques were used to characterize the cellular targets of the tested nanoxides and to verify their potential ability to deeply penetrate inside the cell (e.g. nuclei) both by endocytic process as well as free nanoparticles.

Numerous *in vitro* studies have demonstrated oxidative damage to DNA induced by $nTiO_2$; these findings were attributed to the photocatalytic properties of this MON as well as the crystalline form (Petersen et al., 2011).

In our study we investigated a commercial mixture of anatase and rutile to verify the ability of this formulation to induce cytotoxicity in A549 cells. Then we used different microscopic techniques to characterize the particle uptake and to verify the integrity of the cellular ultrastructure after the exposure to these nanoparticles.

References

Aruoja V., Dubourguier H-C., Kasemets K., Kahru A. 2009. Toxicity of nanoparticles of CuO, ZnO and TiO_2 to microalgae *Pseudokirchneriella subcapitata*. Sci Tot Environ 407, 1461–1468.

Bacchetta R., Santo N., Fascio U., Moschini E., Freddi S., Chirico G., Camatini M. & Mantecca P. 2011. Nano-sized CuO, TiO_2 and ZnO affect Xenopus laevis development. Nanotoxicology, 1–18.

Bantle J.A., Dawson D.A., 1988. In: Adams WJ, Chapman GA, Landis WF, editors. Aquatic Toxicology and Hazard Assessment, ASTM STP 971. ASTM, Philadelphia, PA, p 316.

Bantle J.A., Dumont J.N., Finch R.A., Linder G. 1998. Atlas of abnormalities: A guide for the performance of FETAX. Second Ed. OSU Press, Stillwater, OK.

Barillet S., Jugana M.-L., Laye M., Leconte Y., Herlin-Boime N., Reynaud C., Carrière M. 2010. I*n vitro* evaluation of SiC nanoparticles impact on A549 pulmonary cells: Cyto-,genotoxicity and oxidative stress. Toxicology Letters 198, 324–330.

Becker H., Herzberg F., Schulte A., Kolossa-Gehringa M. 2011. The carcinogenic potential of nanomaterials, their release from products and options for regulating them. International Journal of Hygiene and Environmental Health 214, 231– 238

Gratton S.E., Ropp P.A., Pohlhaus P.D., Luft J.C., Madden V.J., Napier M.E., Desimone J.M. 2008.

The effect of particle design on cellular internalization pathways. Proc Natl Acad Sci USA 105, 11613–11618.

Geiser M., Rothen-Rutishauser B., Kapp N., Schurch S., Kreyling W., Schulz H., Semmler M., Im Hof V., Heyder J., Gehr P. 2005. Ultrafine particles cross

cellular membranes by nonphagocytic mechanisms in lungs and in cultured cells. Environ. Health Perspect. 113, 1555–1560.

Huang Y-W., Wu C-H., Aronstam R.S. 2010. Toxicity of transition metals oxide nanoparticles: recent insights from *in vitro* studies. Materials 3, 4842-4859.

Hund-Rinke K., Simon M. 2006. Ecotoxic effect of photocatalytic active nanoparticles TiO_2 on algae and daphnids. Environ Sci Pollut Res 13, 225–32.

Jomova K., Valko M. 2011. Advances in metal-induced oxidative stress and human disease. Toxicology 283, 65–87.

Kaegi R., Ulrich A., Sinnet B., Vonbank R., Wichser A., Zuleeg S., Simmler H., Brunner S., Vonmont H., Burkhardt M., Boller M. 2008. Synthetic TiO_2 nanoparticle emission from exterior facades into the aquatic environment. Environmental Pollution 156, 233–239.

Kaluza S., Balderhaar J.K., Orthen B., Honnert B., Jankowska E., Pietrowski P., Rosell M.G., Tabarro C., Tejedor J, Zugasti A. 2010. Workplace exposure to nanoparticles. European Agency for Safety and Health at Work (EU-OSHA), Spain.

Landsiedel R., Ma-Hock L., Kroll A., Hahn D., Schnekenburger J., Wiench K., Wohlleben W. 2010. Testing Metal-Oxide Nanomaterials for Human Safety. Adv. Mater. 22, 2601–2627

Martinenaite E., Tavenier J., Dabrowska M.E., Bjerregaa H.F. 2010. Nanoparticle-induced cell death. May, 26th 2011. 4thsemester project Final Report.

Nanoscale Materials Stewardship Program Interim Report - U.S. Environmental Protection Agency Office of Pollution Prevention and Toxics. January 2009.

Nel A.E., Mädler L., Velego D., Xia T., Hoek E.M.V, Somasundaran P., Klaessig F., Castranova V., Thompson M. 2009. Understanding biophysicochemical interactions at the nano–bio interface. Nature materials 8, 543-557.

Oberdörster G., Oberdörster E., Oberdörster J., 2005, Nanotoxicology: An Emerging Discipline Evolving from Studies of Ultrafine Particles, Environ. Health Persp. 113, 823-839.

Ostiguy C., Roberge B., Woods C., Soucy B. 2009. Engineered Nanoparticles: Current Knowledge about OHS Risks and Prevention Measures. REPORT R-656.

Petersen E.J., Nelson B.C. 2010. Mechanisms and measurements of nanomaterial-induced oxidative damage to DNA. Anal. Bioanal. Chem. 398, 613–650.

Sharma V., Shukla R.K., Saxena N., Parmar D., Das M., Dhawan A. 2009. DNA damaging potential of zinc oxide nanoparticles in human epidermal cells. *Toxicol Lett* 185, 211-218.

Som C., Wick P., Krug H., Nowack B. 2011. Environmental and health effects of nanomaterials in nanotextiles and façade coatings. Environment International 37, 1131–1142.

Unfried K., Albrecht C., Klotz L-O., Von Mikecz A., Grether-Beck S., Schins Roel P.F. .2007. Cellular responses to nanoparticles: Target structures and mechanisms,. Nanotoxicology 1, 52-71.

Verma A., Uzun O., Hu Y., Hu Y., Han H-S., Watson N., Chen S., Irvine D.J., Stellaci F. 2008.

Surface-structure-regulated cell-membrane penetration by monolayer-protected nanoparticles. Nature Materials 7, 588-59.

Wilhelm C., Billotey C., Roger J., Pons J.N., Bacri J-C., Gazeau F. 2003. Intracellular uptake of anionic superparamagnetic nanoparticles as a function of their surface coating. Biomaterials 24,
1001–11.

Zong W.X., Thompson C.B. 2006. Necrotic death as a cell fate. Genes & Development 20, 1-15.

CHAPTER 3

Nano-sized CuO, TiO_2 and ZnO affect *Xenopus laevis* development

Renato Bacchetta[1], Nadia Santo[2], Umberto Fascio[2], Elisa Moschini[3], Stefano Freddi[4], Giuseppe Chirico[4], Marina Camatini[3], Paride Mantecca[3]

[1] Department of Biology, University of Milano, Milan, Italy, [2] Interdepartmental Centre of Advanced Microscopy (CIMA), University of Milano, Milan, Italy, [3] Department of Environmental Science, Research Centre POLARIS, University of Milano-Bicocca, Milan, Italy, and [4] Department of Physics, Research Centre POLARIS, University of Milano-Bicocca, Milan, Italy.

3.1 Abstract

The teratogenic potential of commercially available CuO, TiO_2 and ZnO nanoparticles (NPs) was evaluated using the standardized FETAX test. After characterization of NP suspensions by TEM, DLS and AAS, histopathological screening and advanced confocal and energy-filtered electron microscopy techniques were used to characterize the induced lesions and to track NPs in tissues. Except for nCuO, which was found to be weakly embryolethal only at the highest concentration tested, the NPs did not cause mortality at concentrations up to 500 mg/L. However, they induced significant malformation rates, and the gut was observed to be the main target organ. CuO NPs exhibited the highest teratogenic potential, although no specific terata were observed. ZnO NPs caused the most severe lesions to the intestinal barrier, allowing NPs to reach the underlying tissues. TiO_2 NPs showed mild embryotoxicity, and it is possible that this substance could be associated with hidden biological effects. Ions from dissolved

nCuO contributed greatly to the observed embryotoxic effects, but those from nZnO did not, suggesting that their mechanisms of action may be different.

Keywords: nanoparticles; metal oxides; FETAX; embryotoxicity; environmental risk

Nanotoxicology 2011, 1-18, Early online

3.2 Introduction

Nanotechnology is a field of increasing economic and scientific interest that continues to exhibit rapid development. New nanomaterials (NMs) are being manufactured and promptly used in a variety of applications, including cosmetics and personal care products, electronics, drug delivery systems, manufacturing technologies and paints (Ward and Kach 2009). Nanotechnology has been projected to become a $1 trillion market by 2015 (Nel et al. 2006), with an estimated annual production of approximately 60,000 tons of nanoparticles (NPs) by 2020 (Lewinsky et al. 2008). This represents a market associated with great economic interest, which implies that there will be effects on the environment and, consequently, on humans due to exposure to NPs, for which few toxicity data are available.

The lack of toxicological data available for NMs makes it difficult to predict the real risk associated with exposure to these substances and compels the scientific community to undertake research to guarantee the sustainable development of this recently developed technology. The growing use of NPs in a number of applications in different fields is becoming increasingly worthy of attention from institutional organizations related to their possible effects on public health and ecosystems. During their life cycle, NPs will

enter the environment, and experimental evidence has already shown that exposure to NMs may be associated with an increased risk of certain diseases, not only for aquatic organisms (Federici et al. 2007; Baun et al. 2008; Kasemets et al. 2009; Blinova et al. 2010) but also for humans (Pope et al. 2002; Oberdörster et al. 2005). The behavior of NPs in the environment, as well as their fate remain unclear, and it is well known that their state of aggregation and their consequent settlement to sediments depend on the hydrodynamic properties of freshwater systems (Gregory 2006), making prediction of these phenomena almost unreliable.

Despite this significant gap in our understanding, it is well known that aquatic environments are certainly at risk of exposure to these pollutants, as they represent a sink for most environmental contaminants (Scown et al. 2010). Thus, considering NPs as a new class of hazardous material, we aimed to study the effects of metal oxide-based NPs on the amphibian *Xenopus laevis* using the Frog Embryo Teratogenesis Assay-*Xenopus* (FETAX) test. The three endpoints of this test, i.e., mortality, malformations and growth inhibition, render it a powerful and flexible bioassay for evaluating pollutants in water (Dumont et al. 1983). FETAX can be used for testing single compounds (Bantle and Dawson 1988), as well as the joint actions of more than one compound (Dawson 1991). However, despite the great amount of literature available on the effects of many compounds on the larval development of *X. laevis*, only one report exists that deals with the teratogenic potential of a metal NP on this amphibian (Nations et al. 2011). This report paved the way for the present study, in which we investigated the effects of three different nano-sized metal-oxides (nCuO, $nTiO_2$ and nZnO) on *X. laevis* embryos.

Because the release of ions from metals may be a key factor in their toxicity (Kahru et al. 2008; Kasemets et al. 2009; Blinova et al. 2010), the effects of Cu^{++} and Zn^{++} were also evaluated. Luo et al. (1993) showed that these two metal ions were teratogens for *X. laevis*, and some authors (Franklin et al.

2007; Heilaan et al. 2008; Aruoja et al. 2009; Blinova et al. 2010) have reported that in other animals, the toxicity associated with ZnO and CuO NPs was due to dissolved zinc and copper ions. In contrast, Griffitt et al. (2007; 2009) and Ispas et al. (2009) demonstrated that the effects of Cu and Ni NPs in fish are not simply mediated by dissolution, emphasizing the need for additional research on this topic.

In a review entitled "From Ecotoxicology to Nanoecotoxicology", Kahru and Dubourguier (2010) highlighted the most recent frontiers opened in the field of ecotoxicology by nanotechnology. This paper refers to the new scientific problems introduced by engineered nanoparticles (ENPs) in terms of environmental monitoring and modeling, as well as approaches that are useful to screen for their toxicity. These problems are mainly derived from the peculiar physico-chemical characteristics of the nanoworld, as well as from the unpredictable mechanisms of interaction between nanostructures and biological systems. Due to the complexity of phenomena at the nanolevel and the relatively young age of this discipline, no instruments or methods are currently available to provide standardized measures of environmental ENP concentrations, or even their speciation. The urgent need for standardized approaches for NP hazard identification and evaluation prompted our use of *X. laevis* development as a "nanoecotoxicological model" to screen the embryotoxic and teratogenic potential of NPs in a freshwater environment. Using histopathology and advanced confocal and transmission electron microscopy, we focus on the crucial topic of bridging the standard outputs of such toxicity tests with the mode of NP-tissue interaction and internalization.

3.3 Materials and methods

3.3.1 Chemicals and NPs used

All analytical grade reagents, human chorionic gonadotropin (HCG), 3-amino-benzoic acid ethyl ester (MS222), salts for FETAX solutions, $CuSO_4 \cdot 5\ H_2O$, $ZnSO_4$ and metal oxide NPs were purchased from Sigma-Aldrich S.r.l., Italy. The advertised sizes of these particles were <50 nm for nCuO (#544868) and <100 nm for $nTiO_2$ and nZnO (#677469 and #544906, respectively). All suspensions and stock solutions were prepared in FETAX solution with a composition (in mg/L) of 625 NaCl, 96 $NaHCO_3$, 30 KCl, 15 $CaCl_2$, 60 $CaSO_4 \cdot 2H_2O$, and 70 $MgSO_4$ at pH 7.6-8.0. Test suspensions (10, 100, and 500 mg/L) were sonicated for 10 min in a Branson 2510 sonifier and stored in the dark at 4°C. Solutions of $CuSO_4 \cdot 5H_2O$ and $ZnSO_4$ were used as controls for size-dependent and solubility effects at a nominal concentration of the metal ions of 0.5 mg/L, which is very close to the maximum concentrations measured by atomic absorption spectroscopy (AAS) in NP suspensions. These solutions were prepared without sonication.

3.3.2 Characterization of NP suspensions

The effective NP diameters and their size distributions were measured by transmission electron microscopy (TEM). CuO, TiO_2, and ZnO NPs were suspended in distilled water, sonicated for 1 min and vortexed. Aliquots of 3 µl of the NP suspensions (100 mg/L) were immediately pipetted and deposited onto Formvar®-coated 200 mesh Copper grids, and excess of water was gently blotted using filter paper. Once dried, grids were directly inserted into a Jeol-JEM1220 transmission electron microscope operating at 100 kV, and images were collected at a magnification of 50,000X using a dedicated CCD camera. More than 300 NPs from nCuO, $nTiO_2$, and nZnO were measured, and the mean diameter (±SE) of single isolated particles was calculated for each sample.

Dynamic Light Scattering (DLS) was used to characterize the hydrodynamic behavior of the NPs and their extent of aggregation in suspensions in FETAX solution. The light scattered at $\theta = 90^{o}$ by the nanoparticle suspensions was collected using a digital EMI photomultiplier (9863KB, EMI, UK) mounted on a light scattering goniometer constructed in-house (Chirico and Beretta 1999). The corresponding autocorrelation functions (ACFs) were computed using an ISS FCS board (ISS Inc, Urbana, IL). The second order autocorrelation functions (ACFs) of the scattered light were first converted into first order (field) ACFs, G(t), which were analyzed by means of the Maximum Entropy method (Steinbach et al. 2002), thus obtaining the average value of the hydrodynamic radius of each detected component, <R>, and the corresponding distribution width, σ (see Supplementary File F1, available with the online version of this paper).

AAS was used to determine the amount of copper and zinc ions dissolved from the NP suspensions used during embryo exposure. Samples of the NP suspensions (10 and 500 mg/L) were collected soon after their preparation, corresponding to the beginning of the tests (time 0), and then every 24 h until the end of the experiments (96 h). Cu^{++} and Zn^{++} were measured in the supernatants obtained after centrifugation of the samples at 12000 g for 30 min. Supernatants were acidified with 2% HNO_3, and analyses were performed using a Perkin-Elmer SIMAA6000. Samples were collected in duplicate, and each sample was analyzed in triplicate. A five-point standard curve was used to calculate the Cu^{++} and Zn^{++} concentrations.

3.3.3 Animals and experimental design

Adult *X. laevis* were purchased from *Xenopus* Express Inc. (Vernassal, Haute-Loire, France), maintained in aquaria with dechlorinated tap-water at a 22±2°C and alternating 12 h light/dark cycles and fed a semi-synthetic diet (Mucedola S.r.L., Settimo Milanese, Italy) three times a week. FETAX tests were run according to the standard ASTM protocol (1998). Embryos were

obtained from natural breeding pairs of adult *X. laevis* that were previously injected with HCG in their dorsal lymph sac (females: 300 IU; males: 150 IU). Breeding tanks were filled with FETAX solution and well aerated before introducing the couples. Amplexus normally ensued within 2 to 6 h, and the deposition of fertilized eggs occurred from 9 to 12 h after injection. After breeding, adults were removed, and embryos were collected in plastic Petri dishes. Normally cleaved embryos at the midblastula stage (stage 8) 5 h post-fertilization (hpf) (Niewkoop and Faber 1956) were selected for testing and then placed in 6.0-cm glass Petri dishes, with each Petri dish containing 10 ml of the control or test solutions/suspension. For each female, plates were produced in duplicate or triplicate when well-cleaved embryos were available. All of the Petri dishes were incubated in a thermostatic chamber at 23±0.5 °C until the end of the test, 96 hpf. At that time, mortality and malformation data were generated as endpoints of the assay. For each experimental group, the number of dead larvae was recorded, and survivors were anaesthetized with MS-222 at 100 mg/L and evaluated for single malformations by examining each specimen under a dissecting microscope. At the end of the bioassays, the surviving larvae were fixed for growth retardation measurements and for subsequent microscopic analyses. This assay was repeated four times under the same experimental conditions.

3.3.4 Light and electron microscopy analyses

For histopathological analysis, control and exposed larvae were randomly selected, anaesthetized and fixed overnight in Bouin's fluid. After fixation, larvae were rinsed in tap and distilled water, dehydrated in an ascending ethanol series and embedded in Bio-plast tissue embedding medium (Bio-Optica Srl, Italy). Seven-micron transverse or longitudinal serial sections of whole larva were obtained using a Reichert rotative microtome and stained with Hematoxylin-Eosin (HE). All larval organs and tissues were considered. This screening was performed on at least 10 larvae from each

experimental group. All slides were examined under a Leica DMRA2 light microscope, and images were collected with a Leica DC300F digital camera. For visualization of the NPs in tissues, a confocal microscope was used in reflection mode. Larvae were fixed overnight in 10% buffered formalin at RT, rinsed, and finally bleached in a 3% H_2O_2/KOH 0.5% medium for 2 h to avoid reflection by pigmentation (modified by Thisse and Thisse 2008). After processing with standard histological procedures, a Leica TCSNT confocal microscope with reflected-light optics was used to examine *X. laevis* sections at a magnification of 40x (1.25 NA Plan-Apochromat). According to the method of Prins et al. (2006), samples were illuminated with a 488 nm argon/krypton laser using an intensity of the AOTF filter of 10%. A neutral RT 30/70 filter was used as the beam splitter and placed at a 45° angle in the path of the beam.

For ultrastructural analysis, control and exposed larvae were randomly selected and fixed in 4% paraformaldehyde and 2% glutaraldehyde in 0.1 M sodium cacodylate buffered solution at pH 7.4. After several washes in the same buffer, embryos were post-fixed in 1% OsO_4 for 1.5 h at 4°C, dehydrated in a graded ethanol series and, finally, in 100% propylene oxide. Infiltration was subsequently performed with propylene oxide resin (Araldite-Epon) at volumetric proportions of 2:1 for 1.5 h, 1:1 overnight, and 1:2 for 1.5 h. Embryos were then embedded in 100% pure resin for 4 h, and polymerization was performed at 60°C for 48 h. Sectioning was performed using an Ultracut E microtome (Reichert); semithin sections of 1 μm were collected onto a microscope slide and stained with 1% toluidine blue to select the region of interest. Ultrathin sections of less than 50 nm were obtained from the a2 portion of the small intestine (Chalmers and Slack 1998) and collected on 200 mesh uncoated Copper grids. Ultrathin sections were not counterstained to avoid interference with metallic NP visualization. Bright field and then Electron Spectroscopic Imaging (ESI) analyses were performed using a Leo912ab transmission electron microscope (Zeiss) at 80

kV. The distribution of the investigated elements (Cu, Ti, Zn) was obtained by computer processing of images collected at different energy loss values according to the three-window method. The final element map (coded in pseudocolors) was then superimposed on the ultrastructural organization of the same field obtained at 250 eV, i.e., at an energy loss at which most of the elements contribute to the image (Colliex 1986). The nature of the element signals in the different regions of the maps was confirmed by Electron Energy Loss spectra. Digital images were acquired using a CCD-BM/1K system, and image elaboration was performed using Esivision.

3.3.5 Data collection and statistical analysis

The mortality percentages were calculated as the number of dead embryos *versus* their total number at the beginning of the test, and the malformed larva percentages were determined from the number of malformed larvae *versus* the total number of surviving larvae. The relationships between the control and treated groups, along with the percentages of dead and malformed larvae, were investigated with Chi-square test with the Yates's correction for continuity (χ^2 test), or Fisher's Exact test (FE test). When possible, the concentrations causing 50% lethality or malformation at 96 hpf were determined and classified as lethal (LC50) or teratogenic (TC50), respectively. These were obtained following the elaboration of the lethality and malformation data by Probit analysis (Finney 1971) using the US EPA Probit Analysis Program, version 1.5. The Teratogenic Index (TI), which is useful in estimating the teratogenic risk associated with the tested compounds, was the LC50/TC50 ratio (Dawson and Bantle 1987). To evaluate differences in growth retardation among groups, the nonparametric Kruskal-Wallis test and Dunnett's test for post-hoc analysis was used. Statistical comparisons were considered to be significant at the 95% level ($p<0.05$).

3.4 Results

3.4.1 Characterization of NP suspensions

TEM analysis allowed the visualization of single metal oxide NPs, as well as their aggregates. Figure 1 (A-C) shows the morphology of the nCuO, $nTiO_2$, and nZnO particles and their tendency to aggregate once suspended in aqueous medium. Based on measuring hundreds of single NPs by TEM, the calculated mean diameters of nCuO, $nTiO_2$, and nZnO were 34.38±0.76, 46.97±0.89, and 66.91±0.86 nm respectively. As shown by the size distributions (Figure 1D), nCuO mainly clustered in the range of 20-50 nm, with only a few larger particles. nZnO was mainly distributed in the interval between 70 and 100 nm, whereas the $nTiO_2$ population was almost normally distributed around its mean in the interval 20-80 nm.

Despite these measures, single NPs were only rarely detected by TEM, and almost all particles aggregated in small clusters ranging from a few NPs to large aggregates. This behavior was shared by all three types of metal oxide NPs, although $nTiO_2$ and nZnO appeared to produce larger aggregates that were much more regular in shape compared to those of nCuO (Figure 1A-C).

To characterize the degree of aggregation and the effective average size of the particulates used in the experiments, we performed a Dynamic Light Scattering analysis of the NP suspensions in FETAX solution at 10, 100 and 500 mg/L. Based on the analysis of the light scattering autocorrelation functions performed as described in the Materials and methods section (see Supplementary File F1, available with the online version of this paper), we obtained the distribution of sizes reported in Figure 2.

A first qualitative inspection of these distributions indicated the presence of two or three major components, all of which were larger than 250 nm in their hydrodynamic radius and, therefore, larger than the single NPs. This is not unexpected because the light scattered increases with the square of molecular weight, and thus, small components of large aggregates contribute

to the correlation function similarly to much larger components of single NPs. Therefore, rare aggregates that could not be analyzed by TEM are easily detected. Some degree of aggregation was observed, even at a concentration of 10 mg/L, and it increased with the NP concentration. To provide a measure of the average encumbrance of the NP aggregates as a function of the NP concentration in the medium, we computed an average radius for each NP suspension and compared the behavior of the different NPs, as shown in Table I and Figure 2 (inset).

Because copper and zinc ions are well recognized as ecotoxicologically hazardous substances, for the nCuO and nZnO suspensions, the amounts of dissolved ions that entered the test solutions were quantitatively monitored throughout the 96-h experiments by AAS. These data were also helpful in interpreting the contribution of dissolved ions to NP embryotoxicity. The results for the 10 and 500 mg/L NP suspensions are summarized in Figure 3. As can be seen in the figure, the concentration of Cu^{++} and Zn^{++} released did not increase with increasing NP concentration and did not exhibit time-dependent kinetics. The mean ion concentration measured in the FETAX solution during the 96-h experiments ranged from 0.30 mg/L for nCuO at 10 mg/L to 0.45 mg/L for nZnO at 500 mg/L. These data confirmed the relatively low solubility of the metal ions from these NPs, but they also indicated that the increased particle aggregation observed with increasing concentrations contributed to the prevention of ion dissolution. Whereas the percentages by mass of the dissolved ions from nCuO and nZnO 10 were 4.29 and 4.91%, those of nCuO and ZnO at 500 mg/L were 0.07 and 0.12, respectively.

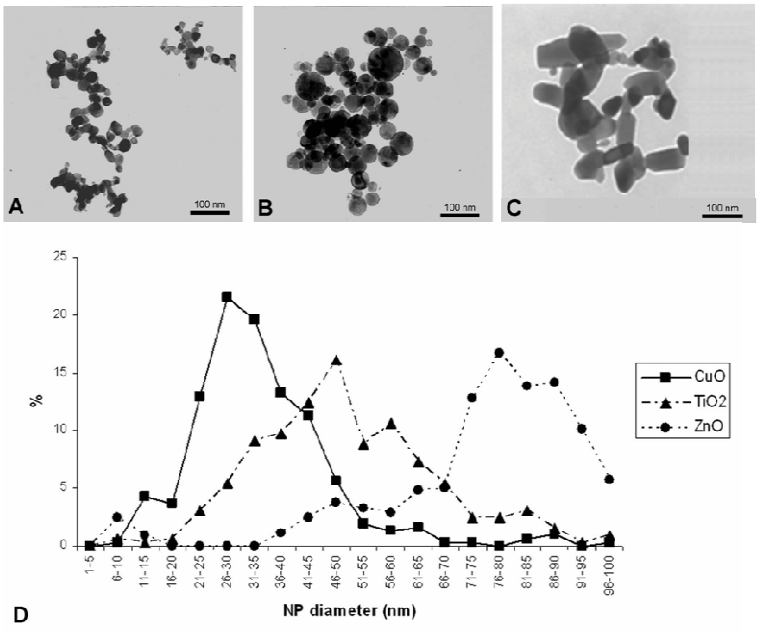

Figure 1. Characterization of metal oxide NPs from 100 mg/L suspensions by Transmission Electron Microscopy. A = nCuO; B = nZnO; C = $nTiO_2$; D = NP size distributions.

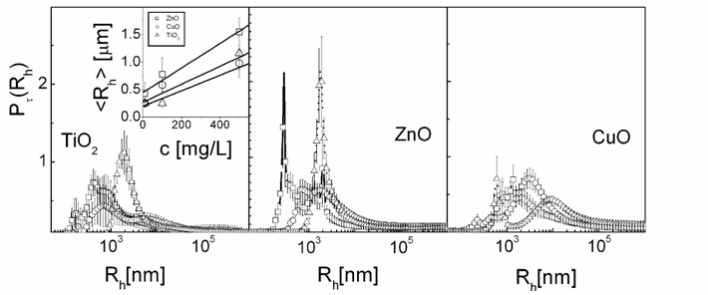

Figure 2. Result of the Maximum Entropy analysis of the DLS autocorrelation functions collected from FETAX suspensions of $nTiO_2$ (left panel), nZnO (middle panel) and nCuO (right panel). In each panel, three distributions are reported, referring to concentrations of 10 (squares), 100 (circles) and 500 mg/L (triangles). The inset reports the average values of the hydrodynamic radii of the NPs as a function of the concentration. The data refer to titanium (triangles), zinc (squares) and copper (circles).

Table I. Dynamic Light Scattering Analysis

NP concentration (mg/L)	CuO	TiO_2	ZnO
10	250±70	250±55	430±200
100	580±125	250±75	775±300
500	980±250	1160±300	1550±250

Average hydrodynamic radii (in nm) of oxide NPs as measured in FETAX suspension as a function of the oxide concentration. The average values and the standard deviations were computed on the distributions shown in Figure 2.

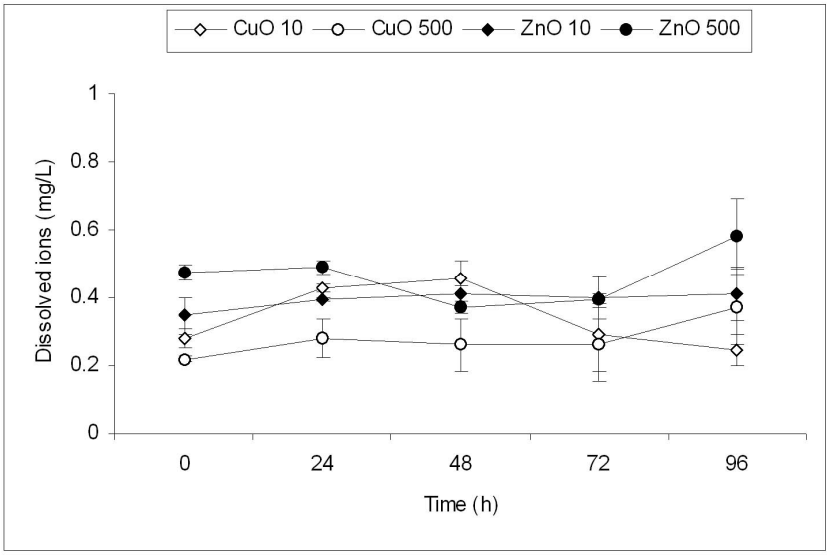

Figure 3. Concentrations of the dissolved Cu^{++} and Zn^{++} ions from NP suspensions during the 96-h exposure, analyzed by Atomic Absorption Spectroscopy. Bars = Standard Error of the means (SE)

3.4.2 Effects of metal oxide-based NPs on X. laevis development

The embryotoxic effects of the tested NP suspensions are shown in Table II. Very low mortality percentages were recorded at the end of the exposure, and the nCuO 500 mg/L group registered the highest value for this parameter

(9.9%; $p<0.001$, $\chi 2$ test). The remaining groups showed values very similar to those of the controls, suggesting that nCuO, $nTiO_2$ and nZnO should not be considered embryolethal for *X. laevis* development. With respect to the malformation rates, values that were significantly different from those in controls were registered in all groups, even at the lowest concentrations tested. In the nCuO-treated groups (though not in the $nTiO_2$ or in nZnO groups), the percentages of malformed larvae obtained using probit analysis allowed us to calculate a TC50 of 304.25 mg/L. However, the low mortality recorded did not allow an estimation of the LC50 or, thus, the TI. Because this latter value would be many times greater than 3, according to Dawson and Bantle (1987), nCuO should be considered "highly teratogenic". No specific terata were observed after nCuO exposure, though the surviving larvae were almost all severely malformed with diffuse edemas often coupled with microcephaly, gut abnormalities and/or axial defects (Figure 5). In contrast to the other groups, the nZnO-treated larvae mainly exhibited abnormal gut coiling as their sole characteristic malformation (see Supplementary Figure S1, available with the online version of this paper). A significant concentration-dependent growth retardation was observed in the nCuO- and nZnO-treated groups, though not in the groups treated with $nTiO_2$ (Figure 4); this last group did, however, present embryos that were significantly shorter than the control embryos in the 500 mg/L group ($p<0.05$; one-way ANOVA on ranks with post-hoc Dunn's test).

The 0.5 mg/L Cu^{++} group showed a very high malformation rate, almost as high as in the 500 mg/L nCuO group (Table II), equally strong growth inhibition (Figure 4), and a mortality value that was statistically different from that of the controls ($p<0.001$, $\chi 2$ test; Table II). In contrast, the effects of 0.5 mg/L Zn^{++} were negligible, as the larvae of this group showed no mortality, no malformations and no growth retardation (Table II, Figure 4).

Table II. Embryotoxic effects in *X. laevis*

		Cuo (mg/L)			Cu^{++} (mg/L)	TiO_2 (mg/L)			ZnO (mg/L)			Zn^{++} (mg/L)
	Control	**10**	**100**	**500**	**0.5**	**10**	**100**	**500**	**10**	**100**	**500**	**0.5**
Utilized embryos (n)	730	374	373	413	225	373	473	401	370	548	398	201
Dead embryos (n)	9	2	4	41	82	12	9	7	3	3	5	2
Mortality (%)	1.2	0.5	1.1	9.9 [c]	36.4 [c]	3.2 [a]	1.9	1.7	0.8	0.5	1.3	1.0
Living larvae (n)	721	372	369	372	143	361	464	394	367	545	393	199
Malformed larvae (n)	41	38	48	291	103	57	46	59	44	135	75	8
Malformed larvae (%)	5.7	10.2 [b]	13 [c]	78.2 [c]	72 [c]	15.8 [c]	9.9 [b]	15 [c]	12 [c]	24.8 [c]	19.1 [c]	4.0

[a] Chi square test; $p<0.05$

[b] Chi square test; $p<0.01$

[c] Chi square test; $p<0.001$

Table III. Pattern of malformations in *X. laevis*

			CuO (mg/L)			Cu^{++} (mg/L)	TiO_2 (mg/L)			ZnO (mg/L)			Zn^{++} (mg/L)
		Control	10	100	500	0.5	10	100	500	10	100	500	0.5
Malformation													
Monster n (%)		0	0	0	6 (1.6)	0	2 (0.6)	0	0	3 (0.8)	3 (0.6)	8 (2.0) [b]	0
Severe n (%)		13 (1.8)	10 (2.7)	12 (3.6)	53 (14.2) [e]	34 (23.8) [e]	11 (3.0)	11 (2.4)	15 (3.8)	14 (3.8)	15 (2.8)	11 (2.8)	1 (0.5)
Gut n (%)		15 (2.1)	12 (3.2)	20 (5.4) [d]	62 (16.7) [e]	26 (18.2) [e]	34 (9.4) [e]	31 (6.7) [e]	34 (8.6) [e]	18 (4.9) [c]	34 (6.2) [e]	41 (10.4) [e]	1 (0.5)
Edema n (%)	*multiple*	0	1 (0.3)	0	0	9 (6.3) [b]	1 (0.3)	0	2 (0.5)	3 (0.8)	0	1 (0.3)	0
	cardiac	0	0	1 (0.3)	3 (0.8)	0	1 (0.3)	0	0	4 (1.1)	1 (0.2)	0	0
	abdominal	0	1 (0.3)	2 (0.5)	0	0	1 (0.3)	0	0	2 (0.5)	19 (3.5) [b]	8 (2.0) [b]	1 (0.5)
Ventral flexure n (%)		8 (1.1)	5 (1.3)	7 (1.9)	11 (3.0) [a]	6 (4.2) [a]	9 (2.5)	2 (0.4)	6 (1.5)	6 (1.6)	14 (2.6)	9 (2.3)	2 (1.0)
Notochord n (%)		0	4 (1.1)	6 (1.6)	1 (0.3)	2 (1.4)	4 (1.1)	7 (1.5)	16 (4.1) [b]	1 (0.3)	6 (1.1)	1 (0.3)	0
Face n (%)		1 (0.1)	3 (0.8)	6 (1.6)	26 (7.0) [e]	14 (9.8) [e]	10 (2.8) [e]	3 (0.6)	3 (0.8)	2 (0.5)	8 (1.5) [c]	8 (2.0) [d]	0

(Percentages based on number of malformations/number of the living)

[a] FE test; $p<0.05$

[b] FE test; $p<0.01$

[c] Chi square test; $p<0.05$

[d] Chi square test; $p<0.01$

[e] Chi square test; $p<0.001$

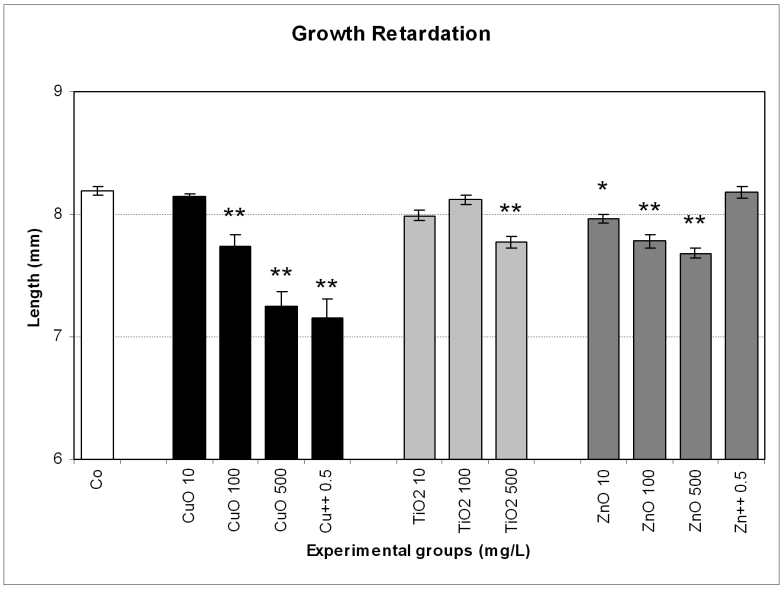

Figure 4. Growth retardation analysis of *X. laevis* embryos. Bars = SE; * = $p<0.05$; ** = $p<0.01$

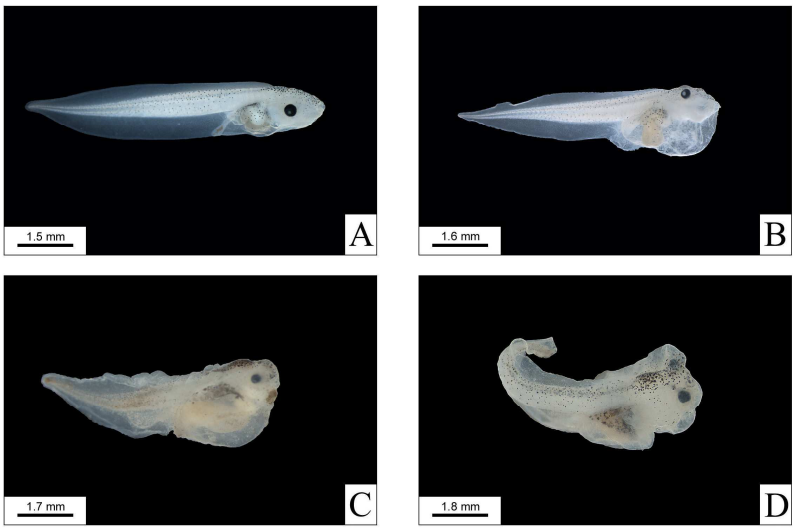

Figure 5. *X. laevis* larvae at 96 h post exposure. (A) Control larva; (B-D) larvae exposed to nCuO: (B) lateral view of a larva exposed to 100 mg/L nCuO affected by cardiac and abdominal edemas; (C) lateral view of a larva exposed to 500 mg/L nCuO showing cardiac and abdominal edemas, microcephaly and bent tail; (D) lateral view of a severely malformed larva exposed to 500 mg/L nCuO.

3.4.3 Histopathological screening

Histological screening performed on 170 larvae showed that the digestive system was the most affected organ system, as the stomach and gut were the preferential sites of NP localization and of the observed damage. Only the nCuO 500 mg/L group presented evident histopathological effects on many organs and cephalic structures (see Supporting Figures S1, S2. Supporting information - PART I) while all of the treated groups presented lesions at the intestinal level. The digestive tract and the epidermis generally represent two of the most crucial exposure routes for *X. laevis* embryos, but no alterations were observed in the skin, suggesting that NPs were likely unable to enter through this route and that gut was the main entry for NPs.

According to Chalmers and Slack (1998), the digestive system of *X. laevis* larvae is composed of the pharynx, esophagus, stomach, small intestine, and large intestine, followed by a proctodeum. No alterations were observed in the first and the last tract, and the large and, especially, the small intestine were the most affected sites. The small intestine is composed of two portions: one of which is ciliated and nonabsorptive (sia1), and the other is absorptive (sia2) and accounts for a large proportion of the gut length. In this tract, the normal absorptive epithelium is composed of columnar cells with nuclei positioned at the base and a well-developed brush border (Figure 6A). Different degrees of alteration were observed in the gut of NP-exposed larvae. Pathological aspects ranged from the presence of small amount of cellular debris in the lumen coupled with a normal morphology of the epithelium (Figure 7A), to very thin epithelia, with cells characterized by densely stained cytoplasm and pyknotic nuclei (Figure 7C). The most affected areas were observed in the nZnO 500 mg/L group, where 90% of the larvae presented the strongest pathological modifications, with considerable disorganization of the entire intestinal tract (Figures 7C, D). Despite this, the brush borders were maintained (Figure 7D). The other tissues presented a normal appearance, indicating that the gut was the

preferential target for nZnO. Embryos exposed to nCuO and $nTiO_2$ also showed pathological morphologies (Figures 6B, C), though the structure of the gut epithelium was almost always maintained. NPs were, however, visible inside the intestinal loops of these two groups, particularly in the $nTiO_2$ group.

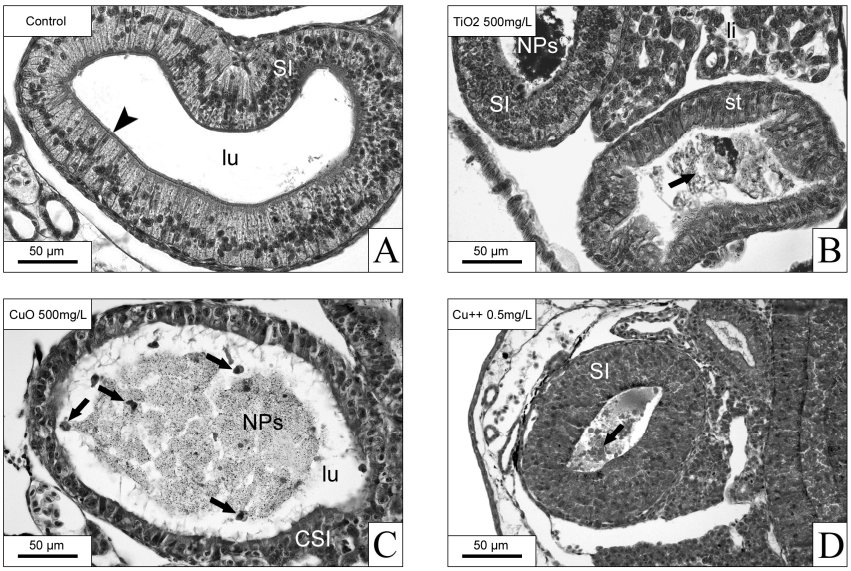

Figure 6. Histological images of 96-h-old *X. laevis* larvae at the gut level. (A) Transverse section of the Small Intestine (SI) from a control larva showing a normal absorptive epithelium with a well-defined brush border (►), lu = lumen. (B) Stomach (st) and Small Intestine (SI) from a larva exposed to 500 mg/L $nTiO_2$ in which TiO_2 NPs and cellular debris (→) are evident, li = liver. (C) Ciliated Small Intestine (CSI) from a larva exposed to 500 mg/L nCuO. Copper oxide nanoparticles (NPs) appear visible inside the lumen together with a small amount of cellular debris (→), lu = lumen. (D) Small Intestine (SI) from a larva exposed to 0.5 mg/L Cu^{++} in which the intestinal wall appeared well preserved, but with cellular debris in the lumen (→).

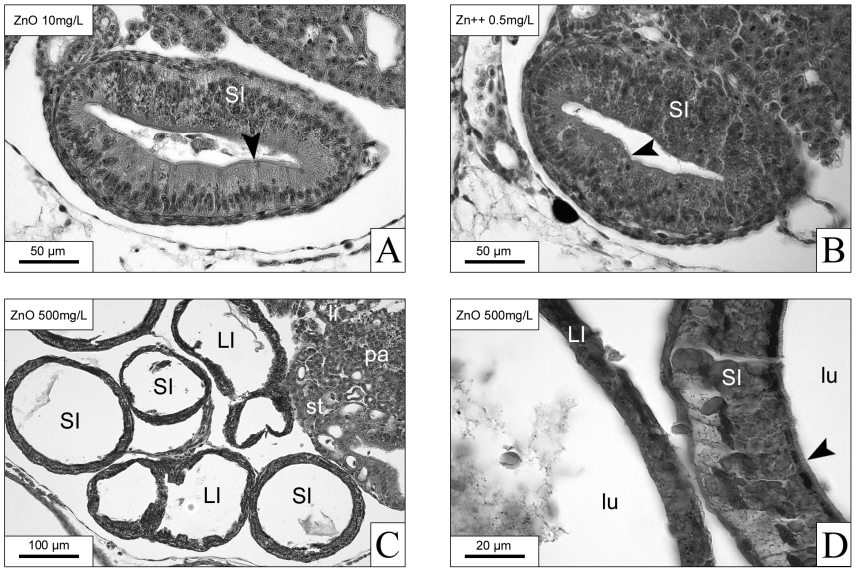

Figure 7. Histological images of 96-h-old *X. laevis* larvae at the gut level. (A) Small Intestine (SI) of larva exposed to 10 mg/L nZnO in which cellular debris is visible in the gut lumen. The brush border appears well preserved (►). (B) Small Intestine (SI) of larva exposed to 0.5 mg/L Zn^{++} in which the intestinal wall appeared regularly shaped without any alteration; the brush border is visible and intact (►). (C) Low magnification of a larva exposed to 500 mg/L nZnO showing several intestinal loops in which the epithelia of both the small and large intestine (SI and LI, respectively) appeared thin and severely damaged; pa = pancreas; st = stomach; li = liver. (D) Detail of two intestinal loops back-to-back from a larva exposed to 500 mg/L nZnO showing necrotic tissues with vacuolated cytoplasm and pyknotic nuclei. The SI still presents a normally shaped brush border (►), SI = Small Intestine; LI = Large Intestine; lu = lumen. The control is the same as Figure 6.

3.4.4 NP visualization at the histological level by reflection analysis

In reflection analysis of histological sections, it was possible to observe aggregates as small as 150-200 nm. TiO_2 NPs clustered very tightly and remained quite visible, even after the histological procedures (Figure 8B). All types of NPs entered the gut epithelium, and they were visible at different depths (Figure 8C; Figures 9B, D). In the nCuO-exposed larvae, the

strongest signals were detected at the brush border level (Figure 9A), whereas in the nZnO-exposed larvae, it was interesting to observe that NPs accumulated near the basement membrane and in the connective tissue among the intestinal loops (Figures 9C, D).

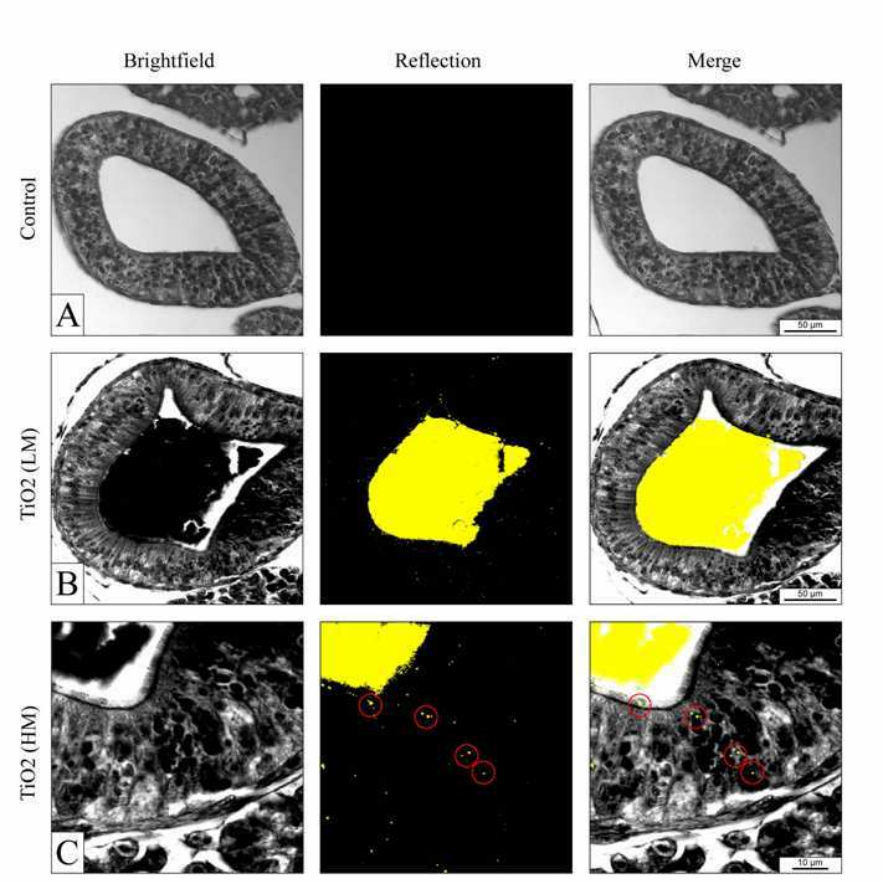

Figure 8. Confocal reflection analysis of histological sections of 96-h-old *X. laevis* larvae. The reflection is coded in yellow pseudocolor. Transverse section of the Small Intestine from control (A) and larvae exposed to 500 mg/L $nTiO_2$ (B, C). The lack of signal in the control and its intensity in the $nTiO_2$-exposed larvae are evident. Red circles emphasize the presence of small NP aggregates at different distances within the epithelial width. LM = Low Magnification; HM = High Magnification.

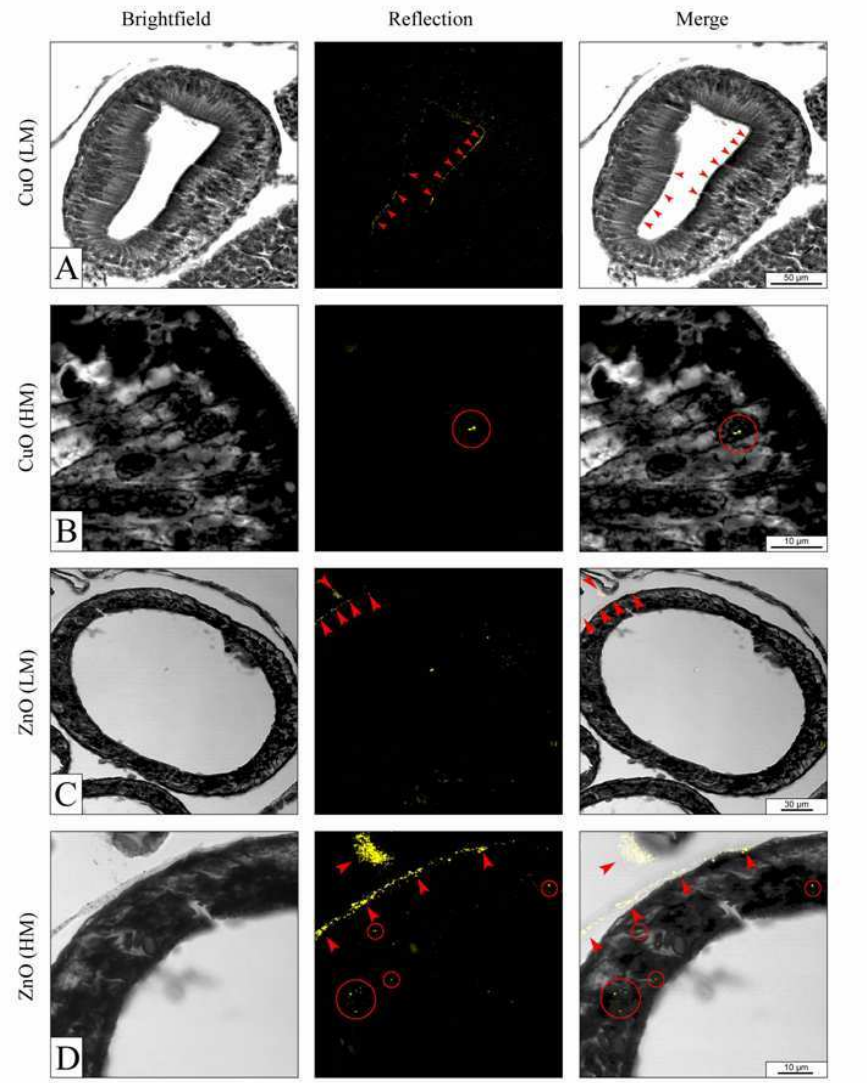

Figure 9. Confocal reflection analysis of histological sections of 96-h-old *X. laevis* larvae. The reflection is coded in yellow pseudocolor. Transverse section of the Small Intestine from 500 mg/L nCuO- (A, B) and 500 mg/L nZnO- (C, D) exposed larvae. The reflection analysis highlights the presence of nCuO along the brush border (A) (red arrowheads), and inside the tissue (B) (red circle). In the nZnO-treated larvae, NPs are present at different tissue levels (red circles), though they mainly accumulate near the basement membrane and beneath the intestinal loops (red arrowheads). LM = Low Magnification; HM = High Magnification.

3.4.5 NP effects and visualization at the ultrastructural level

TEM analysis of control larvae showed that they exhibited a normal gut epithelium, with regular microvilli organized in a well-defined brush border (Figure 10A). The microvilli core was filled with fine filaments, which extended deep into the terminal web of the apical cytoplasm. Numerous mitochondria and multivesicular bodies were visible immediately beneath the terminal web. This structural aspect was maintained in all of the $nTiO_2$-exposed larvae (Figure 10B), which showed a sporadic presence of NPs, including inside the mitochondria, as demonstrated by ESI (Figures 10C, D). Exposure to nCuO caused serious ultrastructural alterations, such as microvilli disruption and anastomosis (Figure 11A) and the presence of large amounts of cellular debris in the lumen. Microvilli appeared to be thicker and shorter than in controls, and the mucosal cells often showed a diffuse blebbing of the apical plasma membranes (Figure 11B). In the less affected nZnO-treated larvae, the basal portions of the cells showed normally shaped nuclei and a detachment from the basement membrane, accompanied by swelling of the paracellular spaces, and the structure of the apical membrane was well preserved (Figure 11D). The epithelial width was reduced compared to the controls, and this became more evident in the 500 mg/L larvae, in which it was sometimes observed that extensive areas of the intestinal wall exhibited disrupted organization (Figure 11E). It was shown by both TEM and ESI analyses that nZnO preferentially localized between adjacent cells (Figure 11F, G), where aggregates of hundreds of nm were easily observable.

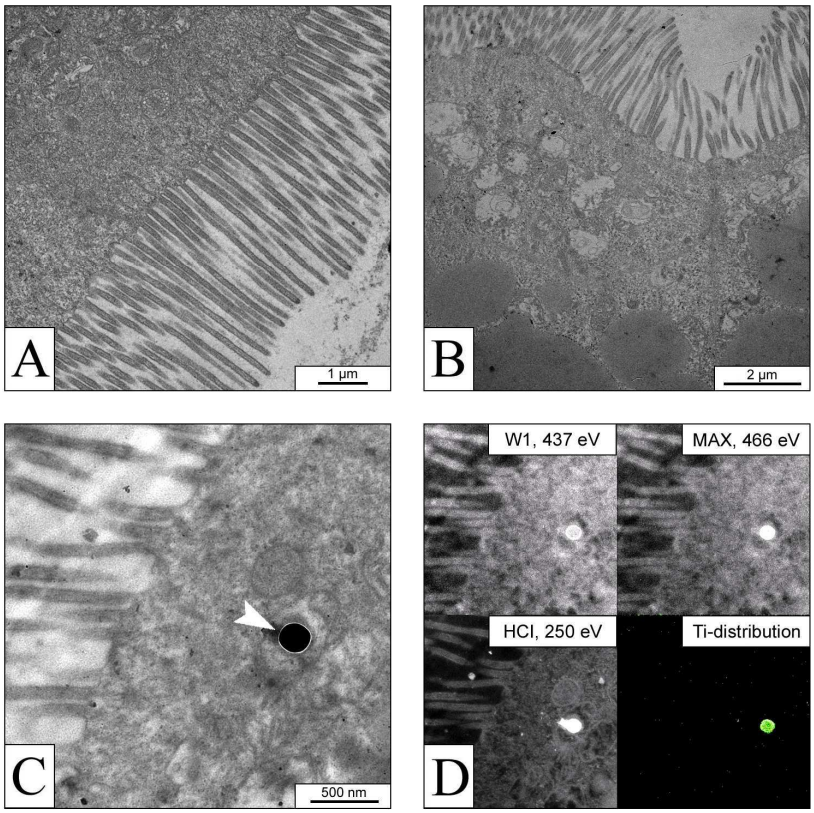

Figure 10. TEM images of 96-h-old *X. laevis* control (A) and 100 mg/L $nTiO_2$- (B-D) exposed larvae. (A) Apical portion of a digestive cell from the Small Intestine of a control. (B) Portion of a digestive cell from a $nTiO_2$-exposed larva with regular arrangement of the microvilli. (C) A $nTiO_2$ aggregate of approximately 300 nm inside a mitochondrion (white arrowhead). (D) Elemental Spectroscopy Imaging (ESI) by the three-window method, showing Ti inside a mitochondrion.

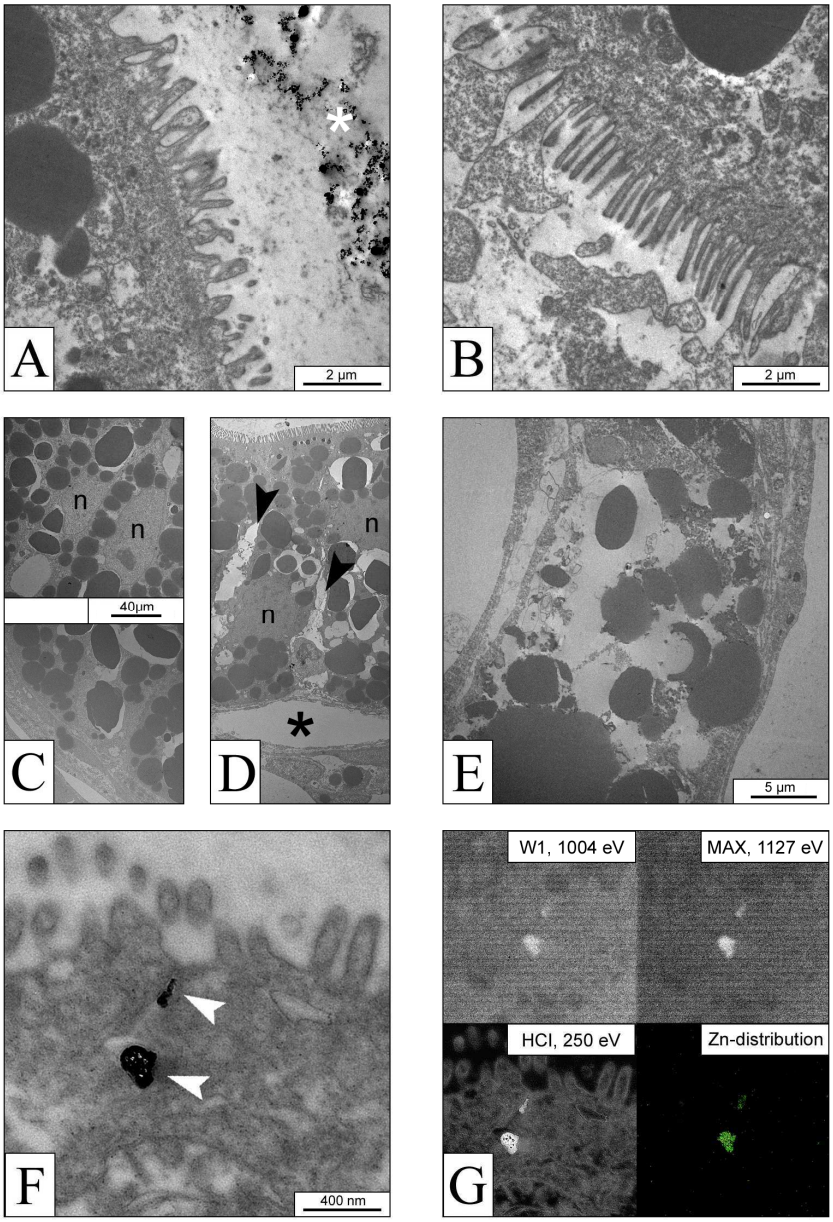

Figure 11. TEM images of 96-h-old *X. laevis* 500 mg/L nCuO- (A, B), control- (C), and 500 mg/L nZnO- (D-G) exposed larvae. All sections are from the Small Intestine. (A) Detail of an apical portion of a digestive cell showing anastomosis of the microvilli, which are thicker and shorter than usual. (*) = nCuO in the lumen. (B) Detail of an apical portion of a digestive cell with diffuse blebbing of the plasma

membrane. (C, D) Control and 500 mg/L nZnO-treated larvae at the same magnification. The height of the entire intestinal wall of the control larva was too great to be put into the picture (C), but the entire width of the epithelium is visible in D, where the swelling of the paracellular spaces is evident (►), n = nucleus; * = cell detachment from the basal membrane. (E) Low magnification of a disintegrated intestinal wall, where ultrastructural details cannot be resolved. (F, G) ESI shows the presence of Zn aggregates between two adjacent cells.

3.5 Discussion

Nanoecotoxicology has recently emerged as a new discipline requiring careful investigation because it presents many important topics for consideration (Behra and Krug 2008), such as the most suitable test for NP characterization, the route of NP entry into organisms, and how to measure of the level of exposure-producing effects. These questions indicate the need to use more sensitive imaging and detection tools to bridge the observed biological responses to NPs with their effective availability. Our research was performed following these requirements and will be discussed here with respect to criticisms of this work and to compare our results with those presented in the literature.

3.5.1 X. laevis development as a nanoecotoxicological model?

The standardized FETAX procedure, which was introduced to test the embryotoxic potential of chemicals, has been applied only once previously in nanotoxicological studies (Nations et al. 2011). Further, the potential embryotoxic effects of NPs on both aquatic organisms and laboratory mammals has not generally received a great deal of attention to date.

The observation that gold NPs can cross the placenta and accumulate in the fetus, as demonstrated in an *in vivo* study in rats (Saunders 2009), as well as by the findings of Wick et al. (2010), who demonstrated that fluorescent

polystyrene NPs up to 240 nm were able to cross the placental barrier without affecting the viability of the placenta, require further attention. The possibility of NP transport through the placenta highlights the urgent need for further studies on this topic, suggesting the use of alternative methods, such as FETAX, to screen for embryotoxicity. Moreover recent researches have demonstrated that several NPs (i.e. silver, gold and silica NPs) are able to overpass the embryonic barriers and deeply penetrate in zebrafish embryos even at early life stages, thus contributing to generate adverse developmental effects (Lee et al. 2007; Browning et al. 2009; Fent et al. 2010)

No data have previously been reported in the literature on the teratogenic potential of NPs on *X. laevis* embryos. The mortality and genotoxic effects of double-walled carbon nanotubes have been investigated in the larval phase (Mouchet et al. 2008), and the chronic effects of nZnO have been evaluated during metamorphosis (Nations et al. 2011). The lack of experimental evidence related to the early developmental phases of *X. laevis* is likely linked to the recent introduction of zebrafish as a new ecotoxicological model, thus allowing the correlation of genomic analyses with traditional embryotoxicity endpoints (Griffitt et al. 2007; 2009). Additionally, *X. laevis* embryos apparently have a considerably greater resistance to NPs in comparison with zebrafish, as our results showed that appreciable developmental effects only appeared at high NP concentrations, raising the question of the comparative protection against NPs along vertebrate evolution. Despite these considerations, *X. laevis* embryos remain a valid tool for the evaluation of the mechanisms of NP-induced toxicity.

3.5.2 Nano-developmental toxicity: priority of the characterization of NPs

The three types of metal oxide NPs investigated here were selected from the Sigma-Aldrich catalog because they are widely diffused and commercially available. Their embryotoxic potential was analyzed

and compared through experiments that were designed to guarantee a realistic exposure scenario, and consequently, no additives (coating proteins or detergents) were added to the test media for the maintenance of NPs in suspension. Because no data on the embryotoxic effects of these NPs were available, a range-finding test was performed to investigate possible concentration-dependent responses and to determine NP concentrations inducing relevant modifications. This approach required detailed knowledge of the hydrodynamic behavior of NPs in suspension, as aggregative phenomena could contribute to the availability of particles in the nano-scale dimension (Johnston et al. 2010). Our samples were constituted of particles ranging from few nm to 100 nm (Figure 1), and the size distributions differed for the three NPs: a large fraction of nCuO particles measured between 20 and 45 nm; the majority of nZnO particles varied from 70 to 90 nm; and the $nTiO_2$ particles presented a mean diameter of approximately 50 nm (Figure 1). Although they showed different dimensions, all of these NPs behaved similarly once dispersed in the FETAX medium. They all exhibited considerable aggregation, forming clusters of hundreds of nm, with a consistent fraction at the micrometer scale. As a consequence, it was easy to observe that larger aggregates were not maintained in suspension but precipitated to the bottom of the exposure chambers. Thus, the exposure system was modified, resulting in an additional substrate for grazing, and implementing the quantity of NPs available for larvae. On day 3 (stage 40/41; Nieuwkoop and Faber 1956), *X. laevis* embryos opened their mouths, and ingestion became the main route of NP intake. The next day, the grazing behavior of the larvae became very active, increasing the numbers of ingested particles. It was already stated that metal oxide NPs behavior in water environment change significantly according to the physicochemical properties of the solvent, and that they easily reach the sediments, thus modifying the exposure scenario in target organisms (Zhang et al. 2008; Sharma 2009).

Our results related to mortality (Table II) are in agreement with those of Nations et al. (2011), who reported that no mortality occurred in embryos during acute studies, but it increased after four days of exposure. The NP exposure conditions in our experiments did not allow us to establish concentration-dependent effects, but they can be considered representative of real exposure, in which insoluble metal-oxide NPs reach sediments, and organisms are continuously exposed to water-dispersed and settled NPs.

In conclusion, NP aggregation played an important role in the bioavailability of NPs and their consequent toxicity. The methods used here and the results obtained are quite comparable to those of other authors who have investigated the acute toxicity and the ecotoxicological potential of metal oxide NPs on aquatic organisms (Kahru and Dubourgier 2010; Krysanov et al. 2010).

3.5.3 Comparative results of NP-induced embryotoxicity

To assess the potential risk of new NMs in the environment, we exposed *X. laevis* embryos to a wide range of NP suspensions for 96 h. No effects were observed at concentrations of 0.1 and 1 mg/L (data not shown). Therefore, embryos were exposed to concentrations ranging from 10 to 500 mg/L. Very low mortality was recorded in all of the treatment groups, suggesting that metal oxide NPs do not affect *X. laevis* embryo survival, even at very high concentrations. These results are in agreement with those of Nations and co-workers (2011), who reported that nZnO did not induce embryo mortality at concentrations up to 1000 mg/L. However, all of our NP-treated groups showed malformation rates that were significantly higher than was observed in controls, suggesting the teratogenic potential of metal-based NPs after short-term exposure (Table II). Nations et al. previously reported significant malformations induced by 100 mg/L nZnO, and we obtained similar results at a concentration as low as 10 mg/L.

Metal oxide NPs are toxic for bacteria, algae, crustaceans, and fish (Kahru and Dubourgier 2010), but the mechanism underlying their toxicity remains unclear. There are data attributing the nCuO and nZnO toxicity observed in these organisms to dissolved ions (Aruoja et al. 2009; Blinova et al. 2010; Heinlaan et al. 2010), whereas other data show that the effects of NPs in fish cannot be explained by particle dissolution alone (Griffitt et al. 2007; Asharani et al. 2008; Griffitt et al. 2009).

Our data from embryotoxicity screening suggest that the toxicity of nCuO was mainly attributable to dissolved copper ions, as the mortality and malformation rates produced by 0.5 mg/L Cu^{++}, which were significantly higher than in controls, were very similar to those observed in the 500 mg/L nCuO group. In contrast, the effect of nZnO apparently did not depend on its soluble ions because no mortality or malformations were recorded in the 0.5 mg/L Zn^{++} group, although the nZnO-exposed groups showed malformation rates that were always significantly higher than in controls.

Histological analysis confirmed the different impacts of the different types of NPs on embryo morphology, with nCuO being found to be the most harmful. The 500 mg/L nCuO and 0.5 mg/L Cu^{++} groups were the only groups presenting severe lesions (see Supporting Figure S2. Supporting information - PART I), confirming the hypothesis that copper ions dissolving from NPs are highly toxic. All of the NPs mainly affected the digestive system, including the stomach and particularly the gut, suggesting that ingestion is the principal exposure route.

Particular attention must be paid to the levels of NPs available in the environment, which are currently estimated to be on the order of a few micrograms per liter (Kaegi et al. 2008; Blinova et al. 2010), whereas the concentrations used in laboratory exposures are almost always higher than this. Despite the fact that such a discrepancy may exist between experimental conditions and actual NP availability and the associated effects, it is important to clarify our understanding of the mechanisms of NP

action when they are used over threshold levels. Moreover, the transfer of NPs through trophic levels must be taken into account, as this phenomenon has been reported by several authors (Moore 2006; Ward and Kach 2009; Kahru and Dubourgier 2010).

Some types of metal oxide NPs have been extensively studied in aquatic organisms, but a conclusive categorization of their toxicological impacts has not yet been achieved. Focusing on freshwater vertebrates, nZnO was able to delay embryo development, decrease survival and cause tissue damage in zebrafish (Zhu et al. 2008; 2009). In *X. laevis*, exposure to a concentration of 2 mg/L nZnO was found to increase mortality to 40% during late larval stages and negatively affected metamorphosis (Nations et al. 2011). Nickel NPs were found to be highly toxic for zebrafish, causing thinning of the gut epithelium and skeletal muscle fiber separation (Ispas et al. 2009). Copper and silver NPs were also observed to be toxic to zebrafish (Asharani et al. 2008; Griffitt et al. 2009), and this toxicity is apparently related to both the NPs and their dissolved ions. TiO_2 NPs, which are usually described as non-toxic at concentrations between 0.1 and 0.5 mg/L, altered gill morphology and induced oxidative stress in the rainbow trout, *Oncorhynchus mykiss* (Federici et al. 2007). More recently, Griffitt et al. (2009) reported that $nTiO_2$ was associated with low toxicity and did not induce gill alterations in zebrafish embryos exposed to this substance for 48 h. In our experiments, the $nTiO_2$-treated groups showed significant malformations (Table II), and because these NPs do not release toxic metal ions (Yamamoto et al. 2004), the effects produced may be dependent on the "mechanical stress" induced by the large quantity of $nTiO_2$ in the digestive tract. Uptake of TiO_2 NPs from the water column through the gills and the gut after a 14 days of exposure has been demonstrated in *O. mykiss* (Johnston et al. 2010), which is in line with our data obtained using reflection analysis showing that TiO_2 NPs entered into the gut mucosa (Figure 8). Additionally, this analysis showed that all three types of NPs entered the gut epithelia, and that nZnO

aggregates were easily detectable at the basement membrane level (Figures 8, 9). Our TEM analyses confirmed the presence of NPs both inside cells and between them (Figure 11). Their presence in the epithelial cell *interstitia* suggests the paracellular space as a possible route of entry (Supporting Figures S5. Supporting information - PART I), followed by translocation to other organs via the bloodstreamDamage to cell binding sites can lead to intestinal barrier leakage and tissue disruption, as demonstrated by our histopathological observations (Figure 7), which showed a disorganization of the intestinal tract in nZnO-treated embryos, as well as by data reported in the literature (Zhu et al. 2008) illustrating ulceration in zebrafish larvae exposed to the same NPs. ZnO NPs were also found to produce cytotoxicity in a human intestinal cell line (RKO), and these effects were independent of the amount of soluble Zinc present, though this effect required NP-cell contact (Moos et al. 2010). The intestine-blood route for NP transport to other organs has been previously suggested by Kashiwada (2006), who exposed *Oryzias latipes* to 10 mg/L fluorescent particles. Particle transport via the blood circulatory system was also proposed by Jani et al. (1990) for the translocation of polystyrene NPs from the oral primary exposure route in rats.

3.6 Conclusion

Our results showed that metal oxide NPs do not affect viability in *X. leavis* embryos at the conditions used in this study, but they induce considerable morphological alterations, especially of the digestive system.

CuO NPs were found to be the most toxic among the investigated particles, with a remarkable teratogenic potential that is apparently dependent on dissolved Cu^{++} ions, though an effect of the particles themselves was also observed to be involved.

The effects of ZnO NPs on aquatic organisms have to be carefully considered in environmental risk assessment.

TiO_2 NPs, which apparently do not induce strong embryotoxicity, may have hidden biological effects that should be taken into account.

All of the types of NPs investigated entered the gut epithelium and were detected beyond the intestinal lumen, suggesting the possibility of their translocation to other organs and, consequently, possible additional teratogenic effects during later developmental stages, which need to be further investigated.

Though the mechanisms underlying the action of nCuO and $nTiO_2$ cannot be explained here, the mechanisms associated with the effects of nZnO are apparently linked to the disruption of the intestinal barrier. This allows nZnO to pass into the paracellular space and to reach the basement membrane, thus permitting translocation to other organs

The main route of entry was found to be the oral route for all of the NPs tested, despite the fact that they have different toxicity potentials and associated mechanisms.

Further investigations are needed to clarify the teratogenicity of NPs, and special attention must be paid to their safe use to minimize their impact.

† This paper is dedicated to the memory of Dr. Claudio Vismara, a colleague and a friend, who spent most of his working life spreading the enthusiasm for using FETAX.

Acknowledgements

The authors wish to thank Drs. Maria Tringali and Daniele Gallinotti for their assistance in the NP suspension characterizations with AAS and TEM. We also strongly acknowledge Dr. Maurizio Gualtieri for his helpful advice and Prof. Giovanni Vailati for valuable assistance in the analysis of *X. laevis*

embryology and histology. This work was partially supported by the Grant PRIN 2008 from the MIUR to M.C.

References

Aruoja V., Dubourguier H-C., Kasemets K., Kahru A. 2009. Toxicity of nanoparticles of CuO, ZnO and TiO_2 to microalgae *Pseudokirchneriella subcapitata*. Sci. Tot. Environ. 407, 1461-1468.

Asharani P.V., Wu Y.L., Gong Z., Valiyaveettil S. 2008. Toxicity of Silver nanoparticles in zebrafish models. Nanotechnology 19, 255102-255109.

ASTM, American Society for Testing and Materials, 1998. Standard guide for conducting the Frog Embryo Teratogenesis Assay-*Xenopus* (FETAX) E-1439-E1498.

Bantle J.A., Dawson D.A., 1988. In: Adams WJ, Chapman GA, Landis WF, editors. Aquatic Toxicology and Hazard Assessment, ASTM STP 971. ASTM, Philadelphia, PA, p 316.

Baun A., Hartmann N.B., Grieger K., Kusk K.O. 2008. Ecotoxicity of engineered nanoparticles to aquatic invertebrates: a brief review and recommendations for future toxicity testing. Ecotoxicology 17, 387-395.

Behra R., Krug H. 2008. Nanoparticles at large. Nat. Nanotechnol. 3, 253-254.

Blinova I., Ivask A., Heinlaan M., Mortimer M., Kahru A. 2010. Ecotoxicity of nanoparticles of CuO and ZnO in natural water. Environ. Pollut. 158, 41-47.

Browning L.M., Lee K.J., Huang T., Nallathamby P.D., Lowman J.E., Xu X.N. 2009. Random walk of single gold nanoparticles in zebrafish embryos leading to stochastic toxic effects on embryonic developments. Nanoscale 1, 138-152.

Chalmers A.D., Slack J.M.W. 1998. Development of the gut in *Xenopus laevis*. Dev. Dynam. 212, 509-521.

Chirico G., Beretta S. 1999. Polyion character of globular proteins detected by translational and rotational diffusion. Phys. Rev. E 60, 2148-2153.

Colliex C. 1986. Electron energy-loss spectroscopy: analysis and imaging of biological specimens. Ann. NY Acad. Sci. 483:311-326.

Dawson DA. 1991. Additive incidence on development malformation for *Xenopus* embryos exposed to a mixture of ten aliphatic carboxylic acids. Teratology 44, 531-546.

Dawson D.A., Bantle J.A. 1987. Development of a reconstituted water medium and preliminary validation of the Frog Embryo Teratogenesis Assay-*Xenopus* (FETAX). J. Appl. Toxicol. 7, 237-244.

Dumont J.N., Schultz T.W., Buchanan M., Kao G. 1983. Frog Embryo Teratogenesis Assay-*Xenopus* (FETAX) - A short-term assay applicable to complex environmental mixtures. In: Waters MD, Sandhu SS, Lewtas J, Claxton L, Chernoff N, Nesnow S, editors. Short-Term Bioassays in the Analysis of Complex Environmental Mixtures. New York: Plenum Press pp 393-405.

Federici G., Shaw B.J., Handy R.D. 2007 Toxicity of titanium dioxide nanoparticles to rainbow trout (*Oncorhynchus mykiss*): gill injury, oxidative stress, and other physiological effects. Aquat. Toxicol. 84, 415-430.

Fent K., Weisbrod C.J., Wirth-Heller A., Pieles U. 2010. assessment of uptake and toxicity of fluorescent silica nanoparticles in zebrafish (*Danio rerio*) early life stages. Aquat. Toxicol. 100, 218-228

Finney D.J. 1971. Probit Analysis, 3rd. Cambridge University Press, Cambridge.

Franklin N.M., Rogers N.J., Apte S.C., Batley G.E., Gadd G.E., Casey P.S. 2007. Comparative toxicity of nanoparticulate ZnO, bulk ZnO, and $ZnCl_2$ to a freshwater microalga (*Pseudokirchneriella subcapitata*): the importance of particle solubility. Environ. Sci. Technol. 41, 8484-8490.

Gregory J. 2006. Particles in water: properties and processes. Taylor & Francis editors. Boca Raton, FL.

Griffitt R.J., Hyndman K., Denslow N.D., Barber D..S. 2009. Comparison of molecular and histological changes in zebrafish gills exposed to metallic nanoparticles. Toxicol. Sci. 107, 404-415.

Griffitt R.J., Weil R., Hyndman K.A., Denslow N.D., Powers K., Taylor D., Barber D.S. 2007. Exposure to Copper nanoparticles causes gill injury and acute lethality in zebrafish (*Danio rerio*). Environ. Sci. Technol. 41, 8178-8186.

Heinlaan M., Ivask A., Blinova I., Dubourguier H-C., Kahru A. 2008. Toxicity of nanosized and bulk ZnO, CuO and TiO_2 to bacteria *Vibrio fischeri* and

crustaceans *Daphnia magna* and *Thamnocephalus platyurus*. Chemosphere 71, 1308-1316.

Heinlaan M., Kahru A., Kasemets K., Arbeille B., Prensier G., Dubourguier H-C. 2010. Changes in the *Daphnia magna* midgut upon ingestion of Copper oxide nanoparticles: a transmission electron microscopy study. Water Res. DOI:10.1016/j.watres.2010.08.026

Ispas C., Andreescu D., Patel A., Goia D.V., Andreescu S., Wallace K.N. 2009. Toxicity and developmental defects of different sizes and shape Nickel nanoparticles in zebrafish. Environ. Sci. Technol. 43, 6349-6356.

Jani P., Halbert G., Langridge J., Florence A. 1990. Nanoparticle uptake by the rat gastrointestinal mucosa: quantitation and particle size dependency. J. Pharm. Pharmacol. 42, 821-826.

Johnston B., Scown T.M., Moger J., Cumberland S., Baalousha M., Linge K., van Aerle R., Jarvis K., Lead J.R., Tyler C.R. 2010. Bioavailability of nanoscale metaloxides TiO_2, CeO_2, and ZnO to fish. Environ. Sci. Technol. 44, 1144-1151.

Kaegi R., Ulrich A., Sinnet B., Vonbank R., Wichser A., Zuleeg S., Simmler H., Brunner S., Vonmont H., Burkhardt M., et al. 2008. Synthetic TiO_2 nanoparticle emission from exterior facades into the aquatic environment. Environ. Pollut. 156, 233-239.

Kahru A., Dubourguier H-C. 2010. From ecotoxicology to nanoecotoxicology. Toxicol. 269, 105-119.

Kahru A., Dubourguier H-C., Blinova .I, Ivask A., Kasemets K. 2008. Biotests and biosensors for ecotoxicology of metal oxide nanoparticles: a minireview. Sensors 8, 5153-5170.

Kasemets K., Ivask A., Dubourguier H-C., Kahru A. 2009. Toxicity of nanoparticles of ZnO, CuO and TiO_2 to yeast *Saccharomyces cerevisiae*. Toxicol. *in vitro* 23, 1116–1122.

Kashiwada S. 2006. Distribution of nanoparticles in the see-through medaka (*Oryzias latipes*). Environ. Health Perpect. 114, 1697-1702.

Krysanov E.Yu, Pavlov D.S., Demidova T.B., Dgebuadze YuYu. 2010. Effect of nanoparticles on aquatic organisms. Biol. Bull. 37, 406-412.

Lee K.J., Nallathamby P.D., Browning L.M., Osgood C.J., Xu X.N. 2007. *In vivo* imaging of transport and biocompatibility of single silver nanoparticles in early development of zebrafish embryos. ACS Nano 1, 133-143.

Lewinski N., Colvin V., Drezek R. 2008. Cytotoxicity of nanoparticles. Small 4, 26-49.

Luo S.Q., Plowman M.C., Hopfer S.M., Sunderman F.W.Jr. 1993. Embryotoxicity and teratogenicity of Cu^{2+} and Zn^{2+} for *Xenopus laevis*, assayed by the FETAX procedure. Ann. Clin. Lab. Sci. 23, 111-120.

Moore M.N. 2006. Do nanoparticles present ecotoxicological risks for the health of the aquatic environment? Environ. Internat. 32, 967-976.

Moos P.J., Chung K., Woessner D., Honneggar M., Shane Cutler N., Veranth J.M. 2010. ZnO particulate matter requires cell contact for toxicity in human colon cancer cells. Chem. Res. Toxicol. 23, 733-739.

Mouchet F., Landois P., Sarremejean E., Bernard G., Puech P., Pinelli E., Flahaut E., Gauthier L. 2008. Characterisation and *in vivo* ecotoxicity evaluation of double-wall carbon nanotubes in larvae of the amphibian *Xenopus laevis*. Aquat. Toxicol. 87, 127-137.

Nations S., Long M., Wages M., Canas J., Maul J.D., Theodorakis C., Cobb G.P. 2011. Effects of ZnO nanomaterials on *Xenopus laevis* growth and development. 2010. Ecotoxicol. Environ. Saf. 74, 203-210.

Nel A., Xia T., Mädler L., Li N. 2006. Toxic potential of materials at the nanolevel. Science, 311, 622-627.

Nieuwkoop P.D., Faber J. 1956. Normal table of *Xenopus laevis* (Daudin). Amsterdam: North Holland Publishing Co.

Oberdörster G., Oberdörster E., Oberdörster J. 2005. Nanotoxicology: an emerging discipline evolving from studies of ultrafine particles. Environ. Health Perspec. 113, 823-839.

Pope III C. A., Burnett R.T., Thun M.J., Calle E.E., Krewski D., Ito K., Thurston G.D. 2002. Lung cancer, cardiopulmonary mortality, and long-term exposure to fine particulate air pollution. JAMA 287, 1132-1141.

Prins F.A., Cornelese-ten Velde I., de Heer E. 2006. Reflection contrast microscopy: the bridge between light and electron microscopy. In Taatjes DJ, Mossman BT,

editors. Cell imaging techniques. Methods and protocols. Totowa: Humana Press. pp 363-401.

Saunders M. 2009. Transplacental transport of nanomaterials. WIREs Nanomed. Nanobiotechnol. 1, 671-684.

Scown T.M., van Aerle R., Tyler C.R. 2010. Do engineered nanoparticles pose a significant threat to the aquatic environment? Crit. Rev. Toxicol. 40, 653-670.

Sharma VK. 2009. Aggregation and toxicity of titanium dioxide nanoparticles in aquatic environment – a review. J. Environ. Sci. Heal.A. 44:1485-1495.

Steinbach P.J., Ionescu R., Matthews C.R. 2002. Analysis of kinetics using a hybrid maximum-entropy/nonlinear-least-squares method: application to protein folding. Biophys. J. 82, 2244-2255.

Thisse C., Thisse B. 2008. High resolution *in situ* hybridization on whole-mount zebrafish embryo. Nat. protoc. 3, 59-69.

Ward J.E., Kach D.J. 2009. Marine aggregates facilitate ingestion of nanoparticles by suspension-feeding bivalves. Mar. Environ. Res. 68, 137-142.

Wick P., Malek A., Manser P., Meili D., Maeder-Althaus D., Diener L., Diener P-A., Zisch A., Krug H.F., von Mandach U. 2010. Barrier capacity of human placenta for nanosized materials. Environ. Health. Perspect. 118, 432-436.

Yamamoto A., Honma R., Sumita M., Hanawa T. 2004. Cytotoxicity evaluation of ceramic particles of different sizes and shapes. J. Biomed. Mat. Res. 68A, 244-256.

Zhang Y., Chen Y., Westerhoff P., Hristovski K., Crittenden J.C. 2008. Stability of commercial metal oxide nanoparticles in water. Water Res. 42, 2201-2212.

Zhu X., Wang J., Zhang X., Cahng Y., Chen Y. 2009. The impact of ZnO nanoparticle aggregates on the embryonic development of zebrafish (*Danio rerio*). Nanotechnology 20, 195103

Zhu X., Zhu L., Duan Z. QI R., Li Y, Lang Y. 2008. Comparative toxicity of several metal oxide nanoparticle aqueous suspensions to Zebrafish (*Danio rerio*) early developmental stage. J. Environ. Sci. Health Part A 43, 278-284.

CHAPTER 4

Metal oxide nanoparticles induce cytotoxic effects on human lung epithelial cells A549

4.1 Abstract

The increase in production and exposure to engineered nanoparticles (NPs) makes necessary to acquire information about NP potential adverse health effects. Many studies, focused on NP toxicity, highlighted their cytotoxic potential but there is still a lack of information about the biological mechanisms involved. The aim of this research is the comparison of cytotoxicity between two types of metal nanoxides (nCuO and $nTiO_2$) on A549 cells. After physico-chemical characterization, NPs were administered to cells. Cell-particle interactions, pro-inflammatory potential, membrane integrity, and cell viability were investigated. nCuO exposure resulted in a significant reduction of cell viability and an increase in chemokines release, while no effects were observed after TiO_2 exposure. Both NPs induced cell cycle alteration, with a significant increase in frequency of cells in G1 and G2/M phases for $nTiO_2$ and nCuO respectively. Confocal microscopy detected NPs in different cell compartments, and TEM imaging highlighted their ability to be internalized as aggregates by phagocytic processes or even as small agglomerates free in the cytoplasm.

Keywords: *copper oxide, titanium dioxide, internalization, ultrastructure*

Parts of this chapter are contained in Moschini E., Gualtieri M., Gallinotti D., Pezzolato E., Fascio U., Camatini M., Mantecca P. 2010. Metal oxide nanoparticles induce cytotoxic effects on human lung epithelial cells A549. Chemical engineering transactions 22, 23-26.

4.2 Introduction

Nanometer-sized particles (<100nm) constitute a fraction of atmospheric particulate matter (PM) and, according to their origin, they are defined "ultrafine particles" (UFPs) or nanoparticles (ENPs). UFP is usually adopted to describe airborne particles deriving from combustion emissions; ENP indicates nanomaterials intentionally produced by industrial processes (Warheit et al., 2008). Because of their peculiar characteristics, frequently different from the bulk materials, ENPs find application in many different fields such as cosmetic, technological and pharmaceutical, allowing a remarkable increase in their production and utilization in the recent years. Therefore the environmental and occupational exposure to NPs is likely increasing and may represent a source of health risk, which determine an urgent need to develop rapid, accurate and efficient testing strategies to assess their biological effects (Hu et al., 2009). Among the different exposure routes, inhalation results to be the most critical; there are significant differences between NPs and larger particles regarding their distribution pattern into the respiratory system. Moreover the common mechanisms of clearance often results to be ineffective (Oberdoster et al., 2005). So inhaled nanosized materials can be both kept within the respiratory system or translocated to other target organs. Furthermore with a reduction in size, the properties can change dramatically regarding electrical conductivity, magnetic characteristics, hardness, active surface area, chemical and biological activity (Karlsson et al., 2008). Chemical analysis of UFPs has highlighted the high presence of metal oxide nanoparticles at sites surrounding factories, when compared to clean areas (Rogaczewska and Matczak, 1985), and epidemiological studies have reported a correlation between the level of UFP and the increase in pulmonary disease including exacerbation of bronchial asthma (Weichenthal et al., 2007). It has been

hypothesized that different MONs are able to generate oxidative stress and affect cell viability through the red-ox potential associated to transition metals (Fahmy et al., 2009), but the role of particle nanostructure in eliciting toxic mechanism remains to be fully understood. The aim of this study is to compare the biological effects induced by commercially available metal oxide NPs (CuO and TiO_2) on A549 lung epithelial cells. In particular we focused on potential cytotoxicity of these nanoxides, on their ability to be internalized in cell compartments and alter the cell cycle. We also investigated the ultrastructural modifications induced by such particles with TEM analysis.

4.3 Materials and methods

4.3.1 Particle suspensions preparation and characterization

CuO (<50nm) and TiO_2 (<100nm) NPs (Sigma-Aldrich) were suspended in ultrapure water, sonicated (1min) and diluted in PBS+BSA (0,1% final concentration) to optimize suspension stability. Working concentrations (1, 5, 10, 50, 100 μg/ml) were obtained by adding NP suspensions directly to culture medium (OptiMEM1X, 1%FBS). nCuO and $nTiO_2$ water suspensions have been observed by TEM (Jeol JEM-1220) to depict particle morphology and size distribution before and after being sonicated; while Dynamic Light Scattering (DLS) (ZetaPlus-Brookhaven Instruments Corporation) was used to assess either the mean size of NPs and their polydispersion into the aqueous medium. Detailed results of particle characterization were reported in Supporting information – PART II.

4.3.2 Cytotoxicity

A549 cells (American Type Culture Collection) were maintained in OptiMEM 1X, 10% FBS at 37°C and 5%CO_2. Cells were seeded in 12-well

plate and exposed for 3 and 24h to increasing concentrations of NPs. Cell viability was assessed by MTT assay and Neutral Red retention; the Optical Density (OD) measured respectively at 540 and 570 nm is proportional to cellular viability. The experiments were replicated at least 3 times and results were expressed as mean±SE. Statistical differences were tested by One-Way Analysis of Variance ANOVA followed by the Dunnett's method. To assess cell proliferation and membrane permeability we performed also the lactate dehydrogenase assay using TOX-7 kit (Sigma–Aldrich) according to the protocol.

4.3.3 Pro-inflammation signalling

For analysis of pro-inflammatory chemochine released in the supernatant we used DuoSet ELISA kits interleukin-8 (IL-8) (R&D Systems Minneapolis, MN) according to the manufacturer's protocols. Briefly, 96-well plates were coated with capture antibody and incubated overnight at room temperature. Supernatants of cultured cells were centrifuged in order to remove nanoparticles and cell debris and then they were added on the plate (100 µl per well). After 2h the detection antibody was loaded to each well for a further incubation. Finally we added streptavidin horseradish-conjugated and the peroxidase substrate. Reaction was stopped with H_2SO_4 and optical density of each well was read with multiplate reader (Multiskan Ascent) at 450nm using 630nm as a reference wavelength. Data were expressed as pg IL-8 /ml of supernatant (mean ±SE).

4.3.4 Cell cycle

After treatment (24h) cells were washed, detached and fixed in ice-cold absolute ethanol. After freezing (-20°C) they were incubated for 30mins (37°) with RNase-free DNase and then labeled with PI (10µM) at the dark. After 7 minutes 10 000 cells per sample were analyzed with EPICS XL-MCL flow cytometer to highlight cycle alterations. Data were analyzed

using the EXPO32 ADC software (Beckman-Coulter). To verify organization of mitotic spindle indirect immunocytochemistry of β-tubulin was performed using a FITC-conjugated secondary antibody.

4.3.5 Particle internalization

Treated cells were severely washed in PBS and fixed in 4% paraformaldheide. Mitochondria were stained with Mitotracker Red and nuclei with SYBR green (Molecular Probes) to be viewed under a Leica TCSNT confocal laser scanning microscope. NPs were imaged by laser reflection technique. For TEM imaging, cells were fixed in 2.5% glutharalheide, post-fixed in 1% OsO_4 and embedded in EPON-Araldite. Unstained ultrathin sections of 50nm thickness were directly inserted in the TEM (Jeol JEM-1220) operating at 80KV and images taken by a CCD camera.

4.4 Results

4.4.1 Particle characterization

TEM analysis confirmed the presence of differently sized aggregates, constituted of NPs well below 100nm for TiO_2 and 50nm for CuO. CuO appeared irregularly shaped, while TiO_2 had a spherical morphology. Mean diameters of 318nm and 613nm for CuO and TiO_2 suspensions (in medium) with a Polidispersity Index of 0,156 and 0,322 respectively were measured with DLS. Sonication did not affect significantly neither the mean diameter nor the size distribution of particles for both the oxides (Supporting Figures S1,S2, S4. Supporting information - PART II).

4.4.2 Cytotoxicity

After exposure to CuO, a time- and dose-dependent significant decrease in cell viability, either with NR (Supporting Figure S6A. Supporting information - PART II) or MTT test (Fig.1A) was observed. The dose-response curve for CuO-induced reduction in viability was estimated as an LC50 of 19,9 μg/ml (Supporting Figure S5. Supporting Information PART II). At the same testing conditions, no mortality was evident after TiO_2 exposure with both the two test applied.(Fig.1B; Supporting Figure S6B. Supporting information –PART II).

Intracellular LDH significantly decreased after 24h exposure to CuO (data not shown), corroborating the data from cell viability assays ($r^{2=}$ 0,923; $p<0,05$). Released LDH did not result in responsiveness, probably for some interactions between nCuO and detection molecules. This hypothesis is supported by cell free system experiments that showed a dose-dependent optical density decrease, when incubating LDH standard (0,25 IU/ml) with nCuO for 24h.

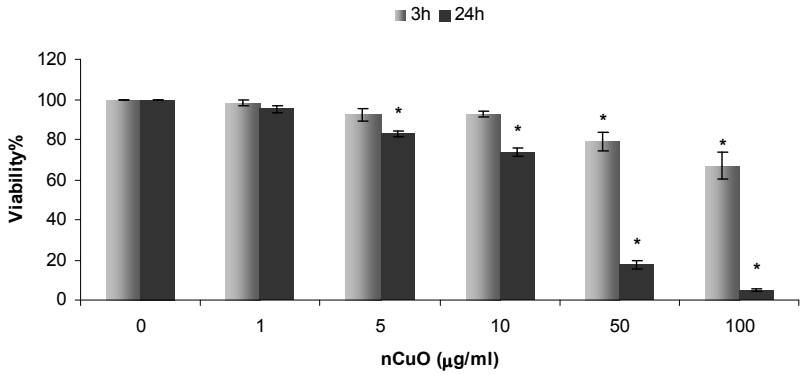

A

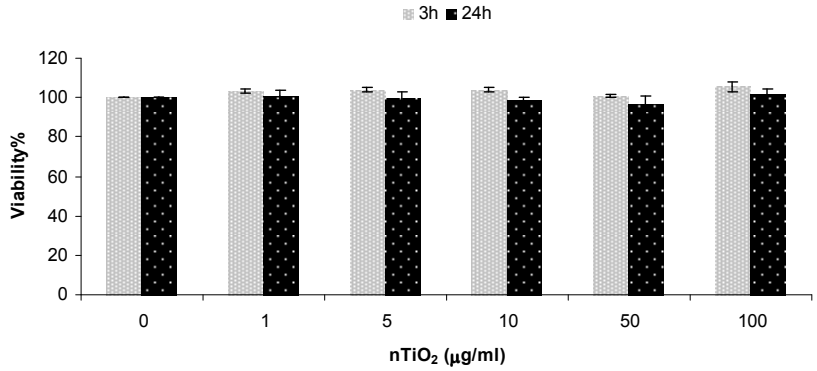

B

Fig. 1. A549 cell viability by MTT assay after exposure to nCuO (A) and $nTiO_2$ (B) for 3h (grey bars) and 24h (black bars). *Significantly different from control (One-way ANOVA + Dunnett's method; p<0,010).

4.4.3 Pro-inflammation signaling

We assessed IL-8 release in the supernatant as marker of pro-inflammatory potential of $nTiO_2$ and nCuO. As reported in Fig. 2 we observed a significant increase in IL-8 production only for cytotoxic concentrations of nCuO after while treatment with titanium dioxide didn't cause IL-8 at the time points investigated.

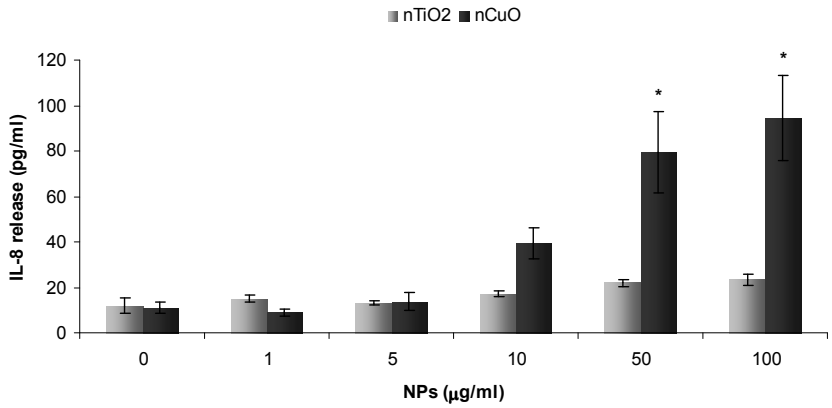

Fig. 2. IL-8 release in colture medium of A549 exposed to increasing concentrations of $nTiO_2$ and nCuO (24h). * Significantly different from control (One-way ANOVA + Dunnett's method; p<0,010).

4.4.4 Cell cycle

The ability of NPs to interact with the cell growth resulted also in a significant alteration of the cell cycle. Fig. 3 shows A549 cell cycle profile after exposure to increasing concentrations of both metal oxides. After 24h of exposure nCuO induced an increase in the frequency of cell at G2/M phase (from 13,6% to 32,1%) while $nTiO_2$ induced a slight increase in frequencies of cells at G1 phase, starting from 10µg/ml (from 63,1% to 73,8%), when compared to the control. Fluorescence microscopy of β-tubulin immunostained cells exposed to nCuO (10µg/ml for 24h) highlighted a serious microtubule alteration supporting this findings (Fig. 4)

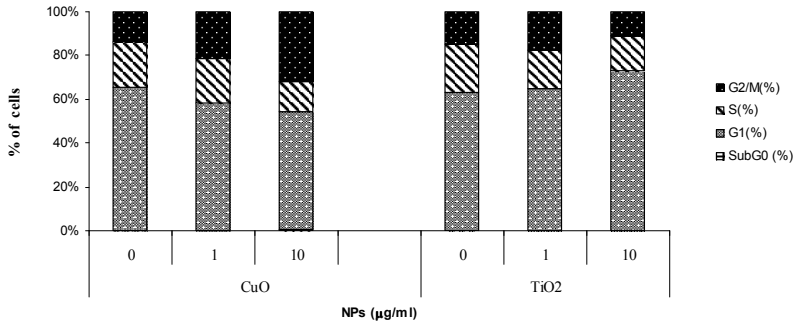

Fig.3. Representative A549 cell cycle frequencies distribution after exposure to increasing concentration of nCuO or $nTiO_2$

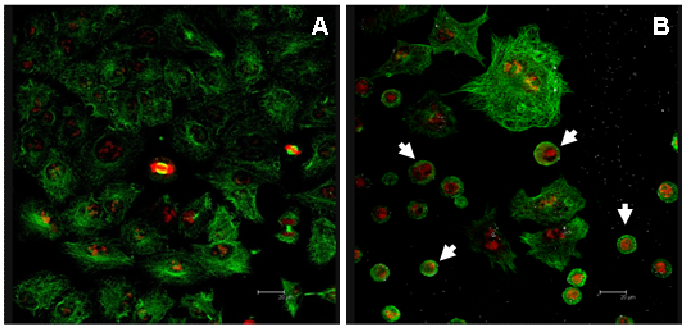

Fig.4. Confocal images of A549 cells immunostained for β-tubulin. A) Control cells; B) nCuO-treated cells (10µg/ml, 24h) with altered microtubules organization (white arrows).

4.4.5 Cell-particle interactions

Different microscopy techniques were applied to better localise the internalised particles. Fig.5 shows interaction and internalization of CuO (c,e) and TiO_2 NPs (b,d) respectively into mitochondria and nuclei (e,d; white bright spots) detected by confocal reflection. Cell-NPs interaction and uptake was quantitatively detected by flow cytometer as increase in laser side scatter (SS) in exposed cells (data not shown). SS can be considered a marker of an augmented cytoplasmic complexity due to NP interactions. TEM analysis evidenced the internalization and subcellular localization of metal oxides and the alterations induced by NPs. Both NPs were internalised into cytoplasm as free aggregates or phagocytised agglomerates (Fig.6b,e,f). In particular nCuO showed an evident ability to modify the cell ultrastructure (Fig. 6c,d). TiO_2 NPs induced slight ultrastructural modifications only at late exposure time (Fig. 6g).

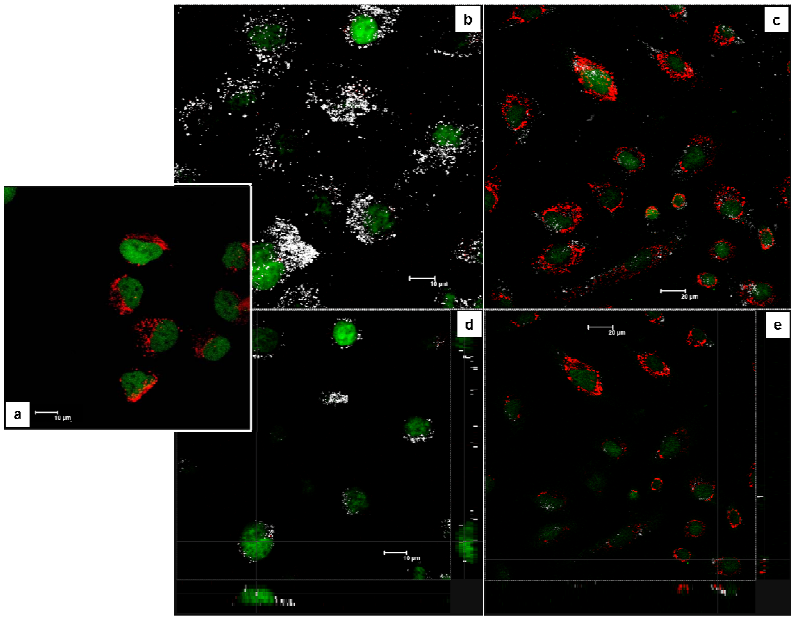

Fig.5. Cell-Particle interaction and uptake detected by confocal microscope in reflection mode: a) control cells b) orthogonal section of $nTiO_2$- treated cells covered by NPs; c) orthogonal section of nCuO- treated cells d) $nTiO_2$ in nucleus; e) nCuO inside the mitochondria.

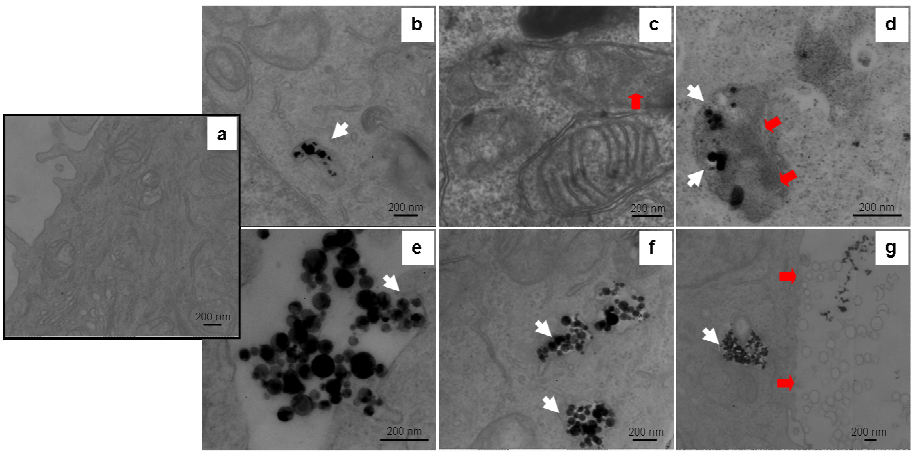

Fig.6. Cell-particle interactions by TEM: a) Cell control; b) internalisation of nCuO (white arrow); c,d) early (3h) damages induced by nCuO (red arrows); e,f) internalization of TiO_2 (white arrow); g) late effects of TiO_2 on membranes (24h) (red arrows).

4.4 Discussion

Although it is reasonable to assume a correlation between metal oxides NPs exposure and increasing in pulmonary or respiratory diseases, there is still a lack of information about the toxicity of these materials on biological systems. Currently MONs, such as nCuO, are reported to display cytotoxicity in *in vitro* studies (Karlsson et al., 2008; 2009; Fahmy et al., 2009), but results may differ depending on many factors such as cell type, NP administration conditions and test sensitivity.

In this work, exposure of A549 cells to nCuO resulted in a time- and dose-dependent cytotoxicity with a significant decrease in cell viability starting from the dose of 5μg/ml. Hence nCuO has to be considered a powerful cytotoxic agent. When exposed to 100 μg/ml nCuO, cell mortality reach about 30% and 100% after 3 and 24h respectively (Fig.1A). Basing on the present data, the LC50 for nCuO was 19,9 μg/ml, quietly higher than that of

10μg/ml measured by Lanone et al., (2009) at very similar experimental conditions (Supporting Figure S5. Supporting Information - PART II). In contrast, no significant cytotoxicity was registered in $nTiO_2$-treated cells (Fig.1B).

Different findings are reported in literature regarding pro-inflammatory potential of metal oxide nanoparticles. In some cases, the activation of pro-inflammatory factors such as IL-1, IL-6, IL-8 and MIP has been found after exposure of human cell lines to MONs. In our study assessing of pro-inflammatory potential by measure of IL-8 release testify that cytotoxic concentrations of nCuO determine also a significant chemokine release after 24h of treatment. In contrast no significant IL-8 release was detected after A549 exposure to $nTiO_2$.

Also the cell cycle progression resulted significantly affected in nCuO-treated cells as well as the spindle machinery assembly. Cells treated with nCuO arrested in G2/M phase and did not duplicate; coupled with the microtubules disorganization, this effect may be ascribed either to DNA damage, already reported for CuO NPs, or to disregulation of intracellular calcium homeostasis for the disruption of the membrane systems.

As shown by TEM analysis, nCuO, was able to induce alteration of the cell and mitochondrial membranes as preliminary event, pointing to a rapid evolution of the cytotoxic pathways leading to the cell necrosis. The localization of nCuO near to these organelles was testified also by confocal images.

Exposure to $nTiO_2$ resulted in a massive internalization of particles as shown by both confocal and TEM analysis. Although cells were treated with the same concentration of NPs (Fig. 5) the quantity of particles interacting with the cell membranes appeared higher in $nTiO_2$ treated cells (Fig.5b). This fact could be due to the aggregation phenomena which characterise TiO_2 nanoparticles. The interaction between cells and $nTiO_2$ brings to structural

damage only at the late exposure stages, as visible in Fig. 6g; while cell viability does not seem be affected by this effect.

An alteration of the cell cycle progression in $nTiO_2$-treated cells was observed, therefore hidden effects induced by these particles cannot be excluded.

Moreover the mechanisms of NPs uptake and the molecular pathways during the initial cell responses are still unclear and need much more investigative effort to properly characterize their potential mechanisms of pulmonary toxicity.

References

Fahmy B., Cormier S. A. 2009. Copper oxide nanoparticles induce oxidative stress and cytotoxicity in airway epithelial cells, Toxicol. In Vitro, 23, 1365–1371.

Hu X., Cook S., Wang P., Hwang H-M. 2009. In vitro evaluation of cytotoxicity of engineered metal oxide nanoparticles, Sci. Total Environ., 407, 3070–3072.

Karlsson H.L., Cronholm P., Gustafsson J., Möller L. 2008. Copper oxide nanoparticles are highly toxic: a comparison between metal oxide nanoparticles and carbon nanotubes, Chem. Res. Toxicol. 21, 1726–1732.

Karlsson H., Gustafsson J., Cronholm P., Möller L. 2009. Size-dependent toxicity of metal oxide particles-A comparison between nano- and micrometer size, Toxicol. Lett. 188, 112-118.

Lanone S., Rogerieux F., Geys J., Dupont A., Maillot-Marechal E., Boczkowski J., Lacroix G., Hoet P. 2009. Comparative toxicity of 24 manufactured nanoparticles in human alveolar epithelial and macrophage cell lines, Part. Fibre Toxicol. 6, 14.

Oberdörster G., Oberdörster E., Oberdörster J. 2005. Nanotoxicology: An Emerging Discipline Evolving from Studies of Ultrafine Particles, Environ. Health Persp. 113, 823-839.

Rogaczewska T., Matczak W. 1985. Evaluation of occupational exposure to cadmium based on air analysis of the work area. I. Cadmium oxide level in the

air of work areas in a cadmium and nickel cumulator factory, Med. Pr. 36, 273–279.

Warheit D. B., Sayes , C.M., Reed, K.L., Swain K.A. 2008. Health effects related to nanoparticle exposures: Environmental, health and safety considerations for assessing hazards and risks, Pharmacol. Ther. 120, 35–42.

Weichenthal S., Dufresne A., Infante-Rivard C. 2007. Indoor ultrafine particles and childhood asthma:exploring a potential public health concern. Indoor Air 17, 81–91.

CHAPTER 5

The role of ion dissolution and particle internalization in nCuO-induced cytotoxicity

5.1 Abstract

Copper oxide nanoparticles are widely diffused in industry and in bio-applications as additive for inks, ingredient for polymers, coating in antimicrobial textiles. Several concerns about human safety of this material arise from its use in cosmetic products (powders and sprays), which lead to human potential exposure by contact and inhalation. Some toxicological studies on mammalian cell lines described nCuO as high cytotoxic and likely genotoxic but the role played by different chemical-physical properties in promoting the adverse effects have not been enough clarified. Among the mainly causes of cytotoxicity, copper release has been investigated but the extent of its effect is different depending on the experimental conditions adopted and the biological model used. Using nCuO as a representative toxic transition metal oxide nanoparticle we investigated the contribution of both extracellular release of copper ions and intracellular dissolution of particles to the cytotoxic events occurring in the A549 cell line.

Exposure to copper ions obtained from nCuO suspensions resulted to be cytotoxic only at the highest concentrations after 24h of treatment, suggesting that particles themselves have a key role in determining the early events responsible for cell injuries. Concomitantly CuO NPs were abundantly internalised in cells by endocytic processes (although it did not appear the unique mechanism by which NPs are taken up), allowing cells to be massively and rapidly loaded by nCuO. These events have been ssociated

ith diffuse oxidative damages , retained to be the main nCuO-mediated effects driving cells to death.

5.2 Introduction

In vitro exposure to nanoparticles can determine adverse effects on cultured cells as a results of multilevel interactions. If we consider, for example, soluble nanocompounds, the first factor inducing cytotocity can be the extracellular dissolution of particles. For completely soluble nanoparticles the toxic potential is likely totally dependent upon the ions dissolved; for partially soluble NPs the degradation of particles may or not contribute to some extent to the effects observed. The second level of action could be represented by the physical interaction between NP and plasma membrane. Particles can be recognised by specific receptor inducing cell death signalling cascade or could generate local alterations of the equilibrium, for example by inducing reactive oxygen species or directly interacting with the molecular components of plasma membrane. (Nel et al., 2009; Martineniate et al., 2011).

The studies performed on different culture cells highlighted the ability of nanoparticles to permeate the membrane or to be also internalised as aggregates or single objects through endocytic processes, diffusion or other mechanisms. Once inside the cell they may interact with intracellular organelles and macromolecules and their toxic behaviour may vary significantly according to several physical-chemical properties, like particle solubility and surface reactivity.

5.2.1 Extracellular copper release

Although metal oxide nanoparticles are commonly considered as insoluble compounds in aqueous media, in certain conditions the dissolution of metal

ions can occur and may contribute to the toxicity of the NPs. Chemical stability of the particles (release of cations), coupled with catalytic properties, is considered one of the most important parameter determining the cytotoxic potential of metallic nanomaterials (zero-valent metals, metal oxides) (Auffan et al., 2008). Zinc and copper oxides (Brunner et al., 2006; Franklin et al., 2007; Aruoja et al., 2009; Karlsson et al., 2008), as well as cobalt oxide (Limbach et al., 2007), showed high cytotoxicity in *in vitro* experiments mainly as a consequence of the particles' solubility. Hence, in nanotoxicological studies , it is essential to distinguish the effects induced by ions dissolved from NPs to that produced by the NPs themselves (Lei et al., 2008).

The amount of ions released depends on particle characteristics (Midander et al., 2009), but even on the properties of the medium. Some studies also indicate that the oxidation state of particle surface can affect the dissolution rate of metal-based nanoparticles. Assessing the antimicrobial effect of CuO and Cu nanoparticles embedded in propylene matrix, Delgado et al. (2011) found that metal dissolution from copper oxide nanoparticles was easier than ion release from Cu nanoparticles. In CuO NPs copper is already at the highest oxidation state so the only mechanism for ion release is the dissolution of the particles. On the contrary, Cu NPs previously require the formation of an oxide layer. The role played by the cover shell of copper oxides in promoting the dissolution/corrosion processes of CuNPs in acidic conditions was reported also in Elzey and Grassian (2010).

In contrast with these considerations Midander et al. (2009) showed no significant differences in copper release from Cu NPs and CuO NPs after 4h of incubation in PBS or DMEM+. Further they found that sonication of particle suspensions in DMEM+ significantly increased the dissolution rate for both nanoparticles, especially for Cu NPs.

5.2.2 Intracellular copper release

Cation release from metal oxide nanoparticles can occur both in the extracellular environment (culture medium) and in the intracellular compartments. Although copper is an essential element for life, it is toxic at high concentrations (Martineniate et al., 2011). Copper ions can be responsible for increased reactive oxygen species levels, DNA damage, and induction of apoptosis (Rana 2008).

Usually the cell membrane is an efficient barrier against the entry of many ions that can be *per se* cytotoxic (Xia et al., 2008). Besides several studies (Limbach 2007; Kim et al., 2009; Foldberg et al., 2010) indicate that nanoparticles are easily internalised by cells in comparison to the parental metal ion. In particular in Studer et al. (2010) presence of carbon-coated copper nanoaparticles (C/Cu) inside the cells was detected by SEM. The metal nanoparticles were found enclosed in vesicles most likely in lysosomes as earlier found for engineered oxide nanoparticles but the internalization process is not still well described.

Once inside the cell, and especially when encapsulated in the, lysosomal compartment, NPs can dissolve, thanks to the low pH values and to the presence of chelating agents. This process, known as “Trojan horse mechanism” (Limbach et al., 2007), determines an intracellular release of free transition metal ions that can compromise internal homeostasis after rupture of lysosomes, changes in osmotic pressure and generation of radicals inside the cells (Brunner et al., 2006; Karlsson et al., 2009; Midander et al., 2009). Usually the evaluation of intracellular particle dissolution is made by simulating lysosomal metal release with artificial lysosomal fluid (ALF) in cell free experiments (Studer et al., 2010; Cho et al., 2011). This allows to calculate the theoretical degree of particle dissolution under conditions similar to those found intracellulary, but on the other hand it is not possible to verify where this process occurs and its real extent after the direct exposure of cells to metal oxide nanoparticles.

The aim of this work was 1) to estimate the contribution to cytotoxicity of the copper ions dissolved from CuO NPs in the culture medium; 2) to verify the intracellular copper release and lysosomal leakiness after internalisation of particles.

We simulated external metal dissolution by incubating NPs in cell culture medium in a cell free system. After having removed particles by centrifugation, the copper concentration in the supernatant was measured with atom absorption spectroscopy. Intracellular dissolution was evaluated by cytochemical technique using a specific molecule (5,4 dimethylaminobenzylidene-rhodanine) for detection of copper ions. These measurements related to copper ion dissolution, both intracellularly and extracellularly, were investigated parallel to cell viability, stress and morphological markers to bridge the cytotoxic effects with the real bio-availability either of NPs or dissolved ions.

5.3 Materials and methods

5.3.1 Reagents

Standard copper oxide nanopowder (CuO<50nm; cod. 544868), 3-(4,5-dimethylthiazol-2-yl)-2,5-diphenyltetrazolium bromide (MTT), 5,4dymethylaminobenzylidene rhodanine (DMABR) were purchased from Sigma-Aldrich (Milan, Italy). A549 cells (American Type Culture Collection) were obtained from LGC Promochem (Sesto S. Giovanni, Italy). The fluorescent probe Lysotracker Red, were purchased from Invitrogen (U.S.A).

5.3.2 Particle characterization

The NPs' morphology, size and hydrodynamic behaviour were characterized by transmission electron microscopy (TEM) and dynamic light scattering (DLS).

Just prior the analyses, NPs were weighted in a micro-balance, suspended in MilliQ water and sonicated with a Ultrasonic bath Soniprep 150 MSE (Sanyo) for 1 min to reduce particle agglomeration.

For TEM imaging, droplets of 5µl of NP suspensions were placed onto Formvar©-coated 200 mesh copper grids, allowed to deposit for 3 min and finally water was gently blotted using filter paper. Once dried, grids were inserted in a Jeol JEM-1220 electron microscope and observed at an acceleration voltage of 100KV. Digital images were taken with a Gatan CCD camera.

The milliQ -stock solutions were supplemented with bovine serum albumine as dispersion stabilizer (0,1% final concentration) and mixed to culture medium just prior to cell exposure. The agglomeration status of particles and Z-potential were determined by DLS using a Zetasizer nano ZS (Brookheaven Instruments).

Soluble copper release from CuO NPs suspensions was analysed by Atomic Absorption Spectroscopy (AAS) using a Perkin Elmer-SIMAA6000. Briefly NPs were suspended in the cell medium and incubated for 24h at 37°C, 5%CO_2; these suspensions were then centrifuged at 12000 g at 4°C for 30 min to remove copper nanoparticles. Supernatants were acidified with 2%HNO_3 and immediately analyzed by AAS. Each sample was read in triplicate and a five point standard curve was used to calculate copper concentrations in culture medium.

5.3.3 Cell culture and treatments

A549 cells (American Type Culture Collection) were routinely maintained at 37°C, with 5% CO_2 in OptiMEM medium at pH 7.2, supplemented with

10% inactivated foetal bovine serum (FBS) and 1% penicillin/streptomycin. To evaluate the contribute to cytotoxicity of extracellular copper ions release from particles cells were exposed in parallel to 1) particle suspensions (nCuO) at working concentrations of 1, 5, 10, 50, 100 μg/ml prepared as described in *Chapter 4*; 2) copper ions released in medium from each of these concentrations after separation of particles by centrifuge; 3) copper ions from soluble salt ($CuSO_4 \cdot 5H_2O$) at concentrations comparable to those measured in (2) by AAS.

Concentration values of nCuO, copper ion released in medium and copper ion from soluble salt used for our treatments were reported in Supporting Table S2 (Supporting information - PART II).

5.3.4 Contribution of NPs and dissolved copper ions to cytotoxicity

For the cytotoxicity tests, cells were seeded at a concentration of $1{,}0x10^5$ in 12-well plates. After 24h from seeding, once reached 70-80% confluence, they were exposed to the conditions previously described.

At 3h and 24h post-exposure to nCuO, MTT assay were performed to assess cell viability. Cells were rinsed with PBS and MTT [3-(4,5-dimethylthiazol-2-yl)-2,5-diphenyltetrazolium bromide] at a final concentration of 0.3 mg/ml in OPTIMEM 10%FBS was added for 3-4h according to the method of Moossmann (1983). The medium was removed and the purple MTT reduction product (formazan crystals) was dissolved in DMSO. The absorbance of each sample, proportional to cell viability, was measured with a multiplate reader spectrophotometer (MultiskanAscent -Thermo) at 570nm, using 690nm as a reference wavelength. Cell viability was expressed as OD percent in comparison to the control (± standard error of the mean). In order to detect possible OD modifications due to the presence of particles not correctly removed we centrifuged representative samples after formazan salt solubilisation and then we measured the relative absorbance. Statistical

differences were tested by One-Way Analysis of Variance ANOVA followed by the Dunnett's method.

5.3.5 Endocytosis of particles

The role of endocytosis as NP-internalizing process was assessed with microscopic technique by immunocytochemistry of Rab5 and Rab7, specific markers for early (EE) and late endosomes (LE) respectively. Cells were seeded onto glass coverslips and vesicle formation were evaluated after 1,3,6 h of treatment. At the end of the exposure cells were rinsed with ice-cold PBS, fixed in 4% paraformaldheyde (20min) and then permeabilised with PBST solution (0,1% TritonX, 2%BSA in 0,1% Tween Phosphate Buffer Solution). Then they were incubated overnight in a wet chamber with the primary antibody at dilution of 1:500 in PBS 1%BSA (anti-Rab5 polyclonal antibody or anti-Rab7 polyclonal antibody - Cell Signaling, Boston, USA). AlexaFluor488 and AlexaFluor594 were used as secondary antibodies at dilution 1:200 in PBS 1%BSA (Invitrogen, CA, USA) to detect respectively early and late endosomes. Finally coverslips were rinsed, mounted on slides with ProLong Antifade (Invitrogen, CA, USA) and observed with Axioplan Zeiss 4.1 microscope.

5.3.6 Early lysosomal functionality

Cells were exposed to particle suspensions (10μg/ml) for 3h and 6h; then were washed and incubated with Lysotracker Red (90 min, 37°C, 5%CO_2) in complete medium. They were rinsed, detached and suspended in phosphate buffer saline for the cytometric analysis. Side scatter, forward scatter and fluorescence intensity of 10 000 events was measured by cytometer EPICS XL-MCL (Beckman-Coulter) using FL3=625nm band pass filter and the data were analyzed using the EXPO32 ADC software (Beckman-Coulter). Gates were made including at least the 90% of total cells analysed.

The experiment was replicated three times in duplicate and the data were expressed as mean% of fluorescence respect to the control (±SE).

5.3.7 Intracellular copper detection

A549 were growth onto glass coverslips and exposed to CuO suspensions (10 μg/ml) for 3h,6h and 24h.

At the end particles were removed and the monolayer was fixed with 10% neutral buffered formalin at room temperature. Cells were wash in several changes of distilled water and then incubated with 5,4-dimethylaminobenzylinene-rhodanine working solution (0,12 g/L) at 37°C, overnight. After several rinses with distilled water the coverslips were stained with pure Mayer's Haemalaun (1min) and then differentiated in water. Coverslips were mounted in a glycerol based medium and observed with Axioplan Zeiss 4.1 microscope.

5.3.8 Lipid peroxidation (LPO)

Detection of aldhehydic products of LPO were performed by immunostaining of 4- Hydroxy-2-nonenal (4HNE). Cells were seeded onto glass coverslips and exposed for 3 and 24h to a sub-lethal concentration of nCuO suspensions (10μg/ml). Then they were fixed in cold 4% paraformaldheide for 30 min, rinsed in PBS and incubated 20 min in 1% H_2O_2 in methanol for the quenching of the endogenous peroxidases. Non-specific binding was blocked with 10% Normal Horse Serum (NHS) (Elite® ABC Kit, Vectastain Laboratories, Burlingame, CA) in a humid chamber at RT. Sections were incubated with monoclonal antibody against 4-Hydroxy-2-nonenal (anti-4-HNE) at 25μg/ml (JaICA, Japan) overnight at 4°C in a humid chamber. Slides were then washed in PBS and incubated with secondary horse anti-mouse antibody conjugated to biotin (ABC Kit) for 1h at RT and washed again in PBS. The Avidin-Biotin complex conjugated with horseradish peroxidase (ABC Kit) was added on each section for 30

min at RT and after three washing with PBS, slides were incubated in 0.75 mg/ml DAB and 0,3‰ H_2O_2 in PBS for 7 min. Slides were abundantly washed in tap and distilled water and then nuclei were counterstained with Mayer's Haemalaun. Lastly they were mounted in a glycerol based medium and observed with a light microscope.

5.3.9 Transmission electron microscopy

Ultrastructural details and endocytosis in nCuO- exposed cells were investigated by TEM. Confluent cell monolayers were directly fixed on dishes with 2.5% glutaraldehyde in 0.2M cacodilate buffer, pH 7.6 for 30min and post-fixed with 1% OsO_4 in the same buffer for 2h. After repeated washings, cells were pre-stained with 1% uranyl acetate for 90 min at the dark, dehydrated in a graded ethanol series and routinely embedded in EPON/Araldite resin. Frontal 60nm ultrathin sections of the cell layers were obtained by Reichert Ultracut Jung E and, placed onto 300 mesh copper grids and then stained with uranyl acetate and lead citrate.

Finally, the grids were viewed with a Jeol JEM1220 TEM operating at 80kV and digital images were taken with a Gatan CCD camera.

5.4 Results

5.4.1 Characterization of particles

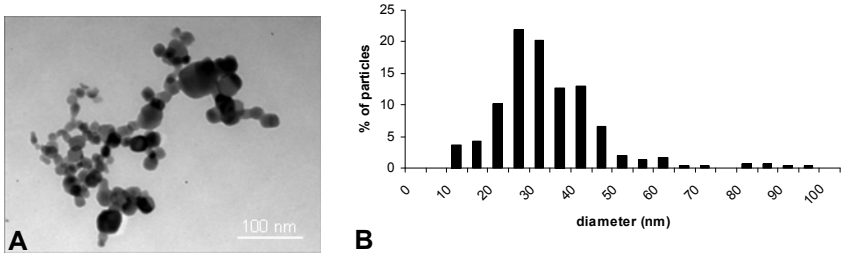

Fig.1 TEM analysis of of nCuO A) particle morphology; B) particle size distribution.

Tab.1. nCuO description and physical chemical characterization

Particle	Particle size in powder [a]	Surface area [a] [m2/g]	mean diameter in powder [b] [nm]	Average size in powder [b] [nm]	mean diameter in solution [c] [nm]	PDI [c]	Z-pot H2O [c] [mV]	max Cu++ release (24h) [d] [μg/ml]
nCuO	<50	29	34	10-50	318	0,156	-20,5 ± 1,6	38

[a] according to the manufacturer Sigma-Aldrich; [b] measured by TEM; [c] measured by DLS; [d] detected by AAS

TEM analysis revealed particles with an irregular shape (Fig.1) and a size distribution ranging from 10 to 50nm and mean diameter of 34nm. Particle size changes dramatically when nCuO was suspended in culture medium: DLS detected the presence of two populations of particles (Supporting Figure S3b. Supporting information - PART II) with a global mean diameter of 318,3nm and a polydispersion index of 0,156 (Table1).

The Z-potential measured in ultrapure water at pH 7 demonstrated a condition of incipient instability of CuO NPs, as defined by a Z value ranging from -30 mV and +30mV.

Despite the use of BSA (0.1% final concentration) as biological stabilizing agent in NP suspensions, these results showed the tendency of CuO NPs to agglomerate once dispersed in culture medium.

Assessing of copper release by particle was evaluated by AAS; significant metal dissolution was observed in nCuO supernatants (data not shown) with a maximum cumulative release found after 24h of incubation in culture medium (CuO 100μg/ml)(Tab.1).

5.4.2 Contribution of NPs and dissolved copper ions to cytotoxicity

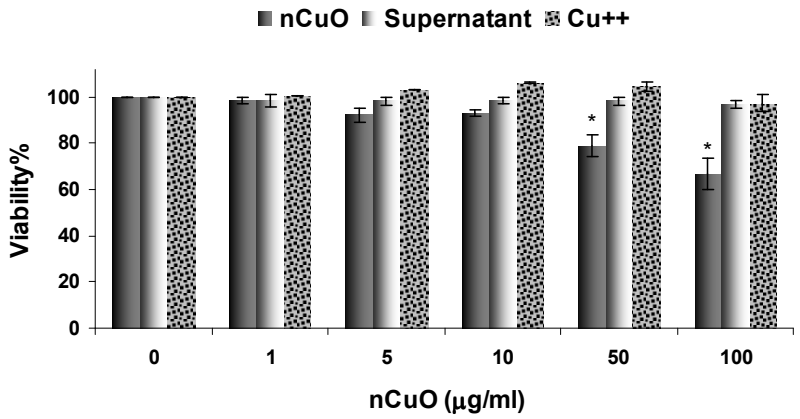

A

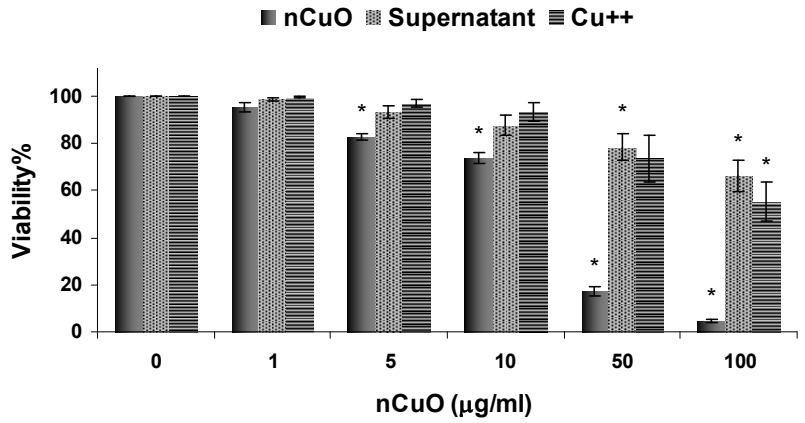

B

Fig.2. Cell viability by MTT assay in A549 cells after exposure for 3h (A) or 24h (B) to: particle suspensions (nCuO); copper ion released from particles (Supernatant); soluble copper from $CuSO_4 \cdot 5H_2O$ (Cu^{++}). Concentrations reported on x-axis are referred to the particle suspensions in medium. Viability data are expressed as mean % to the respect of control (± SE) * Significantly different when compared to control (One-way ANOVA + Dunnet's method; $p<0,010$).

The first objective of the work was to compare the viabilities after cell exposure to nCuO suspensions at increasing concentration or to the NP

soluble fractions containing dissolved metal ions from the correspondent suspensions. Accordingly, viability tests were performed as following 1) with increasing concentrations of particle suspensions; 2) with supernatants obtained from centrifugation of particle suspensions; 3) with a solution of copper ions obtained from a soluble copper salt ($CuSO_4$), using the same concentrations of Cu detected by AAS in the supernatants. The results obtained after cell incubations for 3h and 24h are reported in Fig. 2. Fig.2B shows that copper ions induced a significant reduction of cell viability at 24h, but the effects of the NP suspensions is much more higher. At 3h exposure time only nCuO affected cell viability, while solutions of copper ions did not do it even at the highest concentrations tested (Fig.2A). These observations suggested that NPs, rather than dissolved copper ions, were responsible for the initiation of the cytotoxic events.

5.4.3 Internalization of particles

It was already stated that CuO NPs are effectively taken up by A549 cells (*Chapter 4*) and that already at 3h post-exposure, ultrastructural defects were present concomitantly to a relatively abundant masses of NP internalized in cells. Anyway the induction of active endocytic processes was already observed after 1h of exposure, as shown in Fig.3. At these conditions, under TEM, NPs were in fact mapped inside vesicle buds and cytoplasmic membrane-surrounded vesicles, testifying the beginning of the endocytic process. Fluorescent labelling of endocytic structures revealed as the internalization of nCuO involves the maturation of early vesicles into late endosomes characteristic of CME process (Fig.4 b,d).

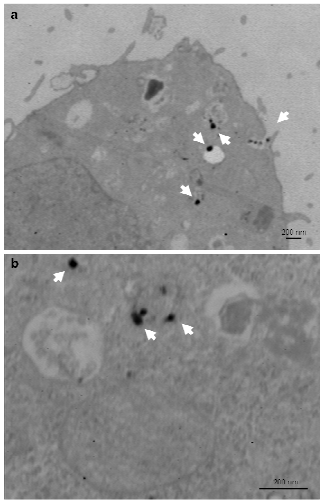

Fig. 3 a) Uptake of nCuO by endocytic process;
b) endocytised particles in vesicles and lysosomes.

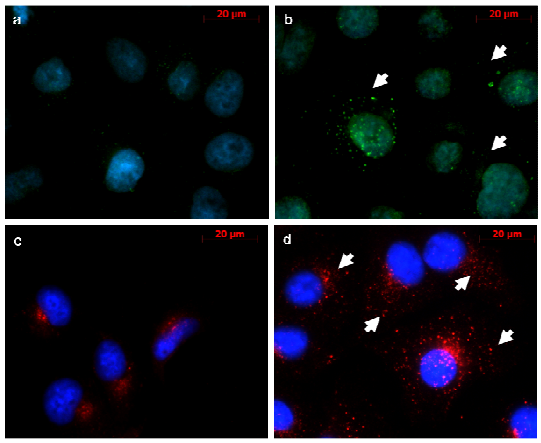

Fig.4. Formation of endocytic vescicles detected by labelling of early endosomes (green spots) an late endosomes (red spots).Nuclei were stained in blue. a,c)Control cells; b,d) nCuO treated cells 10µg/ml

5.4.4 Lysosomal functionality/integrity

By staining cells with the lysosomal fluorescent probe Lysotracker Red, the status of the lysosomal activity in nCuO exposed cells was investigated with cytometric techniques. As shown in Fig.5 a significant decrease of fluorescence intensity was observed after 3h and 6h of exposure to nCuO. At the same exposure condition, soluble Cu^{++} at 40µg/ml did not cause reduction of lysosomal activity (data not shown), confirming that the effect observed is attributable to particle exposure. Fluorimetric analysis of particle suspensions incubated with Lysotracker in a cell-free system allowed to exclude a fluorescence decrease due to quenching or interaction between nCuO and the fluorescent probes used. The effects on lysosomes were clearly seen also under the fluorescent microscope (Fig. 6).

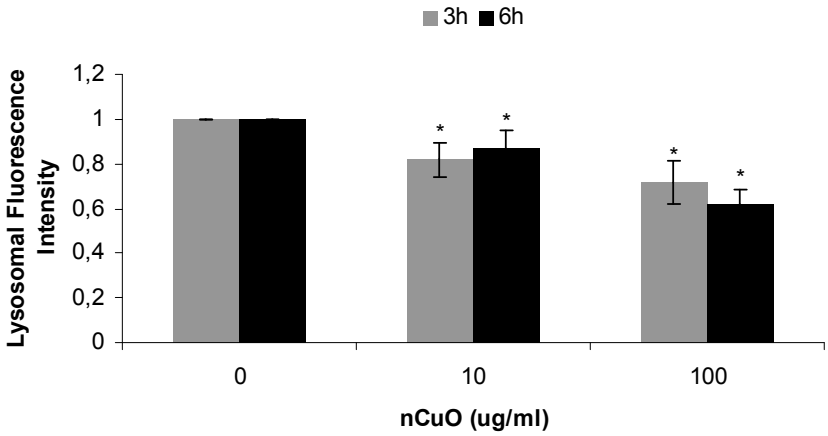

Fig.5 Decrease of lysosomal fluorescence intensity in A549 exposed to increasing concentration of nCuO after staining with Lysotracker Red. Data are expressed as mean % respect to the control (±SE). * Significantly different from control (one-way ANOVA + Dunnett's method; $p<0,01$).

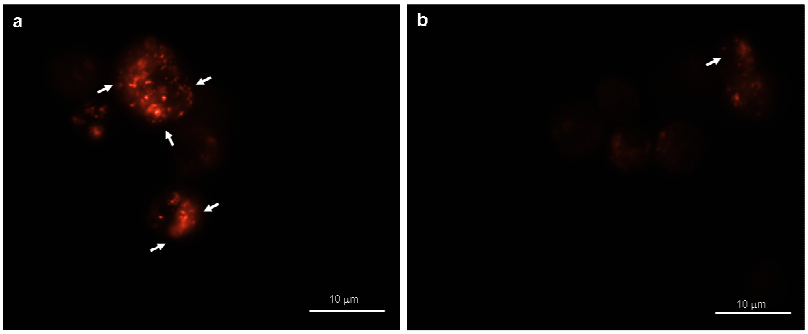

Fig.6 Representative images of lysosomal fluorescence (white arrows) in A549 stained with Lysotracker Red; (A) Control cells; (B) A549 exposed for 3h to nCuO at 10 µg/ml.

5.4.5 Does intracellular copper release drive cytotoxic effects?

The intracellular copper release was evaluated with DMABR staining. Fig.7 showed that metal dissolution was not detectable at early exposure times, since at 3h and 6h no formation of the red DAMBR-Cu precipitate was found in nCuO exposed cells (Fig. 7b,c).

Massive intracellular copper dissolution was instead observed at 24h of treatment (Fig. 7d), when cell viability was decreased by a 25% to the respect of the control (nCuO 10 μg/ml) (Fig. 1A, *Chapter 4*).

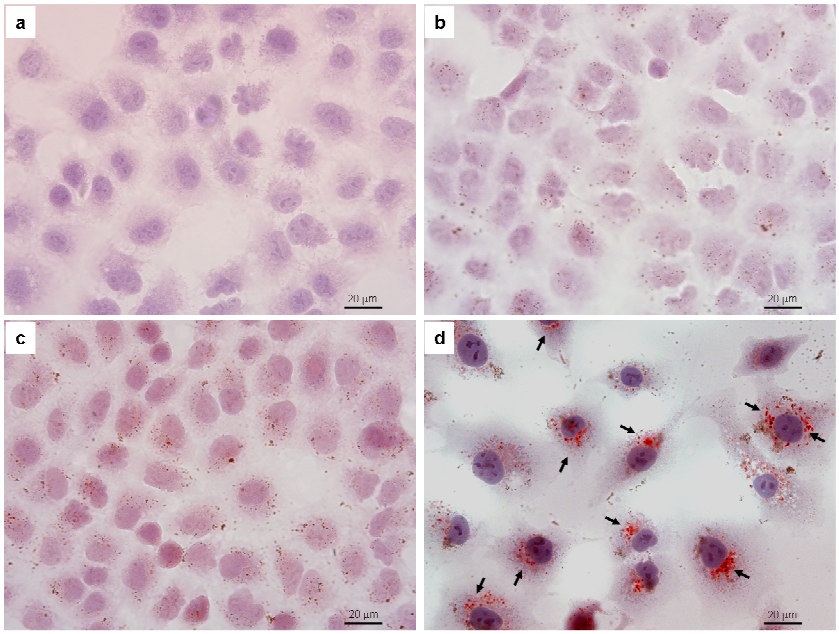

Fig.7. Intracellular copper release in A549 exposed to nCuO 10 μg/ml highlighted by DMABR (red precipitate →). a) Control cells; b) 3h nCuO treated-cells; c) 6h nCuO treated-cells; 24h nCuO treated-cells.

At the same time significant formation of peroxidation products was observed by immunostaining of 4-HNE. As shown in Fig.8 3h treated-cells presented oxidative alterations mainly localised at membrane level (Fig.8b) and sometimes also diffuse in the intracellular space (Fig. 8c). Prolonged exposure to nCuO 10μg/ml (24h) induced severe oxidation state which resulted in different effects. The accumulation of 4-HNE adducts in the nuclear region and presence of dark granules of reaction product in the cytoplasm was observed in cells significantly damaged and characterised by swelling, probably necrotic; in parallel it has been observed cells with altered morphology (reduction in size) with a diffuse peroxidation.

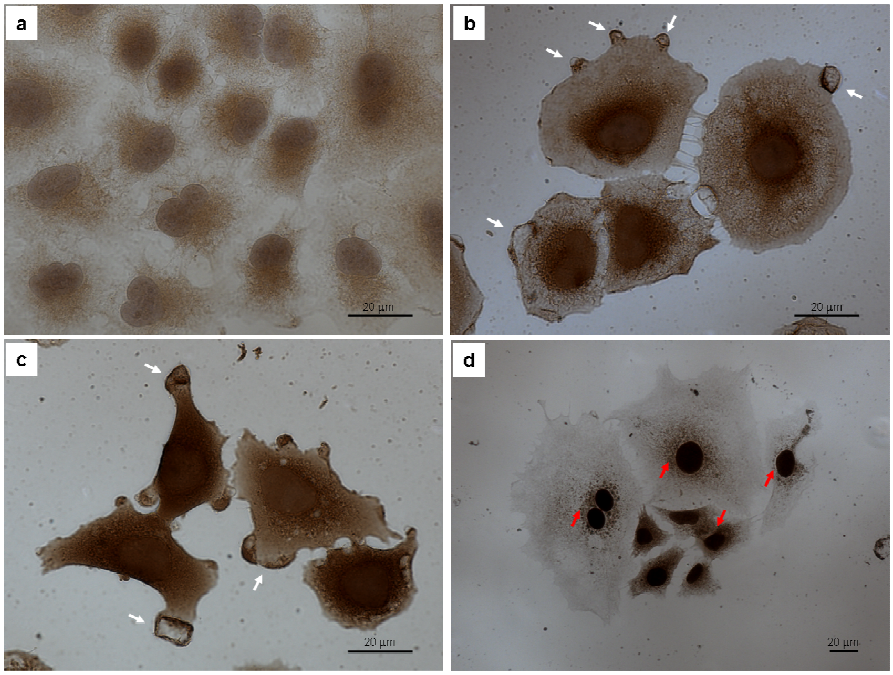

Fig.8 Immunocytochemistry of 4-HNE in A549 exposed to nCuO 10µg/ml. Control cells (a); nCuO- treated cells (3h) with LPO localised at membrane level (b) and diffuse in the intracellular space (c); nCuO- treated cells (24h) with significant accumulation of 4-HNE adducts in the nuclear and perinuclear regions (d).

Evidences of ultrastructural lysosomal alterations were highlighted by TEM analysis as shown in Fig.9 After early exposure stages only few particles were found inside the lysosomes (Fig. 9c), nevertheless their integrity appeared sometimes compromised (Fig.9b). After 24h of treatment internalization of nCuO resulted more significant and associated with rupture of phagocytic organelles at the stage phagolysosome (Fig.9d).

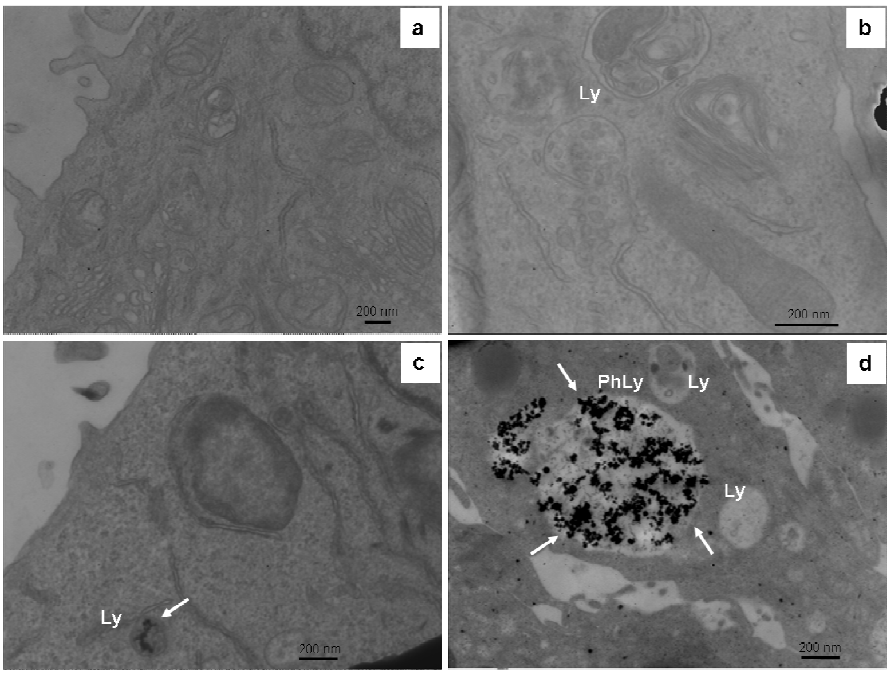

Fig. 9 TEM micrographs of A549 exposed to nCuO. Control cells (a); 3h-treated cells with lysosomal structural alterations (b) or presence of particles inside (white arrows) (c); loss of phagolysosome integrity by presence of particles (white arrows) (d).

5.4 Discussion

Among nanoparticles metal and metal oxides are critical compounds because dissolution phenomena and speciation to which they are subjected in the environmental or in the biological compartments could affect their fate and finally their bioavailability. When metal nanoxides interact with the cellular environment in *in vitro* systems they can exert their toxic potential firstly as metal ions released by particles; secondly by direct interaction with biological system and finally they can compromise the intracellular components after internalisation. Extracellular metal dissolution from particles is one of the hypothesis proposed to justify the toxicity of different

MONs such as copper oxide. The extent of the effects observed and ascribed to copper release greatly changes depending on the model investigated. Thanks to their size NPs distribute into the respiratory three and can theoretically reach the alveolar space as proposed by Oberdoster et al. (2005) where the presence of surfactants may favourite metal release from particles. We used A549 alveolar cells as model to assess the acute lung injury deriving from CuO nanoparticles exposure which should be ascribed to extracellular and intracellular copper release.

The viability trend of A549 exposed to increasing concentrations of nCuO was already shown in the previous section. With this study we investigated the ability of copper ions released into the culture medium to induce a reduction in cell viability after 3 and 24h of exposure, comparing these results with the effect induced by the correspondent concentration of CuO nanoparticles.

After 3h nCuO appears already cytotoxic while no variations were observed in cells exposed to particle extracts; in cells treated with Cu from soluble salt even an apparent increase of cell viability was detected at higher doses.

At 24h we observed about 45% of cells died when treated with extracts of nCuO 100μg/ml. It means that Cu^{++} was responsible for almost the moiety of the total mortality induced by nCuO similarly to that reported in Connolly et al. (2010). The same effects were observed when cells were exposed for 24h to copper ions, confirming that at extracellularly solubilised copper partially contributed to the long term (24h) effects of nCuO, but it can not sustain alone the total mortality induced by CuO nanoparticles.

These findings agree with previous studies on mammalian cells (Karlsson et al., 2008; 2009; Fahmy et al., 2009; Midander et al., 2009; Studer et al., 2010; Hanagata et al., 2011) that reported the significant role of dissolved copper ion in inducing cell toxicity of nCuO, but concomitantly assessed that it was not likely the "only" parameter triggering cell death. Accordingly these results maintain the hypothesis that Cu^{++} may sensitize A549 cells, but

NPs are largely responsible for the cytotoxic effect. In fact after 3h of exposure, when dissolution rate is retained to be high (Midander et al., 2009; Xia et al., 2008), we detected a significant decrease in cell viability only with NP suspensions (at the highest doses), while copper ion (dissolved from NPs or obtained from soluble copper salt) did not cause effects.

According to the above reported data, the so called "Trojan horse mechanism", proposed by Limbach et al. (2007), seemed to work in A549 cells exposed to nCuO at our experimental conditions. Normally plasma membrane is an efficient barrier versus high external ion concentrations but nanoparticles can by-pass this control system serving as carriers for high level of copper inside the cell. Once in lysosomes metal dissolution can occur because of the acidic conditions. Here the high local concentration of Cu^{++} can lead to ROS formation and lipid peroxidation resulting in lysosome leakiness and intracellular release of proteases and phospholipases, with activation of lysosomal pathway of cell death (Pourahmad et al., 2001; Guicciardi et al., 2004).

This mechanisms was verified in nCuO exposed cells by the presence of particle internalization by endocytic process even at early exposure time, as visualized by both transmission electron microscopy and specific markers of early endosome formation, like Rab5, that confirmed a clathrin-mediated endocytosis of NPs. However in literature further endocytic mechanisms have been hypothesized, like caveolin-1 dependent endocytosis and macropinocytosis (Doherty and McMahon 2009).

Rab7 is involved in the transition phase between early and late endosomes and during the process leading to fusion with lysosomes (Lakadamialy et al., 2006; Russel et al., 2006). Fig.3 is referred to 1h- exposure and well summarize the various steps of endocytic pathway but a significant increase of early and late endosomes was detected only after 3 and 6 h of exposure respectively (Fig.4 b,d).

At 3h and 6h post-exposure, sensible increase of the endocytic process was evident, as shown by the immunochemical detection of early and late endosomes (Rab5 and Rab7) (Fig. 4), but at the same time points significant decrease in lysosomal functionality occurred in nCuO exposed cells (Fig.5). The decrease in Lysotracker retention, also confirmed by Neutral Red Retention assay (Supporting Figure S6A. Supporting information - PART II), suggested in fact an increase in lysosomal leakiness likely as a consequence of NP internalization and surface reactivity, rather than of an intracellular dissolution of copper ions that at this time was not evident, at least at the NP dose of 10 µg/ml. Significant accumulation of DMABR reaction products were detected instead after 24h of exposure at the same dose of nCuO, suggesting that intracellular dissolution of particles become important only after prolonged exposure periods. Although no specific co-localizations were performed to demonstrate that copper ion dissolution occurred in lysosomes, the distribution of DMABR-Cu at the perinuclear region, mainly inside globular-shaped cytoplasmic structures, well reflected the typical localization of mature endosomes. Likewise, after 24h of treatment, a similar distribution was observed for 4-HNE adducts (24h). This fact may suggest that copper intracellular dissolution could promote severe lipid peroxidation in the neighbouring space probably responsible for the increased cytotoxicity observed at this time. To explain this finding we hypothesize that dissolution could be a slow process in spite of acidic conditions of lysosomes and DMABR can't be able to highlight the lower concentration of copper released after few hours of treatment. Note that in his work, Studer et al. (2010), found a complete dissolution of CuO nanoparticles (95%) only after 72h of incubation in artificial acidic medium (pH=5.5). Further a massive dissolution could occur when a critical lysosomal concentration is reached that is when endocytic vesicles mature and localized at the perinuclear region. Nevertheless evidences of LPO and alteration of lysosomal activity were found already at early exposure stages

(3,6h) when metal release was negligible. Reactive nanomaterial surface might be able to promote chemical interactions between nanoparticles and membranes by inducing LPO at the interface, causing changes in membrane permeability and dynamics (Nel et al., 2006) also at lysosomal level.

In conclusion this study confirms that the high toxicity of copper oxide nanoparticles on lung epithelial cells is attributable mainly to particles themselves and in a lesser extent to copper extracellular release. Particles internalised by endocytic processes showed the tendency to be dissolved in the intracellular space inside lysosomes, where both NPs and then copper ions promoted severe oxidative damages. After lysosomes' break down oxidative burden is allowed to spread throughout the cell, determining severe oxidative lesions leading to cell death.

However the first signs of lipid peroxidation at the plasma membrane level and the observation that lysosomal instability already begin at 3h post-exposure, with no copper solubilization, suggest that even alternative mechanisms may be involved in the induction of the very early cytotoxic effects of nCuO. It claims for further investigations, that basically constitute the body of the next chapter.

References

Aruoja V, Dubourguier H-C, Kasemets K, Kahru A. 2009. Toxicity of nanoparticles of CuO, ZnO and TiO_2 to microalgae *Pseudokirchneriella subcapitata*. Sci Tot Environ 407:1461–1468.

Auffan M., Achouak W., Rose J., Roncato M.-A., Chaneac C., Waite D. T., Mason A., Woicik J. C., Wiesner M. R., Bottero J.-Y. 2008. Relation between the redox state of iron-based nanoparticles and their cytotoxicity toward Escherichia coli. Environ. Sci. Technol. 42, 6730–6735.

Brunner T. J., Wick P., Manser P., Spohn P., Grass R. N., Limbach L. K., Bruinink A., Stark W. J. 2006. In vitro cytotoxicity of oxide nanoparticles: comparison to

asbestos, silica, and the effect of particle solubility. EnViron. Sci. Technol. 40, 4374–4381.

Cho W-S., Duffin R., Howie S.E.M., Scotton C.J., Wallace W.A.H., MacNee W., Bradley M., Megson I.L., Donaldson K.2011. Progressive severe lung injury by zinc oxide nanoparticles; the role of Zn^{2+} dissolution inside lysosomes. Particle and Fibre Toxicology, 8:27

Connolly S. 2010. Cytotoxicity of copper oxide nanoparticles and associated ions on human epithelial lung cells. NNIN REU Research Accomplishment pg 6,7.

Delgado K., Quijada R., Palma R., Palza H. 2011.Polypropylene with embedded copper metal or copper oxide nanoparticles as a novel plastic antimicrobial agent. Letters in Applied Microbiology doi:10.1111/j.1472-765X.2011.03069.x

Doherty G.J., McMahon H.T. 2009. Mechanisms of Endocytosis. Annu. Rev. Biochem. 78, 857-902.

Elzey S., Grassian V.H. 2010. Nanoparticle Dissolution from the Particle Perspective: Insights from Particle Sizing Measurements. Langmuir 2010, 26 (15), 12505–12508.

Fahmy B., Cormier S. A., 2009, Copper oxide nanoparticles induce oxidative stress and cytotoxicity in airway epithelial cells, Toxicol. In Vitro, 23, 1365–1371.

Foldbjerg R., Dang D.,A., Autrup H. 2010. Cytotoxicity and genotoxicity of silver nanoparticles in the human lung cancer cell line, A549. Arch Toxicol DOI 10.1007/s00204-010-0545-5

Franklin NM, Rogers NJ, Apte SC, Batley GE, Gadd GE, Casey PS. 2007. Comparative toxicity of nanoparticulate ZnO, bulk ZnO, and ZnCl2 to a freshwater microalga (*Pseudokirchneriella subcapitata):* The importance of particle solubility. Environ Sci Technol 41:8484–8490.

Guicciardi M.E., Leist M. and Gores G.J. 2004. Lysosomes in cell death. Oncogene 23, 2881–2890

Karlsson H.L., Cronholm P., Gustafsson J., Möller L. 2008. Copper oxide nanoparticles are highly toxic: a comparison between metal oxide nanoparticles and carbon nanotubes. Chem. Res. Toxicol. 21, 1726–1732.

Karlsson H., Gustafsson J., Cronholm P., Möller L. 2009. Size-dependent toxicity of metal oxide particles-A comparison between nano- and micrometer size. Toxicol. Lett. 188, 112-118.

Kim S., Choi J.E., Choi J., Chung K-H., Park K., Yi J., Ryu D-Y. 2009. Oxidative stress-dependent toxicity of silver nanoparticles in human hepatoma cells. Toxicology in Vitro 23, 1076–1084.

Lakadamialy M., Rust M.J., Zhuang X. 2006. Ligands for clathrin-mediated endocytosis are differentially sorted into distinct populations of early endosomes. Cell 124, 997-1009.

Lanone S., Rogerieux F., Geys J., Dupont A., Maillot-Marechal E., Boczkowski J., Lacroix G., Hoet P., 2009, Comparative toxicity of 24 manufactured nanoparticles in human alveolar epithelial and macrophage cell lines, Part. Fibre Toxicol., 6, 14.

Lei R., Wu C., Yang B., Ma H., Shi C., Wang O., Wang O., Yuan Y., Liao M. 2008. Integrated metabolomic analysis of the nano-sized copper particle-induced hepatotoxicity and nephrotoxicity in rats: A rapid in vivo screening method for nanotoxicity. Toxicology and Applied Pharmacology 232, 292–301.

Limbach L., Manser P., Wick P., Grass R. N., Bruinink A., Stark W. 2007. Exposure of engineered nanoparticles to human lung epithelial cells: influence of chemical composition and catalytic activity on oxidative stress. Environ. Sci. Technol. 41, 4158 – 4163

Martinenaite E., Tavenier J., Dabrowska M.E., Bjerregaa H.F. 2010. Nanoparticle-induced cell death. May, 26th 2011. 4thsemester project Final Report.

Midander K., Cronholm P., Karlsson H. L., Elihn K., Moller L., Leygraf C., Odnevall Wallinder I. 2009. Surface Characteristics, Copper Release, and Toxicity of Nano- and Micrometer-Sized Copper and Copper(II) Oxide Particles: A Cross-Disciplinary Study. Nano micro small 3, 389–399

Nel A.E., Xia T., Madler L., Li N. 2006. Toxic potential of materials at the nanolevel. Science 311, 622–627.

Oberdörster G., Oberdörster E., Oberdörster J., 2005, Nanotoxicology: An Emerging Discipline Evolving from Studies of Ultrafine Particles, Environ. Health Persp. 113, 823-839.

Pourahmad J., Ross., O'Brien P.J. 2001. Lysosomal involvement in hepatocyte cytotoxicity induced by Cu^{2+} but not Cd^{2+}. Free Radical Biology and Medicine 30, 89-97.

Rana SVS, Metals and apoptosis: Recent developments. 2008. Journal of Trace Elements in Medicine and Biology 22, 262-284.

Russell M.R.G., Nickerson D.P., Odorizzi, G. 2006. Molecular mechanisms of late endosome morphology, identity and sorting. Current Opinion in Cell Biology 18, 422–428.

Studer A.M., Limbach L. K., , Van Duc L., Krumeich F., Athanassiou E. K. , Gerber L. C., Moch H., Stark W. J. 2010. Nanoparticle cytotoxicity depends on intracellular solubility: Comparison of stabilized copper metal and degradable copper oxide nanoparticles. Toxicology Letters 197 169–174.

Xia T., Kovochich M., Liong M., Madler L., Gilbert B., Shi H.B., Yeh J.I., Zink J.I., Nel A.E. 2008. Comparison of the mechanism of toxicity of zinc oxide and cerium oxide nanoparticles based on dissolution and oxidative stress properties. ACSNano 2, 2121–2134.

CHAPTER 6

Does early nCuO-induced cytototocity depend upon rapid oxidative events mediated by high particle reactivity?

6.1 Abstract

A large number of studies are nowadays oriented toward the comprehension of the biological mechanisms by which metal oxide nanoparticles exert their toxic effects, in particular on human respiratory cells. nCuO resulted to be highly cytotoxic, but the exact mechanism of action is not still clearly understood. Some results suggested that nCuO can work through either toxic ion release or element-specific catalytic activity (e.g. semiconducting properties). Oxidative stress has been reported to have a key role in MON-induced cytotoxicity and determines a wide variety of injuries ranging from free radical overproduction to cell cycle arrest and oxidative damages. Accordingly to the previously reported results, it is reasonable that such paradigm might match the nCuO toxic behaviour too, that it is even expected to occur in a very short time after cell exposure to NPs.

In this chapter it is demonstrated that nCuO quickly react with A549 cells and induce cytotoxic effects as early events. The alterations to the plasma membrane as well as to the cell internal membranes appeared to be the most relevant event produced by a short exposure to nCuO, as it can be deduced by the high levels of lipid peroxidation, the significantly reduced mitochondrial activity and the severe lesions to the plasma membrane. These effects rapidly compromised cell homeostasis, giving rise to the heavy cytotoxic potential of nCuO. Oxidative burning was likely also responsible

for irreparable DNA damages, as testified by cell cycle arrest in G1 phase soon after nCuO exposure.

Keywords: *copper nanoxide, oxidative stress, lipid peroxidation, mitochondria, cell cycle.*

6.2 Introduction

Literature abundantly reported that the surface properties of nanoparticles are the most important factors driving the biological effects (Nel et al., 2009; Huang et al., 2010). The NP behaviour at the bio-interface is responsible for example for the formation of free radicals. In particular metal based nanoparticles can theoretically contribute to ROS (reactive oxygen species) formation by different mechanisms: semiconductors features (valence and conductance bands) can generate electronic states that lead to the production of $O_2^{-\circ}$; catalytic chemistry and metal ion leaching can promote ROS formation via Fenton and Haber-Weiss reactions; 3) photo-activation of the surface generates electron hole pairs which favourite $O_2^{-\circ}$ and OH° formation (Nel et al., 2006). ROS generation by NPs could potentially lead to adverse biological outcomes through an oxidant injury mechanism (Li et al., 2008).
Many authors consider the oxidative stress paradigm as a rule to explain nanoparticle toxicity (Xia et al., 2006), MONs included (Fahmy et al., 2009). When the intracellular production of free radicals overwhelms the antioxidant defence systems, this condition leads to the expression of stress proteins, the activation of inflammatory pathway, the cell cycle alterations and finally to oxidative damages and cell death (Xia et al., 2008).
ROS production can occur firstly at membrane level, in correspondence of specific enzyme complexes (e.g. NADPH oxidases), but also other structures such as endoplasmic reticulum and mitochondria are considered to be

principal targets of nanoparticle-induced reactive oxygen species. When cells are exposed to nCuO the presence of metal ions and the catalytic activity may trigger the production of the reactive hydroxyl radical OH° (Moriwaki et al., 2008). This molecule has been recognised as very harmful for mitochondrial and cell functionality: it could attack both the mtDNA (compromising the encoding of proteins involved in the electron chain transport) and DNA (inducing cell cycle arrest or programmed cell death). Further it can quickly react with polyunsatured fatty acids constitutive of the inner and outer cell membranes, thus promoting the formation of lipid peroxides. These compounds can in turn alter the mitochondrial metabolism and activity by inducing loss in mitochondrial membrane potential.

The aim of this work was to investigate the early events occurring after exposure of A549 cells to nCuO, focusing the attention on oxidative stress paradigm. Early changes in cell viability and mitochondrial activity were evaluated. These results were coupled with oxidative stress markers (ROS production and lipid peroxidation) and a microscopic evaluation of cell ultrastructure, with particular attention to cell membrane and mitochondrial health. A cell cycle analyses was also performed to evaluated effects on DNA and cell growth.

6.3 Materials and methods

6.3.1 Reagents

Standard copper oxide nanopowder (CuO<50nm; cod. 544868), the nucleic acid fluorescent dyes Propidium Iodide (PI) and Hoechst , were purchased from Sigma-Aldrich (Milan, Italy). A549 cells (American Type Culture Collection) were obtained from LGC Promochem (Sesto S. Giovanni, Italy). The fluorescent probes $DCFH_2$-DA, Mitotracker Red, BODIPY® 581/591 C11 were purchased from Molecular Probes (Invitrogen, CA, USA).

6.3.2 Cell culture and treatments

A549 cells (American Type Culture Collection) were routinely maintained at 37°C, with 5% CO_2 in OptiMEM medium at pH 7.2, supplemented with 10% inactivated foetal bovine serum (FBS) and 1% penicillin/streptomycin. Particle suspensions were freshly prepared before the treatment as described in *Chapter 5*.

6.3.3 MTT assay as tool to test early decrease of cell viability by metabolic mitochondrial activity

Cell viability at early stage of exposure was performed by MTT assay after 1, 2, 3, 6h of exposure to increasing concentration of nCuO. Viability% was expressed as OD percent in comparison to the control (±SE).

6.3.4 Mitochondrial integrity and functionality

Cells were exposed to particle suspensions (10μg/ml) for 3h and 6h; then were washed and incubated in parallel with Mitotracker Red (30 min, 37°C, 5%CO_2) in complete medium. They were rinsed, detached and suspended in phosphate buffer saline for the cytometric analysis. Fluorescence intensity of 10,000 events was measured by cytometer EPICS XL-MCL (Beckman-Coulter) using FL3=625nm band pass filter and the data were analyzed using the EXPO32 ADC software (Beckman-Coulter). Gates were made including at least the 90% of total cells analysed.

The experiment was replicated three times in duplicate and the data were expressed as mean% of fluorescence respect to the control(±SE).

6.3.5 Intracellular ROS production and localization

Cells were seeded onto glass coverslips and treated with 1, 10 μg/ml of particle suspensions for 45 min. At the end of the exposure time they were washed and incubated 20min with carboxy-$DCFH_2$-DA (5uM - Invitrogen) and MitoTracker® Red (50 nM- Invitrogen) diluted in PBS. We removed the

probes and we stained nuclei with DAPI; after 30 seconds we washed with MilliQ water (three times) and mounted the coverslips onto microscopy glass slide with DABCO solution. Qualitative analysis was made using Leica TCSNT confocal laser scanning microscope. Quantification of ROS was made by cytofluorimetric detection; cells were pre-incubated (45min) with 5uM carboxy-$DCFH_2$-DA (Invitrogen, USA) or 10 uM dihydroethidium (Invitrogen, USA) and then they were exposed to particle suspensions. After treatment cells were rinsed, detached and then suspended in PBS for the cytometric analysis.

6.3.6 Lipid peroxidation (LPO)

Assessing of lipid peroxidation was made both by microscopy techniques and TBARS assay.

For the first application cells were seeded onto sterilized glass coverslips and exposed to particle suspensions. After being washed with PBS the monolayers were fixed in 4% paraformaldheide and then incubated with the fluorescent probe BODIPY-C11(10μM, 30 min, 37°C; 5%CO_2), a fatty acids derivative which localised within the lipid bilayer changing its fluorescence from red to green when oxidised. After incubation, coverslips were mounted on glass slides and analysed with Leica TCSNT confocal laser scanning microscope.

Detection of aldhehydic products of LPO were performed by TBARS assay according to Akhtar et al. (2010) with minor modifications.

For malondialdehyde (MDA) determination cells exposed to NPs suspensions for 3h and 6h were rinsed and frozen at -80°C overnight. They were thawed on ice and scraped in 150μl of PBS supplemented by protease inhibitors and BHT (0,2%). Each sample was sonicated three times and cell homogenates were centrifuged at 4000g, 4°C for 10mins to remove particles and cell debris. Supernatants were collected, mixed with the LPO solution (20%acetic acid and 0,67% thiobarbituric acid) and boiled for 60 mins. Then

they were cold on ice and centrifuged at 12 000 rpm for 5mins. Optical density was measured at 532nm with a multiplate reader (Multiskan Ascent Thermo). The experiment was replicated three times and results were expressed as mean percent in comparison to the control (±SE). Statistical differences were tested by the One-way ANOVA + followed by the Dunnett's method.

6.3.7 Cell cycle

A549 were exposed to nCuO for 3 and 6h and then processed for the cell cycle analysis as described in *Chapter 4* (see the section Material and methods). Data were referred to a representative cell cycle of treated cells.

6.3.8 Effect of nCuO treatment on nuclear morphology

Cells were cultured in presence of nCuO suspensions; then they are washed, detached and incubated with a mixture of Hoechst 33342 for 30 minutes. After centrifugation they are re-suspended in foetal calf serum, deposed onto glass slide and observed with Axioplan Zeiss 4.1. Nuclear morphology, presence of chromatin condensation were evaluated.

6.4 Results

6.4.1 Early decrease in metabolic activity and mitochondrial integrity and functionality

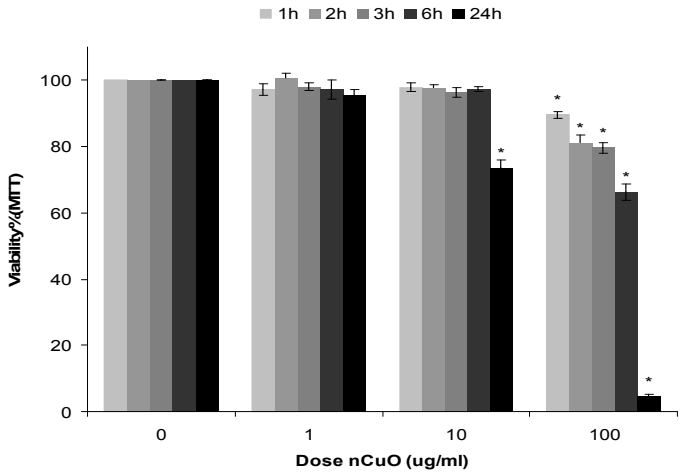

Fig.1 Early viability by MTT assay in CuO- treated A549 cells. *Significantly different from control cells. (One-way ANOVA + Dunnett's method; p<0,010).

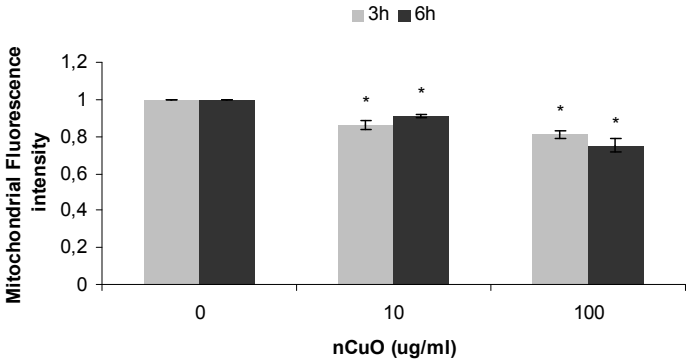

Fig.2. Cytometric analysis of mitochondrial perturbation by staining with Mitotracker Red after exposure to nCuO at 10 μg/ml. Data are expressed as fluorescent intensity% respect to the control. *Significantly different if compared to the control cells (One-way ANOVA + Dunn's method; p<0,05).

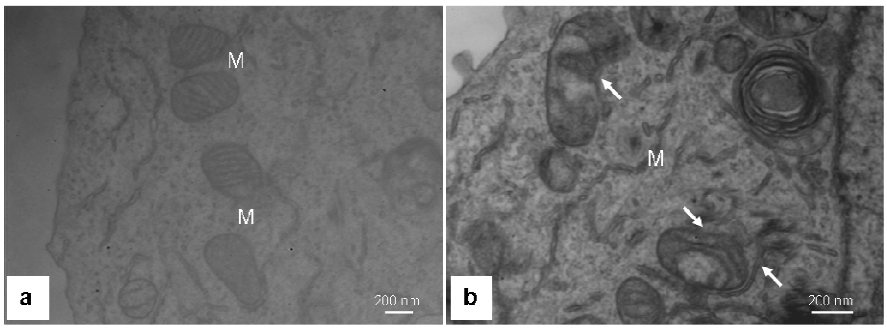

Fig.3. TEM analysis of oxidative damage; A) control cells; B) alteration of mitochondrial structure after 3h (nCuO 10μg/ml).

After treatment with increasing concentrations of nCuO we observed a dose dependent decrease in cell viability at early exposure stages. Significant reduction of the metabolic activity (12%) was observed already after 1h for the dose 100 μg/ml.

With cytometric analyses we investigated the state of mitochondria in living cells after exposure to nCuO. As showed in Fig.2 we observed a significant decrease of fluorescence intensity after 3h and 6h, related to a decrease of stain retention ability by mitochondria. The reduction of the mitochondrial functionality in A549 treated with a sublethal dose of nCuO (10μg/ml), was about the 14% and 19% respect to the control after 3 and 6h respectively. Exposure to higher concentration of soluble Cu^{++} (40μg/ml) didn't cause any reduction of FI value demonstrating that the effect observed is attributable mainly to nanoparticles (data not shown). Evidences of oxidative damages to mitochondrial structure were highlighted by TEM analysis; as shown in Fig.3 nCuO induced morphological mitochondrial alterations with changes in cristae ultrastructure.

6.4.2 Oxidative stress/damage

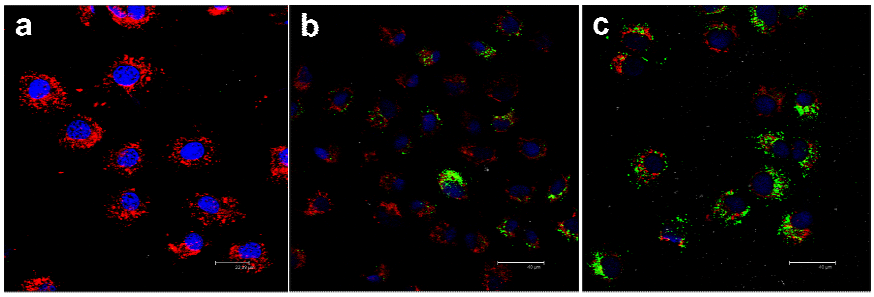

Fig.4. Intracellular ROS production after 45 minutes in control cells (a) nCuO-treated cells at 1 µg/ml (b); nCuO- treated cells at 10 µg/ml (c). Nuclei are stained in bleu, mitochondria in red and ROS are represented by the green spots.

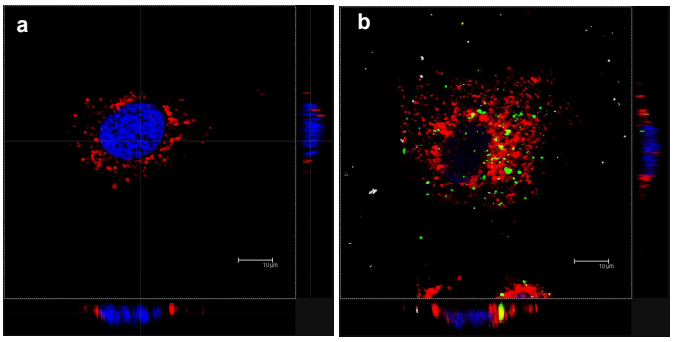

Fig.5. Confocal analyses of ROS (green spots) – mitocondria (red) colocalization (orange-yellow) in (a) control cells; (b) cells exposed to nCuO at 10µg/ml.

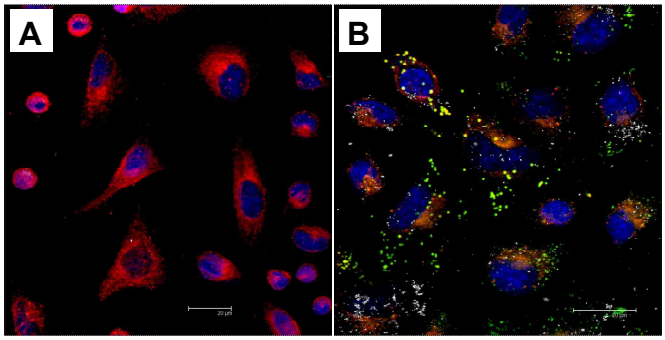

Fig.6. Lipid peroxidation (LPO) in A549 cells. Confocal images of control (A) and 3h CuO-treated cells (10µg/ml) (B) stained with BODIPY-C11. Nuclei (bleu), lipid reduced (red), lipid oxidised (green), nCuO (white spots).

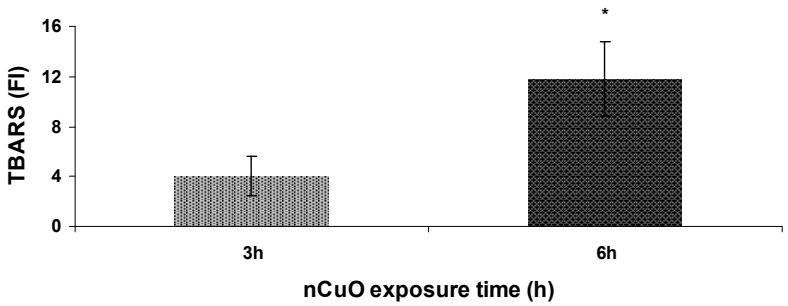

Fig.7. Lipid peroxidation by TBARS assay in A549 after 3h and 6h of exposure to nCuO (10μg/ml); data are expressed as increase% of MDA analogues respect to the control.* Significantly different if compared to the control (One-way ANOVA + Dunnett's method; $p<0,01$)

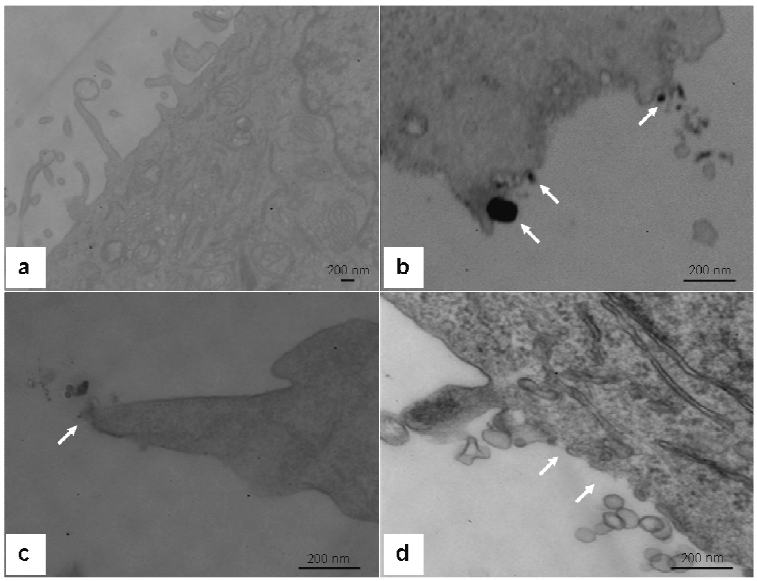

Fig.8. TEM micrographs of plasma membrane ultrastructure. Control cells (a); A549 treated with nCuO 10μg/ml respectively for 1h (b) and 3h (c,d).

Production of intracellular ROS resulted significant in cell treated with nCuO (1, 10μg/ml) starting from 45 minutes of exposure, as shown in

Fig.4b,c. Confocal analysis testify only a partial co-localization between mitochondria and DCF fluorescence Fig.5b.

Oxidative stress due to nCuO appeared at the early stages of exposure as demonstrated by BODIPY-C11 staining which detect presence of lipid peroxidation after 3h (Fig.6B); quantification of MDA analogues by TBARS assay confirm these findings and revealed a dose and time- dependent increase in lipid peroxides respect to the control (Fig.7) after 3 and 6h of treatment.

The oxidative pressure induced by nCuO associated to cell-particle interaction probably acted also at plasma membrane level by inducing serious ultrastructural alterations as testified by TEM analyses (Fig.8).

6.4.3 Cell cycle

Cytometric analysis of cell cycle revealed a slight increase in cells at G1 phase after 3h of exposure. This trend was confirmed for a 6h when we observed also a weak increase in SubG1 phase for low concentrations of nCuO (Fig.9).

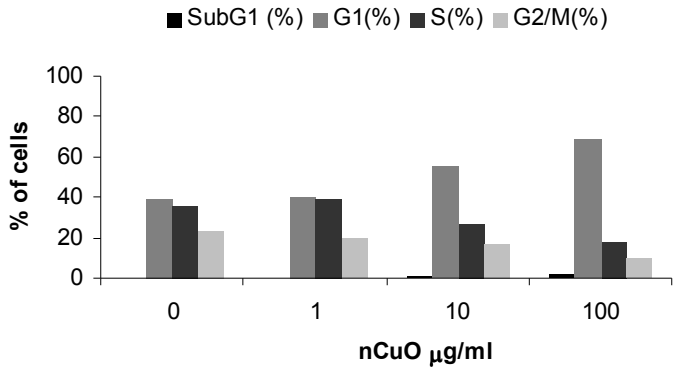

Fig.9. Representative cell cycle profile of A549 by flow cytometry. Evident increase of treated cells in G1 phase after exposure to nCuO for 6h.

6.4.4 Effect of nCuO treatment on nuclear morphology

By nuclear staining we detected after 6h of exposure the prevalence of viable cells associated with the presence of nuclei characterized by abnormal chromatin condensation (Fig.10) and necrotic cells. Although similar morphology may be associated with apoptosis no apoptotic bodies formation was found. The frequency of cells with this nuclear morphology increased when cells were treated with nCuO100μg/ml. Decrease in number of mitotic cells respect to the control was observed (data not shown).

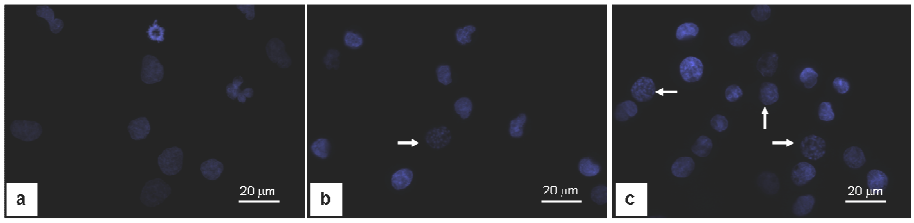

Fig.10. Hoechst staining of A549 cells (6h). a) Control cells; b) nCuO- treated cells (10 μg/ml); c) nCuO- treated cells (100 μg/ml). White arrow = abnormal chromatine condensation in treated cells.

6.5 Discussion

In the previous chapter it was demonstrated that extracellular and intracellular dissolution of copper ions from nCuO contributed to the cytotoxic effects occurring in A549 cells at 24h after exposure. However solubilised metal ions did not play role in the early stages of the cytotoxic induced pathway. So in this chapter the capability of nCuO to perturb very quickly the cell metabolism and structure was investigated basically following as a paradigm the NPs' capacity to induce oxidative stress.

By using confocal microscopy, it was shown that CuO nanoparticles induced an evident increase in ROS production after 45 min in A549 exposed to 1, 10μg/ml. Parallel cytometric analysis of intracellular ROS formation (as

evaluated with two different fluorescent probes, $DCFH_2$-DA and DHE) evidenced only a slight increase in free radical production (data not shown).
This troubleshooting in quantifying very unstable ROS in our samples could be due to the high reactivity of these species (e.g. OH°) or to the fluorescence quenching they might cause (Kroll et al., 2009; Stone et al., 2009).
The ROS formation, analysed by confocal microscopy, was evident and nCuO exposed cells and further experiments revealed a good (even not total) co-localization of ROS and mitochondria (Fig.5b). Nevertheless mitochondrial activity was soon compromised after treatment with nCuO (Fig.2), as shown by the significant decrease in fluorescence intensity in cells incubated with Mitotracker Red. This probe forms specific bindings with sulfidrilic groups localised on mitochondrial proteins (Charzotte 2011) and can be consider as a marker of mitochondrial depolarization (Gilmore and Wilson, 1999). Basing on the observations above, nCuO might interacts with -SH groups, inducing their oxidation and the consequent decrease in mitochondria-probe affinity.
Changes in the mitochondrial membrane potential (ϕ_{mit}) were also reported in Karlsson et al. (2008), where 90% of cells exposed for 16h to nCuO showed a significant mitochondrial depolarization. This effect was observed despite a not significant increase in ROS formation, even at high nCuO concentrations ($20\mu g/cm^2$). Also in Fahmy et al. (2009), who maintained the role of oxidative stress to justify the nCuO cytotocity on HEp-2 cells, the ROS production (measured by $DCFH_2$-DA method) was very little.
The oxidative stress early induced by nCuO in A549 cells was confirmed by the significantly increased levels of lipid peroxidation.
LPO occurring in the first hours after nCuO exposure is likely a consequence of the physical-chemical interactions of NPs with outer and inner membrane systems, which justifies the mitochondrial structural alterations, membrane depolarization and loss of their metabolic activity, as also previously

described (Gutteridge et al.,1995; Li et al., 2003; Xia et al., 2007). In conclusion this findings supported the hypothesis of a direct interaction between copper oxide nanoparticles and biological components, followed by the transient formation of ROS that quickly reacted with macromolecules such as lipids to give lipid peroxides.

Many highly reactive oxidants have indeed short half-life within the cellular milieu and their reactivity is consequently regulated by the type of biomolecule residing close to the ROS generation site (Dickinson et al., 2011). The sensitivity of lipids to free radicals has largely discussed in Orrenius et al., 2007; Clark et al., 2008.

Plasma membranes are sensitive targets of nCuO according to Xie et al. (2012) and serious damages occurred in A549 cells even after few hours of exposure (Fig.3). The hypothesized key role of nCuO surface properties rather than the effect being solely due to the release of metal ions is also supported by the implementation in the use of metal nanoparticles in antimicrobial applications. It was in fact demonstrated that they actively interact with bacterial membranes to induce cell toxicity and death. (Morones et al., 2005).

In addition to membrane an mitochondrial dysfunction, sub-lethal concentrations of copper oxide NPs increased the frequency of cells in G1 phase at 3h and 6h post-exposure. The role of the G1 phase is to allow the cell to grow before chromosome replication. In presence of DNA damage, cells do not go through the G1/S transition until the lesion is repaired. Then, if cells do not go on with the cycle, or do not rest in G0 phase, they consequently begin apoptosis (Alberts et al., 2007). We did not perform a direct evaluation of oxidative DNA lesions, but the genotoxic potential of nCuO was already verified by Karlsson et al. (2009) using comet assay (+ FPG enzyme) in A549 cells after 4h nCuO exposure. Very similar results were also obtained by Ahamed and co-workers (2010). The analysis of cell cycle also revealed a small increase in the frequency of cells arrested in

SubG1 phase at 6h exposure, parallel the nuclear staining by Hoechst highlighted a significant presence of cell with abnormal chromatin condensation, but without any formation of apoptotic bodies. Probably the cells which were able to repair the DNA lesions returned into the cycle, but the oxidative pressure (internal and external) determine the accumulations of further DNA lesions that, coupled to the alteration of the cytoskeleton integrity, determined the cell cycle arrest in G2/M phase at later exposure times (see *Chapter 4).* In a recent study (Hanagata et al., 2011) it has been observed that nCuO was able to induce a cell cycle arrest in different phases depending on the component (copper ions released or particles): the arrest in G1 phase was attributed to particle effect, while that in G2/M to the copper ions dissolved. These observations well agree with the present results showing cell cycle arrest in G1 at early nCuO exposure times, when copper ion dissolution was not detected while the G2/M arrest happened after 24h of exposure (*Chapter 4),* when extracellular and intracellular ion release was massive (*Chapter 5*).

In conclusion this research demonstrated that copper oxide nanoparticles induce early metabolic and structural alterations, mainly as a consequence of lipid peroxidation. Plasma membranes and mitochondria appeared to be sensitive targets of nCuO. Moreover the persistence of a significant oxidative pressure could be responsible for the DNA damages and the consequent cell cycle arrest occurring soon after few hours of exposure to nanoparticles. However, further investigations are still required to better clarify the molecular mechanisms leading to cell death.

References

Ahamed M., Siddiqui M.A., Akhtar M.J., Ahmad I., Pant A.B., Alhadlaq H.A. 2010. Genotoxic potential of copper oxide nanoparticles in human lung epithelial cells. Biochemical and Biophysical Research Communications 396, 578–583.

Akhtar M.J., Ahamed M., Kumar S., Siddiqui H., Patil G., Ashquin M., Ahmad I. 2010. Nanotoxicity of pure silica mediated through oxidant generation rather than glutathione depletion in human lung epithelial cells. Toxicology 276, 95–102.

Alberts B, Johnson A,Lewis J, Raff M, Molecular Biology of the Cell. 2007; Chapter 13-17-18.

Charzotte B. 2011. Labeling mitochondria with mitotracker dyes. Cold Spring Harbor Protocols

Clark R.A.F. 2008. Oxidative stress and "Senescent" fibroblasts in non-healing wounds as potential therapeutic targets. Journal of Investigative Dermatology 128, 2361-2364.

Dickinson B.C., Chang C.J. 2011. Chemistry and biology of reactive oxygen species in signalling or stress responses. Nature chemical biology doi:10.1038/NCHEMBIO.607.

Fahmy B., Cormier S. A., 2009, Copper oxide nanoparticles induce oxidative stress and cytotoxicity in airway epithelial cells, Toxicol. In Vitro 23, 1365–1371.

Gilmore K. and Wilson M. 1999. The use of chloromethyl-X-Rosamine (Mitotracker Red) to measure loss of mitochondrial membrane potential in apoptotic cells is incompatible with cell fixation. Cytometry 36, 355-358.

Gutteridge J.M.C. 1995. Lipid-peroxidation and antioxidants as biomarkers of tissue-damage. Clin. Chem. 41, 1819–1828.

Hanagata N., Zhuang F., Connolly S., Li J., Ogawa N., Xu M. 2011. Molecular responses of human lung epithelial cells to the toxicity of copper oxide nanoparticles inferred from whole genome expression analysis. ACSNano 10.1021/nn202966t.

Huang Y-W., Wu C-H., Aronstam R.S. 2010. Toxicity of transition metals oxide nanoparticles: recent insights from *in vitro* studies. Materials 3, 4842-4859.

Karlsson H.L., Cronholm P., Gustafsson J., Möller L. 2008. Copper oxide nanoparticles are highly toxic: a comparison between metal oxide nanoparticles and carbon nanotubes. Chem. Res. Toxicol. 21, 1726–1732.

Karlsson H., Gustafsson J., Cronholm P., Möller L. 2009. Size-dependent toxicity of metal oxide particles-A comparison between nano- and micrometer size. Toxicol. Lett. 188, 112-118.

Li N., Hao M., Phalen R.F., Hinds W.C., Nel A.E. 2003. Particulate air pollutants and asthma. A paradigm for the role of oxidative stress in PM-induced adverse health effects. Clin. Immunol. 109, 250–265.

Li N., Xia T., Nel A.E.2008. The role of oxidative stress in ambient particulate matter-induced lung diseases and its implications in the toxicity of engineered nanoparticles. Free Radical Biology & Medicine 44, 1689-1699.

Martinenaite E., Tavenier J., Dabrowska M.E., Bjerregaa H.F. 2010. Nanoparticle-induced cell death. May, 26th 2011. 4th semester project. Final Report.

Moriwaki H., Osborne M.R., Phillips D.H. 2008. Effects of mixing metal ions on oxidative DNA damage mediated by a Fenton-type reduction. Toxicology in Vitro 22, 36-44.

Morones J.R., Elechiguerra J.L., Camacho A., Holt K., Kouri J.B., Ramirez J.T. 2005. The bactericidal effect of silver nanoparticles. Nanotechnology 16, 2346–53.

Nel A.E., Xia T., Madler L., Li N. 2006. Toxic potential of materials at the nanolevel. Science 311, 622–627.

Nel A.E., Mädler L., Velego D., Xia T., Hoek E.M.V, Somasundaran P., Klaessig F., Castranova V., Thompson M. 2009. Understanding biophysicochemical interactions at the nano–bio interface. Nature materials 8, 543-557.

Orrenius S., Gogvadze A., Zhivotovsky B. 2007. Mitochondrial oxidative stress: Implications for cell death. Annual Review of Pharmacology and Toxicology 47, 143-183.

Stone V., Johnston H., Schins R.P.F. 2009. Development of in vitro systems for nanotoxicology: methodological considerations. Critical Reviews in Toxicology 39, 613–626.

Xia T., Kovochich M., Brant J., Hotze M., Sempf J., Oberley T., Sioutas C., Yeh J.I. Wiesner M.R., Nel, A.E. 2006. Comparison of the abilities of ambient and manufactured nanoparticles to induce cellular toxicity according to an oxidative stress paradigm. Nano. Lett. 6, 1794–1807.

Xia T., Kovochich M., Nel A.E. 2007. Impairment of mitochondrial function by particulate matter (PM) and their toxic components: implications for PM-induced cardiovascular and lung disease. Front. Biosci. 12, 1238–1246.

Xia T., Kovochich M., Liong M., Madler L., Gilbert B., Shi H.B., Yeh J.I., Zink J.I., Nel A.E. 2008. Comparison of the mechanism of toxicity of zinc oxide and cerium oxide nanoparticles based on dissolution and oxidative stress properties. ACSNano 2, 2121–2134.

Xie X., Xu L., Gao D. 2012. Effect of CuO nanoparticles on the cell membrane permeability of A549 and its exclusion. Advanced Materials Research Vols. 343-344, 77-80.

CHAPTER 7
General conclusions

Due to the large production of manufactured nanoparticles, human occupational and environmental exposure are supposed to increase. It has been assessed that emission quantities prioritize metal nanomaterials for risk assessment (Landsiedel et al., 2010).

The present work improves the current knowledge of the toxicological profile of three widely used MONs: $nTiO_2$, nCuO, nZnO. The major findings obtained from the experiments in *in vivo* and *in vitro* models, for NP aquatic toxicology and respiratory toxicology respectively, are listed below.

7.1 *In vivo* model

The effects of $nTiO_2$, nZnO and nCuO were investigated on the amphibian *Xenopus laevis* embryos, commonly used as *in vivo* model for aquatic toxicity of chemicals. The results revealed that even high NP concentrations (up to 500 mg/ml) were not lethal for such NPs with the exception of nCuO but all NPs induced relevant malformations.

The embryotoxic effects induced by nCuO were however almost completely dependent upon the NPs copper ion release in solution.

Exposure to titanium dioxide did produce only slight embryotoxic effects, but these NPs were able to penetrate inside the embryo tissues and translocate throughout the body.

The intestine appeared to be the main target of nZnO. It induced severe histological alterations of the gut epithelium and over passed the intestinal barrier. These effects were not produced by embryo exposure to soluble Zn, confirming that nZnO embrytoxicity was exerted by NPs. The mechanisms by which nZnO works are now under investigation and preliminary results

indicate lipid peroxidation and alteration of cell junctions as mainly causes of epithelial lesions and NP paracellular translocation (Supporting Figures S4, S5, S6. Supporting information - PART I).

7.2 *In vitro* model

Our study demonstrates that the different effects promoted by MONs on A549 cells depend on the chemical composition, aggregation state, particle dissolution and surface reactivity/properties.

Large $nTiO_2$ particles or aggregates were easily internalised by cells trough the endocytic process. They distributed at different level but they didn't induce structural alterations even at 24 hours of exposure, despite their massive uptake. At this time, the plasma membrane appeared as the major target structure , even cytotoxicity was not significant.

At the same time the observed cell cycle alteration suggests that $nTiO_2$ might induce genotoxic effects but this aspect deserves further investigation.

nCuO resulted to be a very toxic compound and a dose- and time- dependent effects were observed .

Surface reactivity and copper dissolution were the main causes of nCuO cytotoxicity . After few hours of exposure, particles themselves were responsible for significant alterations. The increase in reactive oxygen species and formation of lipid peroxidation products were evident already after 3h of exposure. These effects were associated with the presence of nCuO inside the cells, visible as ultrastructural alterations at the mitochondria and the plasma membrane. The increase in oxidative damage is probably responsible for DNA damage, as suggested by cell cycle perturbation and morphological nuclear alterations, observed at 6h of exposure.

A prolonged exposure allows particles to dissolve in the extra and intracellular milieu. Extracellular release of Cu from particles account for about the moiety of the cyototoxicity registered at 24h. At the same time point the significant intracellular dissolution of copper ions induced high levels of lipid peroxidation and was responsible for significant ultrastructure alterations

Anyway, basing on the results listed above, the following considerations can be made:

- Metabolic processes change between the *in vivo* and *in vitro* models, so the fate of the internalised nanoparticles may be different.
- The extent of citotoxicity induced by metal ions released from MON depends on a series of elements: solubility, metal ion species, growth medium composition (presence of chelating agents) and pH, and finally by the particular chemical species sensitivity of the model used.
- Testing the bulk form of a MON, the specific cation obtained from a soluble salt and the MON in parallel may consent to attribute to a particular component of the particle the observed effects. Moreover the use of an extract of particles realised in the growth medium to reproduce the cation release allows to better simulate the conditions occurring during the exposure, taking into account also the speciation phenomena.
- Focusing on *in vitro* models, the internalization mechanism may determine the fate of the particles inside the cells, the extent of a specific effect and the sequence of events occurring. If NPs are internalised exclusively by an endocytic process, the probability to directly interact with other intracellular components decreases until they remain inside the vesicles, where they may increase their ionic

dissolution. When different entry pathways are followed, much more interactions with cell compartments are possible and other reaction cascade could be involved.

- Lysosomal dissolution of nCuO during the time can be followed from a series of events: 1) increase in copper ion concentration in medium after cell death; 2) exclusion of the excess of intracellular copper by active mechanisms; 3) expulsion (by exocytosis pathways or after cell death) of particles with reduced size which are newly available for the other cells. So the cytotoxicity observed at 24h of exposure must be the result of these processes.
- The association between genomic studies and biochemical end points can help in the understanding of the different phases of the cytotoxic pathway.
- A further attention has to be dedicated to the characterization of the oxidative damage occurring after exposure of alveolar epithelial cells to MONs to better understand their role in the induction of the DNA damage.

In conclusion, due to the complexity of intrinsic variables and the plurality of potential interactions between MONs and the biological systems, harmonised protocols for testing toxicity of nanoparticles should be adopted and interlaboratory comparisons of results should be made.

Anyway, attention has to be posed to the interpretation of the results from toxicity studies on NPs, since the effects produced by the nanomaterials could be different from those induced by the same compounds released in the environment, where significant modifications can occur.

Supporting information - PART I

Translocation of nCuO

Confocal microscope was used on *Xenopus laevis* sections obtained from liver and central nervous system. Briefly control and exposed embryos were fixed fixed overnight in 10% buffered formalin at RT, rinsed, and finally bleached in a 3% H_2O_2/KOH 0.5% medium for 2h to avoid reflection by pigmentation (modified by Thisse and Thisse 2008). Presence of particles was detected using CLSM in reflection mode.

TBARS assay

At the end of FETAX, 15 embryos from each sample (for 3 replicates) were dried and kept at -80°C until the execution of the test. They were thawed on ice and homogenised in 500 ml of cold buffer phosphate with 1% BHT (2% in ethanol). Samples were centrifuged (4000 rpm, 15 min) and 100 ml of supernatant were mixed with 500 ml of thiobarbituric acid (TBA 0,67% water solution) and 500 ml of acetic acid (20% water solution). After mixing they were boiled at 95°C for 45 minutes, cooled on ice and centrifuged at 12000 rpm for 10 min. Optical density of each sample were measured by Multiplate reader (Multiskan Ascent – Thermo) at λ=540nm using λ=630nm as a reference wavelength. MDA analogues concentration was calculated using tetraetoxipropane as a standard and normalised by protein content measured by BCA method. The experiment was repeated and data were expressed as %increase in MDA content respect to the control.

4-hydroxy-nonenal immunostaining

Paraffin embedded sections of intestine of ZnO- treated embryos were incubated 20 min in 1% H_2O_2 in methanol for the quenching of the endogenous peroxidases. Non-specific binding was blocked with 10%

Normal Horse Serum (NHS) (Elite® ABC Kit, Vectastain Laboratories, Burlingame, CA) in a humid chamber at RT. Sections were incubated with monoclonal antibody against 4-Hydroxy-2-nonenal (anti-4-HNE) at 25μg/ml (JaICA, Japan) overnight at 4°C in a humid chamber. Slides were then washed in PBS and incubated with secondary horse anti-mouse antibody conjugated to biotin (ABC Kit) for 1h at RT and washed again in PBS. The Avidin-Biotin complex conjugated with horseradish peroxidase (ABC Kit) was added on each section for 30 min at RT and after three washing with PBS, slides were incubated in 0.75 mg/ml DAB and 0,3‰ H_2O_2 in PBS for 7 min. Slides were abundantly washed in tap and distilled water and then nuclei were counterstained with Mayer's Haemalaun. Lastly they were mounted in a glycerol based medium and observed with a light microscope.

Supporting results

Supporting Figure S1 show the presence of CuO nanoparticles inside the liver and central nervous system (cephalic region) in embryos exposed to 500 mg/L. These findings testify the ability of particles to migrate and accumulate in other districts of the organism investigated.

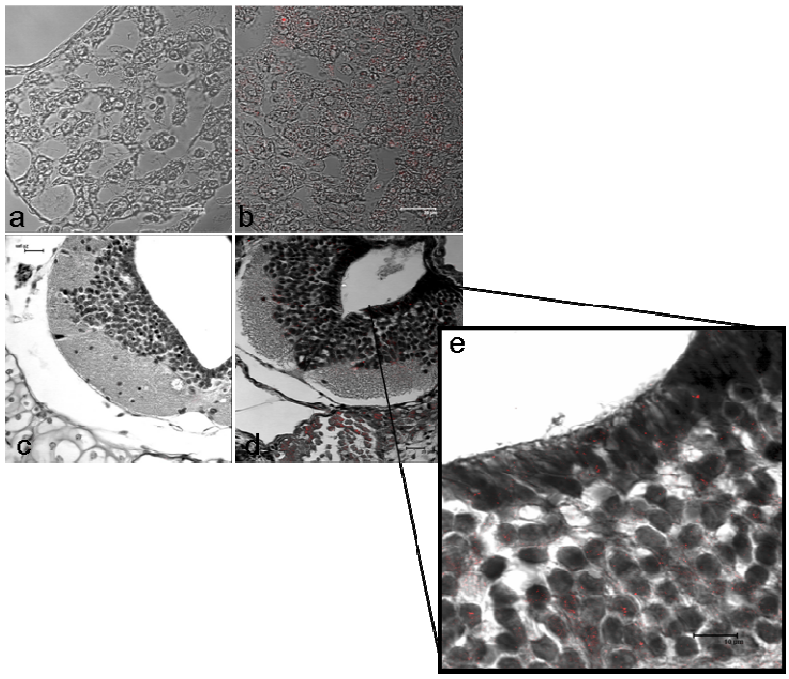

Supporting Figure S1. Histological images of 96-h-old *X. laevis* embryos: control liver (a); liver of nCuO- exposed embryo with particles finely distributed and histological lesions (b); cephalic section of *Xenopus* control (c) ; cephalic section of nCuO-exposed embryo with presence of particles; low magnification (d); high magnification (e). Reflection of particles coded in red pseudocolor.

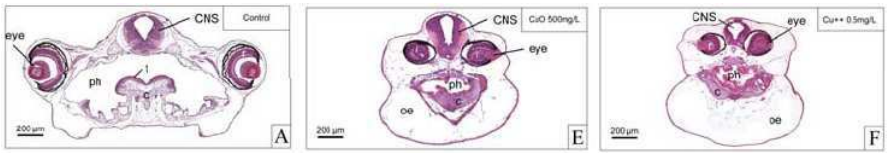

Supporting Figure S2. Cephalic sections from *Xenopus* control (A); *Xenopus* exposed to nCuO 500mg/L with significant malformation of the cephalic structures (B); *Xenopus* exposed to Cu^{++} 0,5 mg/L (CNS= central nervous system).

TBARS assay and 4-hydroxy-nonenal immunostaining

Supporting Figures S3,S4 testify the increase of two different marker of lipid peroxidation in nZnO-exposed embryo at the end of the test (96h).

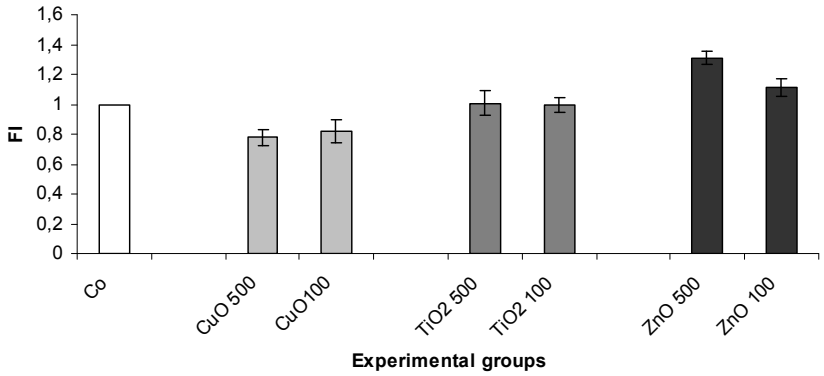

Supporting Figure S3. Lipid peroxidation in *Xenopus laevis* exposed to metal oxide nanoparticles by TBARS assay. Data are expressed as malondialdheyde content (nmolMDA/mg protein) normalised for control embryos (±SE).

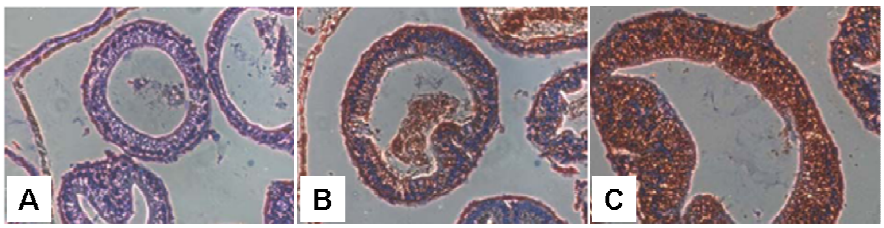

Supporting Figure S4. A) Antibody specificity control; B) intestine of control embryo; C) intestine of ZnO- treated (100mg/L) embryo.

Intestinal distribution of nZnO and ultrastructural effects

Confocal laser scanning microscopy allowed to detect the presence of particles inside the intestine with a significant accumulation during the time. By ESI we localised the particles in the intercellular space and TEM analyses highlighted significant ultrastructural alterations probably induced by disruption of cell junction by particles. So they can migrate at different levels of depth by the paracellular way. The ability of nZnO to cross the intestinal wall and potentially to translocate in other district was confirmed also by TPE microscopy.

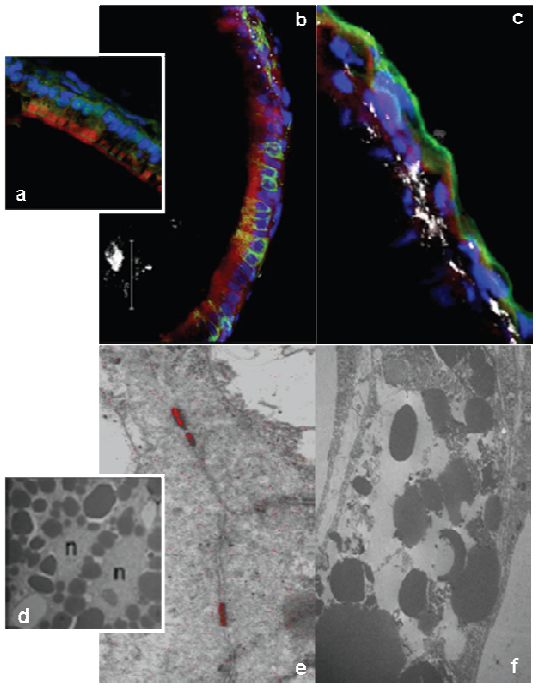

Supporting Figure S5. Early and late distribution and effects of nZnO in *X. laevis* intestine. Confocal 3D images of whole mount intestine in Control embryo(a); ZnO-exposed embryos at early and late exposure stages of treatment respectively (b,c). TEM images of *X. laevis* control (d); Elemental Spectroscopy Imaging (ESI) by the three window method, showing Zn (100 mg/L) in the intercellular space at early exposure stage (e); 100 mg/L nZnO- exposed larvae with disintegrated intestinal wall after prolonged treatment (f).

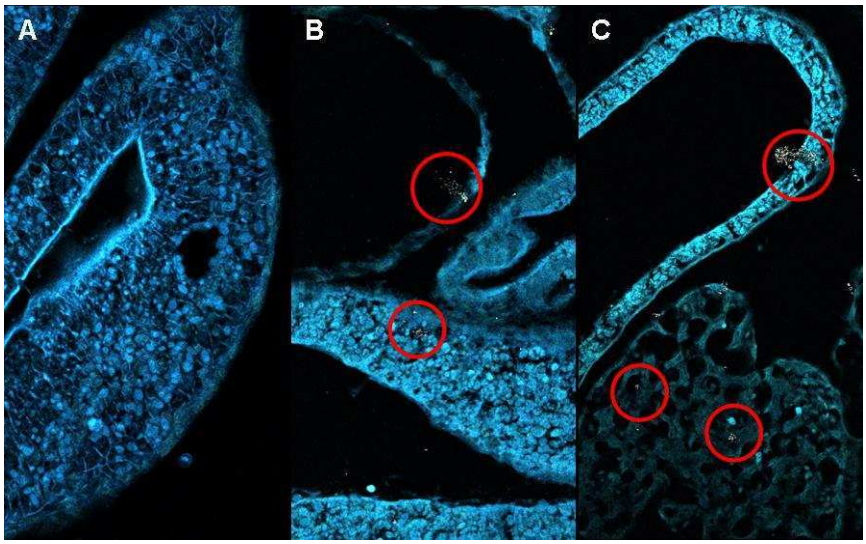

Supporting Figure S6. TPE microscopy of Xenopus embryos intestine. Unexposed embryo (A); ZnO-exposed embryo (500mg/L) with nZnO localised in the intercellular space (white spots) (B); exposed embryo (nZnO=500 mg/L) with nanoparticles crossing the intestinal wall or localised in liver (C).

Supporting information - PART II

Particle characterization

Morphology, agglomeration state and size distribution of TiO_2 (sonicated or not) were analysed by TEM as described in *Chapter 4* for sonicated nCuO. Hydrodynamic behaviour (diameter, polydispersion index) was assessed by dynamic light scattering (DLS) as well as Z-potential.

The same characterization was performed also for nCuO non-sonicated particles.

Cell culture and treatments with nCuO, CuO extracts and soluble copper

A549 exposure to nCuO, copper oxide supernatants and copper ions was performed as described in *Chapter 5*. Copper ion concentration in supernatant were measured by AAS and the same concentration of copper from soluble salt were obtained using $CuSO_4 \cdot 5H_2O$. The concentrations used are reported in Supporting Table S2.

Determination of LC50 in A549 exposed to nCuO

Viability data from MTT assay (24h) were used to calculate the LC50 for nCuO on A549 cells. Exponential regression was used and the resulting equation was reported as well the correlation coefficient.

Neutral Red assay as viability test and lysosomal leakiness index

For Neutral Red assay (NR) the dye solution was added directly to each well (10% of the medium). NR retained at lysosomal level was recovered after 3h with the solubilization solution (1% acetic acid in 70% ethanol). Optical density (OD) was measured with a multiplate reader spectrophotometer (MultiskanAscent -Thermo) at 540nm using 690nm as a reference wavelength. Cell viability was expressed as OD percent in comparison to the

control (± standard error of the mean). The experiments were preformed in triplicates and data were presented as mean values ± standard error of the mean values. Statistically significant differing data sets ($p<0.010$, using one-Way ANOVA + Dunnett's method) were indicated by a star (*).

Supporting results

Particle characterization

Supporting Figures S1, S2, S3 and Supporting Table S1 show the results of $nTiO_2$ characterization. TEM analysis of TiO_2 nanopowder revealed different aggregation state in non sonicated particles compared with sonicated particles, but morphology, average size and mean diameter didn't show significant changes. Aggregation phenomena occurred also in culture medium and the DLS analyses revealed the presence of two main population of particles with a mean diameter of 613nm and a polydispersion index of 0,322. TiO_2 nanoparticles in water (pH=7) appeared as negatively charged.

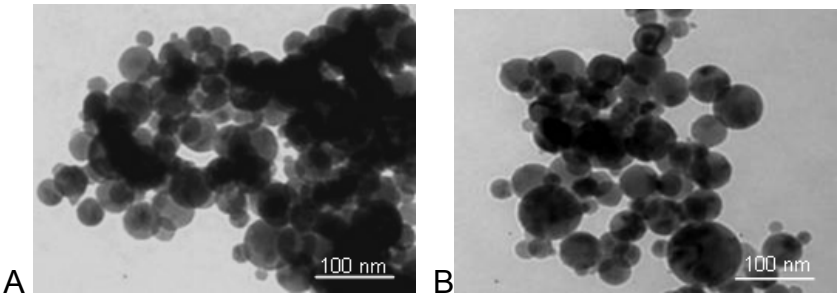

Supporting Figures S1. Morphology and aggregation state of $nTiO_2$ by TEM A) non sonicated- particles B) sonicated- particles.

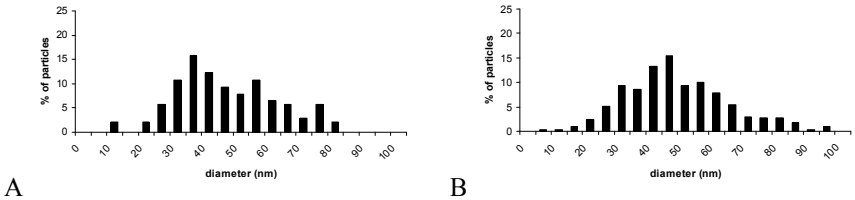

Supporting Figure S2. Size distribution of $nTiO_2$ by TEM A) Non sonicated particles (mean diameter = 48 nm; B) Sonicated particles (mean diameter = 50 nm).

Supporting Table S1: $nTiO_2$ description and physical chemical characterization

Particle	Particle size in powder a	Surface area a [m2/g]	mean diameter in powder b [nm]	Average size in powder b [nm]	mean diameter in solution c [nm]	PDI c	Z-pot H2O c [mV]
nTiO2	<100	>14	50	5-100	613	0,322	-18,4 ± 3,2

[a] according to the manufacturer Sigma-Aldrich; [b] measured by TEM; [c] measured by DLS; [d] detected by AAS

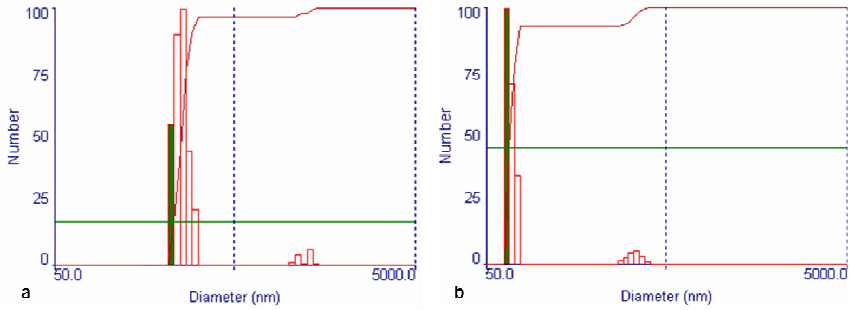

Supporting Figure S3. Characterization of particle suspensions by Dynamic Light scattering (DLS) analysis. a) $nTiO_2$; b) nCuO.

Supporting Figure S4 shows TEM characterization of non sonicated nCuO; particles appeared much more aggregated than sonicated CuO NPs but average size and mean diameter in powder don't significantly differ from sonicated particles.

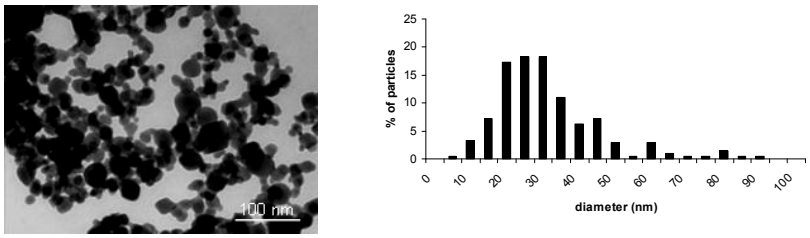

Supporting Figure S4. Aggregation and size distribution of non sonicated nCuO by TEM (mean diameter = 34 nm)

Cell culture and treatments with nCuO, CuO extracts and soluble copper

Supporting Table S2 summarize the amount of copper released after 24h of incubation in Optimem 1%FBS (37°C, 5%CO_2), for each suspension, measured by AAS. In parallel we reported the correspondent nominal $CuSO_4$ dose mass simulating the release from the correspondent concentration of nCuO.

Supporting Table S2. Correspondences among copper concentration in extracts and from soluble salt for each dose of nCuO tested.

[a] nCuO dose μg/ml	[b] Cu in extracts μg/ml	[c] $CuSO_4 \cdot H_20$ μg/ml
100	38	160
50	21	80
10	4	16
5	2	8
1	0,2	0,8

[a] nominal dose of copper oxide nanoparticles administered to cells; [b] Cu concentration in medium (OptiMEM 1%FBS incubated for 24h, 37°C, 5%CO_2) by AAS, after centrifugation (12 000g, 30mins); [c] nominal concentration of $CuSO_4 \cdot 5H_2O$ in medium simulating the [Cu] released from particles.

Determination of LC50 in A549 exposed to nCuO

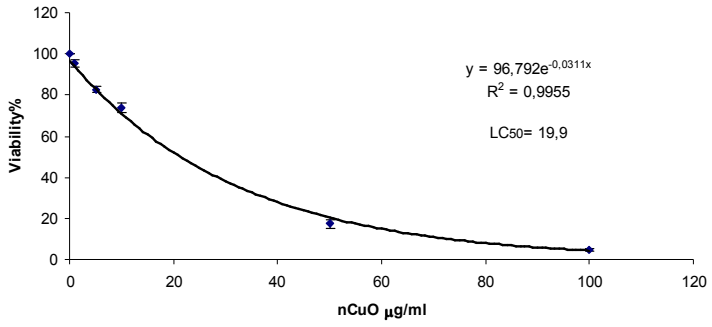

Supporting Figure S5. Dose–response relationship by exponential regression in A549 cells exposed (24h) to increasing nCuO concentrations (1, 5, 10, 50,

100μg/ml). Viability was measured by MTT assay and data are expressed as percentage of the optical density (OD) of treated samples versus control. Correlation coefficients (R^2) and the equation used to calculate LC50 are indicated. Each point represents the mean and standard deviation of at least three independent experiments.

Neutral Red assay as viability test and index of lysosomal leakiness

Supporting Figure S6 shows the viability profile of A549 exposed to nCuO by Neutral Red assay. Reduced stain retention by lysosome can be also attributed to lysosomal leakiness.

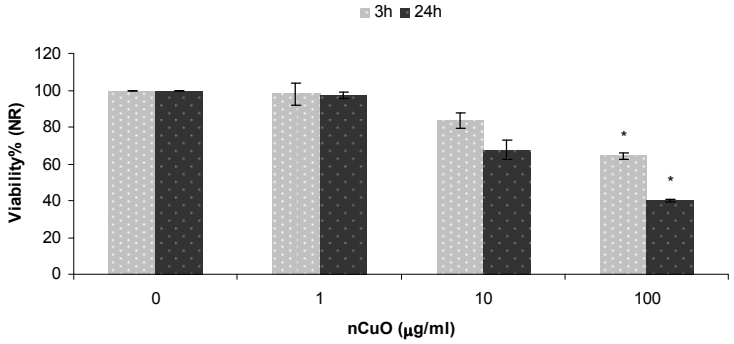

A

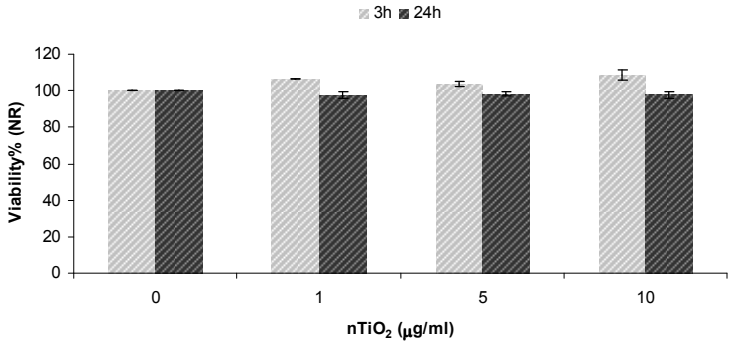

B

Supporting Figure S6. Neutral Red retention in A549 exposed to increasing concentrations of nCuO (A) and TiO_2 (B) (3,24h).

List of abbreviations

AAS	Atomic Absorption Spectroscopy
ALF	Artificial Lysosomal Fluid
BHT	Butylated hydroxytoluene
BSA	Bovin Serum Albumin
C_{60}	Fullerene
CB	Carbon black
CME	Clathrin Mediated Endocytosis
CLSM	Confocal Laser Scanning Microscopy
CNT	Carbon Nanotubes
DAPI	4',6-diamidino-2-phenylindole
$DCFH_2$-DA	2,7 dichlorofluorescein diacetate
DHE	Dihydroethidium
DLS	Dynamic Light Scattering
DMABR	5,4 dimethylaminobenzylidene-rhodanine
DMSO	Dimethyl Sulfoxide
EC	European Commission
EDX	Energy Dispersive X-Ray analysis
EE	Early Endosomes
EELS	Electron Energy Loss Spectra
ENPs	Engineered Nanoparticles
EPA	Environmental Protection Agency
ESI	Electron Spectroscopy Imaging
FETAX	Frog Embryo Teratogenesis Assay-*Xenopus*
FBS	Foetal Bovin Serum
GSH/GSSG	Reduced Glutathione/Oxidized Glutathione
HCG	Human Chorionic Gonadotropin
HNE	Hydroxy-nonenal
ICP-MS	Inductively Coupled Plasma Mass Spectroscopy
ICP OES	Inductively Coupled Optical Emission Spectrometry
ISO	International Organization for Standardization
ITO	Indium Tin Oxide
LC50	Lethal Concentration
LDH	Lactate dehydrogenase
LE	Late Endosomes
LPO	Lipid Peroxidation
MDA	Malondialdehyde
MONs	Metal Oxide Nanoparticles
MTT	3-(4,5-dimethylthiazol-2-yl)-2,5-diphenyltetrazolium bromide
MWCNT	Multi-Walled Carbon Nanotubes
NMs	Nanomaterials
NPs	Nanoparticles

NR	Neutral Red
OD	Optical Density
OECD	Organization for economic Co-operation and Development
PECs	Predicted Environmental Concentrations
PM	Plasma Membrane
QDs	Quantum Dots
REACH	Registration, Evaluation, Authorization and restriction of Chemicals
ROO•	Peroxyl radical
ROS	Reactive Oxygen Species
SEM	Scanning Electron Microscopy
SS	Side Scatter
SWCNT	Single-Walled Carbon Nanotubes
TC50	Teratogenic Concentration
TEM	Transmission Electron Microscopy
TI	Teratogenic Index
TPE	Two-Photon Excitation
UFPs	Ultrafine Particles
nAl_2O_3	Aluminum nanoxide
nCuO	Copper nanoxide
$nTiO_2$	Titanium nanoxide
nZnO	Zinc nanoxide

Ringraziamenti

Ringrazio Paride Mantecca, Alessandra Bulbarelli, Renato Bacchetta, Umberto Fascio, Nadia Santo per il supporto tecnico-scientifico e il Centro Polaris, in particolar modo nella persona della prof.ssa Marina Camatini, per la fiducia accordatami nel portare avanti questo progetto.

Un ringraziamento particolare va anche a tutti i colleghi con cui ho condiviso questi tre anni…Eleonora, Ross, Laura, Betta, Eleonora (Pez), Maurizio, Tiziano, Diego, Jack, Daniele, Pasquale…

E non posso dimenticare, al di fuori dell'università, gli amici e i miei genitori, che in momenti diversi non hanno mancato di incoraggiarmi.

Un grazie di cuore.